

**ENGINEERING MEGAKARYOCYTIC MICROPARTICLES
FOR NUCLEIC ACID DELIVERY AND THEIR BIOLOGICAL EFFECTS TO
HEMATOPOIETIC STEM/PROGENITOR CELLS**

by

Chen-Yuan Kao

A dissertation submitted to the Faculty of the University of Delaware in partial fulfillment of the requirements for the degree of Doctor of Philosophy in Chemical Engineering

Spring 2019

© 2019 Chen-Yuan Kao
All Rights Reserved

**ENGINEERING MEGAKARYOCYTIC MICROPARTICLES
FOR NUCLEIC ACID DELIVERY AND THEIR BIOLOGICAL EFFECTS TO
HEMATOPOIETIC STEM/PROGENITOR CELLS**

by

Chen-Yuan Kao

Approved: _____
Eric M. Furst, Ph.D.
Chair of the Department of Chemical and Biomolecular Engineering

Approved: _____
Levi T. Thompson, Ph.D.
Dean of the College of Engineering

Approved: _____
Douglas Doren, Ph.D.
Interim Vice Provost for Graduate and Professional Education

I certify that I have read this dissertation and that in my opinion it meets the academic and professional standard required by the University as a dissertation for the degree of Doctor of Philosophy.

Signed:

Eleftherios T. Papoutsakis, Ph.D.
Professor in charge of dissertation

I certify that I have read this dissertation and that in my opinion it meets the academic and professional standard required by the University as a dissertation for the degree of Doctor of Philosophy.

Signed:

Wilfred Chen, Ph.D.
Member of dissertation committee

I certify that I have read this dissertation and that in my opinion it meets the academic and professional standard required by the University as a dissertation for the degree of Doctor of Philosophy.

Signed:

April M. Kloxin, Ph.D.
Member of dissertation committee

I certify that I have read this dissertation and that in my opinion it meets the academic and professional standard required by the University as a dissertation for the degree of Doctor of Philosophy.

Signed:

Donna S. Woulfe, Ph.D.
Member of dissertation committee

ACKNOWLEDGMENTS

It's been a great journey toward the doctoral degree and I still cannot believe what I have accomplished. There are so many people that I would like to thank, including my advisor, colleagues, family and friends.

First, I would like to thank my advisor, Dr. Terry Papoutsakis. Thank you for giving me the opportunity to join the lab, guiding me step by step with tremendous patient, and always leading me to look at the bright side. With all the training within the past six year, I feel the great improvement in every aspect, including presenting skill from the conferences that I have attended, writing techniques after participating with one after one proposal application, and for the most importantly, being confident and believing in what I am doing is right.

I am always grateful for joining this lab, and would like to give a big thank you to my mentor, Dr. Jinlin Jiang, with all your guidance in research and as a good friend after work. I would also like to thank the former and current members in Papoutsakis Lab: Dr. Stephanie Luff for her help in research and bouncing idea during conversations, Dr. Robert Bennett for the help in microbial research and force me to have critical thinking, Julia Rohlhill for a great lunch accompany and friend; and all the other lab members including Dr. Alan Fast, Kamil Charubin, Hannah Streett, Samik Das, Erica Winter, Jessica Belliveau, Will Thompson, Bryan von Hagel, and Ben Dubner. I would also like to give a special thanks to Jasmine Shirazi from Gleghorn Lab for her expertise and for the great experience of cooperation between the two labs.

Lastly, I would like to thank my beloved family. Without your support, I couldn't make it to what I am now. Thanks mom and dad for giving me the idea to study abroad, allowing me to pursue what I want to do with no worries. Thanks my girlfriend for her fully support. It has been a wonderful year with you. Your perseverance to pursuing the goal and optimistic to everything largely encourage me to get to the end.

Thank you everyone in this journey.

TABLE OF CONTENTS

| | |
|-----------------------|------|
| LIST OF TABLES..... | xii |
| LIST OF FIGURES | xiii |
| ABSTRACT..... | xvi |

Chapter

| | | |
|-------|--|----|
| 1 | EXTRACELLULAR VESICLES: A MECHANISTIC VIEW OF EXOSOMES, MICROPARTICLES, THEIR PARTS AND THEIR TARGETS TO ENABLE THEIR BIOMANUFACTURING AND CLINICAL APPLICATIONS | 1 |
| 1.1 | Introduction..... | 1 |
| 1.2 | How Do EVs Recognize and Deliver Cargo to Target Cells?..... | 3 |
| 1.3 | EVs Alter the Biology and Fate of Target Cells through Diverse Mechanisms, Resulting in a Multitude of Cellular Phenotypes..... | 5 |
| 1.4 | Translational Applications of Native, Whole EVs | 6 |
| 1.4.1 | Mesenchymal Stem/stromal Cell (MSC)-derived EVs..... | 9 |
| 1.4.2 | Endothelial Progenitor Cell-derived EVs (EPC-EVs)..... | 10 |
| 1.4.3 | Megakaryocyte and Platelet-derived EVs (Mk-EVs and P-EVs)..... | 10 |
| 1.5 | Engineering Using EVs or their Components for Cargo (gene/drug) Delivery | 11 |
| 1.5.1 | Cargo Loading | 13 |
| 1.5.2 | Surface Modifications..... | 14 |
| 1.5.3 | EV-based Hybrid Technologies: Merging EV Membranes with Synthetic Membranes..... | 15 |
| 1.5.4 | New Technologies Based on Cellular-membrane-wrapped Nanoparticles or Loaded Membrane Vesicles | 15 |
| 1.5.5 | Cargo-function Relationships as a Basis for Discovery and Diagnostic Applications..... | 16 |
| 1.6 | Mechanisms of EV Biogenesis | 17 |

| | | |
|----------|--|-----------|
| 1.6.1 | Mechanisms of MP Formation..... | 18 |
| 1.6.2 | Inducers of MP Formation..... | 18 |
| 1.7 | Biomanufacturing of EVs: Exosomes and MPs..... | 19 |
| 2 | HOW DO MEGAKARYOCYTIC MICROPARTICLES TARGET AND DELIVER CARGO TO ALTER THE FATE OF HEMATOPOIETIC STEM CELLS?..... | 23 |
| 2.1 | Background..... | 23 |
| 2.2 | Materials and Methods..... | 26 |
| 2.2.1 | Materials and Antibodies..... | 26 |
| 2.2.2 | Megakaryocytic (Mk) Culture and Kinetics of Mk Microparticle (MkMP) Formation..... | 26 |
| 2.2.3 | Isolation of MkMPs and MkExos..... | 27 |
| 2.2.4 | Characterization of MkMPs and MkExos with Dynamic Light Scattering (DLS)..... | 27 |
| 2.2.5 | Characterization of MkMPs and MkExos with Flow Cytometry..... | 28 |
| 2.2.6 | Preparation of Human Platelets and PMPs..... | 28 |
| 2.2.7 | Human Umbilical Vascular Endothelial cells (HUVECs), Mesenchymal Stem Cells (MSCs) and Granulocytic Cultures.... | 29 |
| 2.2.8 | Co-culture of Human CD34+ Lineage Negative (Lin-) Cells, HUVECs, Human MSCs and Human Granulocytes with MkMPs..... | 30 |
| 2.2.9 | MkMP Binding and Uptake Analyses..... | 30 |
| 2.2.10 | Cell Ploidy and CD41 Expression Analyses..... | 31 |
| 2.2.11 | Scanning Electron Microscopy (SEM) Analysis..... | 31 |
| 2.2.12 | Transmission Electron Microscopy (TEM) Analysis..... | 32 |
| 2.2.13 | Thrombin Treatment of MkMPs and Generation of MkMPs from Thrombin-treated Mks..... | 33 |
| 2.2.14 | Western Analysis..... | 33 |
| 2.2.15 | Antibody Blocking Assays..... | 34 |
| 2.2.16 | Inhibitor Studies for Interrogating Specific MkMP-uptake Mechanisms..... | 34 |
| 2.2.17 | RNase Treatment Assay, RNA Size Distribution Measurement and Co-culture Experiments..... | 35 |
| 2.2.18 | Statistical Analysis..... | 36 |
| 2.3 | Results..... | 36 |
| 2.3.1 | Characterization of MkMPs as Distinct from Mk Exosomes..... | 36 |

| | | |
|-------|---|----|
| 2.3.2 | MkMPs Promote Mk Differentiation and CD34+-cell Maintenance and Expansion of Primitive Lin-CD34+ Stem Cells | 39 |
| 2.3.3 | Target Specificity: MkMPs Cannot Transdifferentiate Human Granulocytes, MSCs or HUVECs into Mk Cells..... | 43 |
| 2.3.4 | Endocytosis is a First Mechanism by which MkMPs Deliver their Cargo to HSPCs..... | 43 |
| 2.3.5 | Cell Fusion is a Second Mechanism by which MkMPs Deliver Cargo to HSPCs..... | 47 |
| 2.3.6 | Role of Macropinocytosis and Lipid Rafts in MkMP Uptake by HSPC | 52 |
| 2.3.7 | PMPs Interact with and Induce Aggregation of HSPCs, but cannot Apparently Deliver Cargo to HSPCs; Thrombin-mediated Platelet-like Activation may Account for the Different Effects of MkMPs vs PMPs | 55 |
| 2.3.8 | HSPC Uropods are the Preferred Area of Interaction with MkMPs, with the Uropod-enriched CD54 (ICAM-1), CD43, CD11b, and CD18 Mediating Binding and/or Uptake of MkMPs..... | 58 |
| 2.3.9 | RNA Transfer Mediates the Impact of MkMPs on HSPCs | 62 |
| 2.4 | Discussion..... | 65 |
| 2.4.1 | MkMPs Target and Induce the Megakaryocytic Differentiation of Primitive Lin-CD34+ and all HSPCs but not so of MSCs, HUVECs or Granulocytes..... | 65 |
| 2.4.2 | MkMPs are Taken up by HSPCs via Endocytosis and Cell fusion, whereby Macropinocytosis and Lipid Rafts Play an Important Role | 66 |
| 2.4.3 | MkMP RNA is in Part at least Responsible for their Biological Effects | 68 |
| 2.4.4 | A Role for HSPC Uropods, CD54 and CD43, and why PMPs cannot Act on HSPCs Like MkMPs Do | 69 |
| 3 | ENGINEERING HUMAN MEGAKARYOCYTIC MICROPARTICLES FOR TARGETED DELIVERY OF NUCLEIC ACIDS TO HEMATOPOIETIC STEM & PROGENITOR CELLS..... | 71 |
| 3.1 | Background..... | 71 |
| 3.2 | Materials and Methods..... | 74 |
| 3.2.1 | Experimental Design..... | 74 |
| 3.2.2 | Chemicals and Reagents | 74 |
| 3.2.3 | Cultures of HSPCs and CHRF cells. | 75 |

| | | |
|--------|--|------------|
| 3.2.4 | Isolation of Megakaryocytic Microparticles (MkMPs) and MPs (CMPs) from CHRf cells..... | 76 |
| 3.2.5 | Determination of Microparticle-Size Distribution..... | 76 |
| 3.2.6 | Exogenous loading of pDNA to CMPs or MkMPs..... | 76 |
| 3.2.7 | Exogenous Loading of Small RNAs to MkMPs..... | 77 |
| 3.2.8 | Quantification of Plasmid-DNA Loading of CMPs or MkMPs..... | 78 |
| 3.2.9 | Setup of co-cultures of HSPCs with pDNA-loaded CMPs/MkMPs, or small RNA-loaded MkMPs..... | 79 |
| 3.2.10 | Quantitative RT-PCR..... | 80 |
| 3.2.11 | Super-Resolution Microscopy..... | 81 |
| 3.2.12 | Nuclei Isolation..... | 81 |
| 3.2.13 | Statistical Analysis..... | 82 |
| 3.3 | Results and Discussion..... | 83 |
| 3.3.1 | Efficient Exogenous Loading of pDNA into Megakaryocytic MPs through Electroporation Demonstrates the Large Cargo Capacity of MPs Compared to that of Exosomes..... | 83 |
| 3.3.2 | Delivery of pDNA to HSPCs using CMPs or MkMPs..... | 90 |
| 3.3.3 | Effective Delivery of pDNA to HSPC Nuclei..... | 95 |
| 3.3.4 | Functional Synthetic-RNA Delivery to HSPCs using MkMPs..... | 99 |
| 4 | ROLE OF MICRORNAS FROM MEGAKARYOCYTIC MICROPARTICLES (MKMPS) IN MKMP-INDUCED MEGAKARYOCYTIC DIFFERENTIATION OF HEMATOPOIETIC STEM/PROGENITOR CELLS..... | 106 |
| 4.1 | Background..... | 106 |
| 4.2 | Materials and Methods..... | 108 |
| 4.2.1 | Chemicals and Reagents..... | 108 |
| 4.2.2 | Megakaryocyte (Mk) Culture from CD34+ HSPCs..... | 108 |
| 4.2.3 | Isolation of Megakaryocytic Microparticles (MkMPs)..... | 109 |
| 4.2.4 | Isolation of Platelet-like Particles (PLPs) and Mk-derived Microparticles (MkMPs)..... | 109 |
| 4.2.5 | MiRNA Transfection into CD34+ HSPCs..... | 109 |
| 4.2.6 | Signaling Inhibitor Study..... | 110 |
| 4.2.7 | Preparation of Human Platelets and PMPs..... | 110 |
| 4.2.8 | RNA Extraction and Library Preparation..... | 111 |
| 4.2.9 | RNA Sequencing Data Analysis..... | 112 |
| 4.3 | Results..... | 113 |

| | | |
|-------|--|-----|
| 4.3.1 | MicroRNAs (miRNAs) in Human Megakaryocyte-derived Microparticles (MkMPs)..... | 113 |
| 4.3.2 | Effect of Individual, Most-abundant in MkMPs, miRNAs on Mk Differentiation and Expansion of CD34+ HSPCs..... | 118 |
| 4.3.3 | Effect of Combinations of the Most-abundant in MkMPs miRNAs on Mk Differentiation and Expansion of CD34+ HSPCs..... | 121 |
| 4.3.4 | Outcomes from Using of Specific Pathway Inhibitors Suggest that JNK, p38, PI3K, and mTOR Signaling Regulates MkMP-induced Mk Differentiation of HSPCs..... | 123 |
| 4.3.5 | MiR-486-5p Inhibitor Suppressed MkMP-induced Mk Differentiation of CD34+ HSPCs..... | 126 |
| 5 | ROLE OF P53 AND TRANSCRIPTION-INDEPENDENT P53-INDUCED APOPTOSIS IN SHEAR-STIMULATED MEGAKARYOCYTIC MATURATION, PARTICLE GENERATION, AND PLATELET BIOGENESIS | 128 |
| 5.1 | Background..... | 128 |
| 5.2 | Materials and Methods..... | 132 |
| 5.2.1 | Megakaryocytic Culture of CD34+ Hematopoietic Stem Cells and the CHR-288-11 Megakaryoblastic Cell Line..... | 132 |
| 5.2.2 | Shear Stress Experiments..... | 132 |
| 5.2.3 | Immunofluorescence Assays..... | 133 |
| 5.2.4 | Western Blot Analysis..... | 134 |
| 5.2.5 | Transfection of Primary Stem Cell-derived Mks..... | 135 |
| 5.2.6 | Sandwich ELISAs..... | 136 |
| 5.2.7 | qRT-PCR Assay on MDM2 Expression..... | 138 |
| 5.2.8 | Annexin V Binding Assay..... | 139 |
| 5.2.9 | Mk Particle Assays and Co-culture with Hematopoietic Stem Cells..... | 139 |
| 5.3 | Results..... | 140 |
| 5.3.1 | Shear-forces Induce Increased Acetylation of Transcription Factor p53 in Immature and Mature Mks..... | 140 |
| 5.3.2 | Shear Flow Stimulates Activation of Caspase 9 in Both Immature and Mature Mks, which Occurs Concurrently with PS Externalization..... | 143 |
| 5.3.3 | Transcription-independent p53-induced Apoptosis is Important in the Shear-stimulated Mk-particle Generation and the Biological Effectiveness of these Particles..... | 149 |

| | | |
|----------|--|-----|
| 5.4 | Discussion..... | 153 |
| 6 | CONCLUSIONS AND FUTURE DIRECTIONS | 157 |
| 6.1 | Conclusions..... | 157 |
| 6.2 | Future Directions | 161 |
| | REFERENCES | 164 |
| Appendix | | |
| A | SUPPLEMENTARY MATERIAL FOR CHAPTER 2..... | 179 |
| B | SUPPLEMENTARY MATERIAL FOR CHAPTER 3..... | 182 |
| C | SUPPLEMENTARY MATERIAL FOR CHAPTER 4..... | 186 |
| D | SUPPLEMENTARY MATERIAL FOR CHAPTER 5..... | 187 |
| E | PUBLICATION PERMISSIONS..... | 189 |
| F | IRB APPROVAL LETTER FOR BLOOD COLLECTION | 192 |
| G | IRB EXEMPT LETTER OF USING HUMAN CD34+ CELLS | 193 |

LIST OF TABLES

| | | |
|-----------|--|-----|
| Table 1.1 | Translation applications of EVs..... | 7 |
| Table 4.1 | Highly abundant (CPM >100), significantly enriched ($p < 0.01$; differential expression \geq two-fold) miRNAs in MkMPs compared to Mks. | 116 |
| Table 4.2 | The top 10 most abundant miRNAs in MkMPs, Mk cells, PLTs, or PMPs..... | 117 |
| Table 4.3 | List of the combination of miRNA mimics | 122 |
| Table 4.4 | List of signaling inhibitors, their targets, and concentrations used | 124 |
| Table B.1 | Primers for amplification in PCR and q-RT-PCR..... | 184 |
| Table B.2 | Estimation of DNA copies in loaded-EVs from literature..... | 185 |

LIST OF FIGURES

| | | |
|-------------|--|----|
| Figure 1.1 | A systems view of EV-based applications..... | 3 |
| Figure 1.2 | Engineering inspired by EVs and their components: together & separately. | 12 |
| Figure 2.1 | Kinetic of MkMP generation and characterization of MkMPs and MkExo. | 39 |
| Figure 2.2 | MkMPs promote Mk differentiation of primitive Lin ⁻ CD34 ⁺ stem cells and this effect is target specific for HSPCs. | 42 |
| Figure 2.3 | MkMPs are quickly endocytosed by HSPCs. | 46 |
| Figure 2.4 | MkMPs can fuse into HSPC membranes and release their content into the target HSPCs. | 50 |
| Figure 2.5 | TEM details the fusion of MkMPs into HSPC membranes..... | 51 |
| Figure 2.6 | Macropinocytosis, lipid-raft and dynamin are engaged in uptake of MkMP by HSPCs. | 54 |
| Figure 2.7 | PMPs are not taken up by HSPCs and a thrombin-mediated platelet-like activation may account for the different effects of MkMPs vs PMPs..... | 58 |
| Figure 2.8 | CD54 (ICAM-1), CD18/CD11b (Mac-1) and CD43 mediate the uptake of MkMPs, with the HSPC uropods being the preferred interaction area..... | 62 |
| Figure 2.9 | RNA profile of Mk and MkMP with or without RNase treatment..... | 64 |
| Figure 2.10 | RNase treatment reduces the biological effect of MkMPs on HSPCs..... | 65 |
| Figure 3.1 | Loading of pDNA into CHRF-derived MPs (CMPs) or megakaryocyte-derived MPs (MkMPs) through electroporation. | 90 |
| Figure 3.2 | Delivery of pDNA to HSPCs via MPs. | 94 |

| | | |
|------------|---|-----|
| Figure 3.3 | Super-resolution images of HSPCs co-cultured with Cy5-pGFPns-loaded MPs. | 95 |
| Figure 3.4 | Examine the delivery of pDNA to HSPC nucleus via nuclei analysis. | 98 |
| Figure 3.5 | Silencing of <i>c-myb</i> through MkMP delivery of siRNA to HSPCs and enhance megakaryocytic differentiation. | 103 |
| Figure 3.6 | Functional delivery of miR-486-5P to HSPCs via MkMPs enhanced megakaryocytic differentiation. | 104 |
| Figure 4.1 | Venn diagram showing the number of miRNAs detected (CPM \geq 1) in Mks, MkMPs, PLPs, PLTs, and PMPs, and the number of miRNA shared between MkMPs with others. | 114 |
| Figure 4.2 | Volcano plot showing the results from the differential expression analysis of miRNAs in MkMPs vs. Mk cells. | 115 |
| Figure 4.3 | Pie chart showing the miRNA distribution in MkMPs. | 118 |
| Figure 4.4 | The effect of single miRNAs on Mk differentiation. | 120 |
| Figure 4.5 | Effect of miRNA combinations on Mk differentiation. | 122 |
| Figure 4.6 | Impact of signaling inhibitor on MkMP-induced Mk differentiation. | 125 |
| Figure 4.7 | Proposed signaling pathways in MkMP-induced Mk differentiation. | 126 |
| Figure 4.8 | Co-culture of miR-486-5p inhibitor-loaded MkMPs with CD34+ HSPCs. | 127 |
| Figure 5.1 | Shear flow alters p53 acetylation and sub-cellular localization in Mks. | 141 |
| Figure 5.2 | Shear flow exposure modulates expression of acetyl-modifying enzymes. | 143 |
| Figure 5.3 | Caspase 9 activation in Mks is enhanced upon shear-flow exposure. | 144 |
| Figure 5.4 | Shear-induced Caspase 9 activation in Mks is TIPA-dependent while Shear-induced PS externalization is p53-dependent, TIPA-independent. | 148 |
| Figure 5.5 | Shear-stimulated Mk particle biogenesis is dependent upon transcription-independent p53-induced apoptosis. | 151 |

| | | |
|------------|---|-----|
| Figure 5.6 | CHRF-derived MPs (CMPs) from p53-KD CHRF cells induce megakaryocytic differentiation of HSCs to a lesser extent than CMPs from wild-type CHRF cells. | 153 |
| Figure A.1 | CD235a, CD11b and CD15 expressions of cells in MkMP co-cultures and vehicle control cultures. | 179 |
| Figure A.2 | Kinetics of MkMP binding to cells. MkMPs were stained with dye CFDA-SE and then co-cultured with d3 HPCs. | 180 |
| Figure A.3 | CD43 antibody induces cell aggregation of d3 HPCs. | 181 |
| Figure B.1 | Physical and functional characterization of CMP..... | 182 |
| Figure B.2 | The effect of electroporation temperature on pDNA loading efficiency. | 183 |
| Figure B.3 | Flow cytometry histograms. HSPCs were co-cultured with..... | 184 |
| Figure C1 | Dose effect of miRNA transfection to HSPCs..... | 186 |
| Figure D1 | Western blotting analysis of p53 expression in CHRF cells with p53 knock-down (p53-KD) or p53-KD followed by rescuing with wild-type p53. | 187 |
| Figure D2 | Transfection efficiency from pmaxGFP-transfected or negative control d12 Mks. | 187 |
| Figure D3 | Representative images of wild-type, p53 knock-down, or p53 overexpression d12 Mks. | 188 |

ABSTRACT

Megakaryocytes (Mks) are large polyploid cells derived from hematopoietic stem and progenitor cells (HSPCs) in the bone marrow and give rise to platelets and megakaryocytic microparticles (MkMPs), the most abundant MPs in circulation. MkMPs can induce the differentiation of hematopoietic stem and progenitor cells (HSPCs) into functional Mks. In this study, we show that MkMPs target HSPCs with high specificity. Using fluorescent confocal microscopy and electron microscopy, we identify two mechanisms by which MkMPs deliver cargo to HSPCs: endocytosis, and specifically macropinocytosis and lipid raft-dependent endocytosis, and direct fusion of MkMPs into HSPCs. We show that HSPC uropods are the preferential site for MkMP binding, and that CD54 (ICAM-1), CD11b, CD18 and CD43, localized on HSPC uropods, are involved in MkMP binding to HSPCs. We also investigate the role of miRNAs from MkMP in MkMP-induced Mk differentiation of HSPCs. Our study identified the importance of three miRNAs, miR-486-5p, miR-92a-3p, and miR-22-3p, alone and in combination, in mediating Mk differentiation of HSPCs in the absence of thrombopoietin. Signaling pathways JNK, p38, and PI3K/mTOR are also identified as mediating the MkMP-induced Mk differentiation of HSPCs.

Since HSPCs are important target cells for gene therapy applications, we developed a nonviral system based on MkMPs for targeted delivery of plasmid DNA

(pDNA) and small RNAs to HSPCs. With an optimized electroporation protocol, an average of 4200 plasmid copies per MP were loaded into MPs, thus enabling effective delivery of green fluorescent protein (GFP)-encoding pDNA to HSPCs and HSPC nuclei, with up to 81% of the nuclei containing pDNA. Effective functional small interfering RNA (siRNA) and microRNA (miRNA) delivery were also demonstrated.

Finally, we examine the role of p53 in the Mk shear-stress response. We demonstrated that shear flow stimulates p53 acetylation and Caspase 9 activation, and demonstrated that shear-stimulated Caspase 9 activation and Mk particle biogenesis depend on transcription-independent p53-induced apoptosis (TIPA), but PS externalization is not.

Chapter 1

EXTRACELLULAR VESICLES: A MECHANISTIC VIEW OF EXOSOMES, MICROPARTICLES, THEIR PARTS AND THEIR TARGETS TO ENABLE THEIR BIOMANUFACTURING AND CLINICAL APPLICATIONS

1.1 Introduction

Extracellular vesicles (EVs) are generated by most if not all mammalian cells [1-3], and carry RNAs, proteins and lipids from their parent cells during EV generation, which takes place frequently under cellular activation or stress [2]. Among EVs, the submicron-size microparticles/microvesicles (MPs/MVs; also known as ectosomes) are the larger ones ranging from 100 to 1000 nm in size. They bud off the cytoplasmic membrane of the parent cell under normal physiological or pathophysiological conditions, including coagulation, inflammation, tumorigenesis, and differentiation [2]. Exosomes (Exos), distinct from MPs, are nano-size particle (<100 nm) which originate from multivesicular bodies through exocytosis [2, 4]. Besides mammalian cells, outer membrane vesicles (OMVs), derived from bacteria (especially Gram-negative bacteria) are involved in stress response, promoting survival, pathogenesis, and interaction between bacteria in a community [5].

Cells use EVs to communicate with other cells by delivering signals through their content [2]. As reviewed (e.g., [6-8]), over the last few years, EVs have emerged as important mediators of intercellular communication regulating an ever-expanding

range of biological processes, both on normo- and patho-physiology. The former include enhancing and accelerating native developmental programs in immunology, vascular repair and angiogenesis, while the latter include carcinogenesis and cancer metastasis, neurodegenerative disorders, and infectious and cardiovascular diseases. As such, EVs are currently considered for a broad range of applications, from minimally invasive diagnostic applications to therapeutic interventions, like cell therapies and macromolecular drug delivery. It is now widely accepted that EVs are excellent candidates for enabling safe and potent cell and gene therapies to treat a broad spectrum of diseases or iatrogenic phenotypes. Yet, in order to pursue such applications involving EVs, better EV characterization, as well as better understanding of the mechanisms of cell targeting and methods for EV biomanufacturing are needed (Figure 1.1).

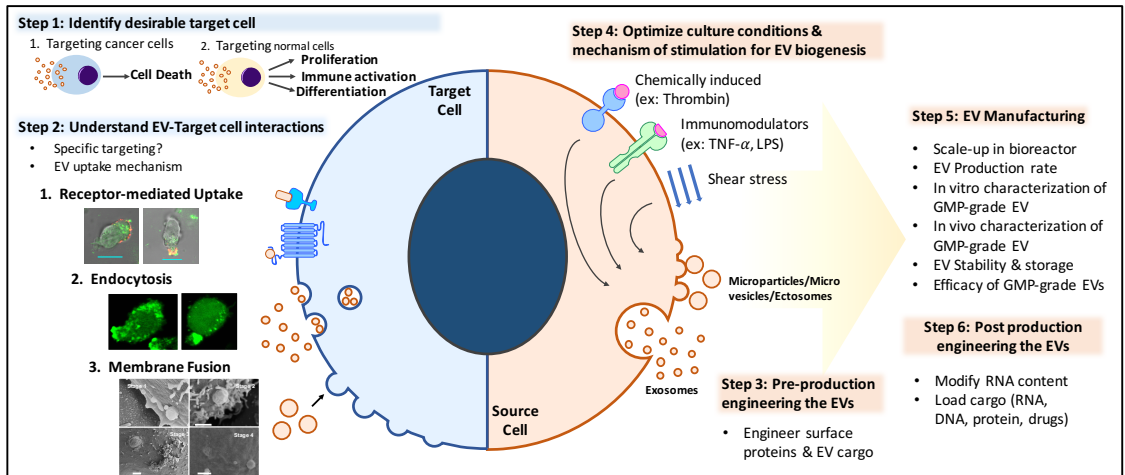


Figure 1.1 A systems view of EV-based applications. Development for EV-based applications detailed in six steps. Step 1: Determination of the target cell type. One could target and induce tumor-cell death, or target normal cells to enhance cell proliferation, differentiation or trigger other positive phenotypic responses. Step 2: Identify one or more EV types for targeting the desirable cell type from Step 1, based on the biology of EV-to-target-cell interactions. Narrow down the options from EV's target specificity or biological outcomes. Step 3: Surface modification on EVs to enhance recognition of and uptake of EVs by target cells, if there are no naturally-targeting EVs. Step 4: Determination and optimization of the method for EV biogenesis (chemically-, physically, starvation-, stimulation-induced or other). Step 5: Manufacturing of EVs from bench to bioreactor scale, and optimization of EV purification and characterization for GMP-grade EVs. Step 6: Post-biomanufacturing modification of EVs to engineer membrane characteristic and content.

1.2 How Do EVs Recognize and Deliver Cargo to Target Cells?

Understanding the recognition/uptake process of EVs to target cells is crucial for further applications in engineering EV for targeted delivery or diagnosis. Several studies have examined mechanisms by which EVs interact with target cells [9, 10].

The interaction typically starts with a ligand-receptor mediated binding, adhesion, or docking of EVs to target cells (Figure 1.1), and, in some cases, this initial interaction

is sufficient to alter the fate of target cells [11-13]. As logically expected, the ligands and receptors involved are EV and target-cell specific. Although ligand-receptor interactions are a first step in the target recognition process, in most cases, EVs exert their biological effect through transferring of signaling molecules (miRNAs , mRNAs, proteins, phospholipids, or generally, a morphogen), which likely requires uptake of EVs by the target cells [2, 14].

It has been suggested that the two major mechanisms are used by targeted/recipient cells to integrate or take up EVs are endocytosis and membrane fusion [2, 14] (Figure 1.1), and that cells use one of these two mechanisms to take up EVs [15, 16]. In general, it appears that the mechanisms of EV uptake largely depends on the recipient cell type [17]. Several endocytosis pathways have been found and studied in EV uptake. For example, macropinocytosis and clathrin-independent endocytosis are dominant in the uptake of EVs by tumor cells [18], while phagocytosis of EVs is usually engaged by immune cells such as dendritic cells, macrophages, or T cells [19]. Receptor-mediated endocytosis such as clathrin-dependent or caveolin-dependent endocytosis, which is usually related to dynamin in the formation of endocytic vesicles, were found in the case of microglia, macrophages or tumor cells, [10, 20]. Lipid raft-mediated endocytosis of EVs depends on membrane content of recipient cells such as cholesterol [21]. Besides endocytosis, direct fusion of EVs with cells was claimed in some studies [16, 22], but the evidence for such fusion events was challenged [23]. The fusion event requires the interaction of two surface protein from

EV and recipients cell, such as syncytin and its receptor Major Facilitator Superfamily Domain 2a (MFSD2a) [24].

EV uptake is examined in *in vitro* co-cultures of EVs with target cells. EVs are typically stained with lipid-membrane dye (ex: PKH26 or DiD) or cytosolic dye (ex: CFSE) for tracking the EVs and the cargo delivery into target cells. Co-localization analysis can be used for further tracking of EVs in the target cells after endocytosis. For example, active endocytosis of platelet-derived MPs by human brain endothelial cells was demonstrated by co-localization of MPs with endosomes and lysosomes [15]. To identify EV uptake via membrane fusion, transferring of fluorescence dye or EV-specific membrane proteins to target cells were detected by confocal or electron microscopy [16, 22].

1.3 EVs Alter the Biology and Fate of Target Cells through Diverse Mechanisms, Resulting in a Multitude of Cellular Phenotypes

Uptake of EVs enables delivery of EV cargo to recipient cells, thus triggering a broad spectrum of biological phenotypes. Tumor-derived EVs regulate the tumor microenvironment and impart an invasive effect in cancer progression and angiogenesis [25, 26]. A recent study reported that exosomes derived from attached hepatocellular carcinoma cells delivered both SMAD Family Member 3 (SMAD3) protein and mRNA to circulating hepatocellular carcinoma cells, enhanced their adhesive ability, and supported their metastasis [27]. EVs also play roles in cell differentiation and reprogramming. A few key examples follow. In a recent study,

ultrasound-induced exosomes released from human dermal fibroblasts carried reprogramming factors and quickly induced cell differentiation of fibroblasts to neural-progenitor cells [28]. MPs from endothelial progenitor cells activated angiogenic affect by transferring of mRNA to other endothelial cells [29]. Delivery of miRNA-150 by monocyte-derived MPs to endothelial cells promoted angiogenesis [30]. EVs also demonstrated therapeutic potential. For example, MPs derived from human bone marrow mesenchymal stem cells stimulated proliferation of tubular epithelial cells and protected cells from apoptosis through RNA delivery [31].

1.4 Translational Applications of Native, Whole EVs

As discussed, native EVs (MP and exosomes) possess multiple biological functionalities that include programming cell differentiation, promoting cell proliferation, preventing apoptosis and cell death, or impairing growth of bacteria. These characteristics suggest that native EVs have a good potential as therapeutic agents in translational applications. Below, we review the target specificity and the nature of the native cargo of EVs derived from a few select cell types. These and additional reports are summarized in Table 1.1.

Table 1.1 Translation applications of EVs.

| Mesenchymal stem cell (MSC)-derived EV | | | | |
|---|---|---------------------|----------------------------------|------------|
| In vitro/In vivo | Functionality | Native Cargo | Target Cell | Ref |
| In vitro | MSC-EVs targeted monocytes and B cells | N/A | monocyte, B cells | [32] |
| In vitro | MSC-EVs increased the expression of anti-apoptotic genes (ex: Bcl-xL, Bcl2, and BIRC8) and decreased the expression of proapoptosis genes (ex: Caspase 1, Caspase 8, and lymphotoxin alpha) in human tubular epithelial cells | N/A | tubular epithelial cells | [33] |
| In vivo (xenograft tumor model) | MSC-EVs promote cell growth of lung adenocarcinoma cancer cells | miR-410 | lung adenocarcinoma cancer cells | [34] |
| Endothelial progenitor cell (EPC)-derived EV | | | | |
| In vitro/In vivo | Functionality | Native Cargo | Target Cell | Ref |
| In vitro and In vivo (SCID mice) | EPC-derived MVs were incorporated in endothelial cells by interaction with alpha-4 and beta-1 integrins expressed on the MV surface, and trigger angiogenesis , promoted endothelial cell survival, proliferation. | mRNA | Endothelial cell | [29] |
| In vitro and In vivo (LPS-induce ALLI in mice) | Administration of EPC- Exos ameliorated LPS-induced ALLI and restored the in vivo pulmonary integrity. EPC- Exos enhanced the proliferation, migration and | miR-126 | Endothelial cell | [35] |

| | | | | |
|--------------------------------------|---|------------------------|---|------|
| | tube formation of the endothelial cells (ECs) | | | |
| In vitro and In vivo (Sepsis mice) | EPC exosomes treatment improved survival, suppressing lung and renal vascular leakage, and reducing liver and kidney dysfunction in septic mice. | miR-126-3p, miR-126-5p | HMVECs | [36] |
| In vitro and In vivo (AKI rat model) | EPC-MV protect the kidney from ischemic acute injury by enhancing tubular cell proliferation, reduced apoptosis, and leukocyte infiltration, by delivering of miR-126 and miR-296. EPC-MVs specifically targeted endothelial cells and epithelial cells, but fibroblast-MVs do not. | miR-126, miR-296 | Tubular endothelial cell, Tubular epithelial cell | [37] |

Megakaryocyte (Mk)-derived and Platelet-derived EV

| In vitro/In vivo | Functionality | Native Cargo | Target Cell | Ref |
|------------------|--|--------------|-------------------------------------|------|
| In vitro | Human megakaryocyte-derived microparticles induced megakaryocytic differentiation of hematopoietic stem/progenitor cells via transferring of RNA | mRNA, miRNA | Hematopoietic stem/progenitor cells | [23] |
| In vitro | P-EVs bind to neutrophil or endothelial cells through specific markers, and promoted the interaction between neutrophil and endothelial cells | N/A | Neutrophil or endothelial | [38] |

| Red Blood cell-derived EV | | | | |
|---------------------------|---|--------------|--------------------------|------|
| In vitro/In vivo | Functionality | Native Cargo | Target Cell | Ref |
| In vitro | RBC-EVs bind to monocyte through CD11b/CD18 to activate endothelial cells | - | Monocyte and Granulocyte | [39] |

1.4.1 Mesenchymal Stem/stromal Cell (MSC)-derived EVs

MSCs have been extensively examined in cell therapy applications for tissue regeneration [40]. In recent years, MSC-derived EVs (MSC-EVs) have shown therapeutic effects in tissue repair based on their anti-apoptotic, anti-inflammatory, or anti-oxidant effects (reviewed in Ref. [40]). MSC-EVs can enhance proliferation, and/or reduce apoptosis of epithelial cells in kidney disease, hepatocytes in liver diseases, or cardiomyocytes in heart disease, apparently by delivery of RNA (mRNA or miRNA) or growth factors [40]. Trapani *et al* have shown that MSC EVs specifically target monocytes and B cells, but not other lymphocytes (T, NK cells) in peripheral blood mononuclear cell population [32]. Bruno *et al* demonstrated specific anti-apoptotic effect from MSC-EVs, but not from fibroblast EVs, to human tubular epithelial cells by upregulating anti-apoptotic genes and down-regulating pro-apoptotic genes [33]. Different from studies reporting positive effects from MSC-EVs, in a recent study, Dong *et al* demonstrated that human umbilical cord MSC-EVs promote cell growth of lung adenocarcinoma cells mediated by miR-410, thus suggesting another therapeutic option (miR-410 inhibition) in order to inhibit tumor progression [34].

1.4.2 Endothelial Progenitor Cell-derived EVs (EPC-EVs)

EPC-EVs have been shown to specifically target endothelial cells or epithelial cells. *In vitro*, exosomes derived from EPCs (EPC-Exos) were able to enhance proliferation and migration of endothelial cells [35]. *In vivo*, injection of EPC-Exos into mice alleviated LPS-induced acute lung injury by transferring miR-126 to endothelial cells [35]. In another study, EPC-Exos, which were found to be enriched in miR-126-3p and -5p, were able to improve cell survival in a murine sepsis model [36]. Other than exosomes, Deregibus *et al* demonstrated that microvesicles derived from EPC (EPC-MVs) specifically target endothelial cells via the surface proteins VLA-4 (alpha-4 and beta-1 integrins), thus triggering angiogenesis and enhancing endothelial survival [29]. In an acute kidney injury (AKI) rat model, EPC-MVs enhanced tubular endothelial/epithelial cells proliferation mediated by the delivery of miR-126 and miR-296 [37]. Cantaluppi *et al* further demonstrated the specificity of these EPC-MVs in only targeting endothelial/epithelial cells but not fibroblasts [37].

1.4.3 Megakaryocyte and Platelet-derived EVs (Mk-EVs and P-EVs)

Mk-EVs and P-EVs are the most abundant EVs in circulation, with Mk-EVs being the most abundant of the two [41]. Although they have the same ontogeny and they both present the megakaryocytic surface proteins (CD41 or CD42b), they differ in that P-EVs are CD62P⁺ while Mk-EVs are not, and these and other unknown differences makes them target different cell types. P-EVs are able to trigger angiogenesis, and a play a role in tissue repair and tumor progression [42]. In a recent study, P-EVs

(mostly platelet-derived microparticles, PMPs) were shown to efficiently bind to neutrophils or endothelial cells through different surface markers, and subsequently enhance the interaction between neutrophils and endothelial cells. CD62P or CD11b mediated the recognition of neutrophils by P-EVs, while CD61, CD21, and CD51 were involved in the interaction between P-EVs and endothelial cells [38].

1.5 Engineering Using EVs or their Components for Cargo (gene/drug)

Delivery

EVs exhibit several desirable natural characteristics that makes them suitable as vehicles for cargo (gene or drug) delivery (Figure 1.2). Applications of native, unmodified EVs were discussed above. Here we examine engineering of EVs or using key EV components to enhance or enable efficient cargo delivery, respectively, or to deliver non-native cargo. As summarized in Figure 1.2, all key EVs components, including their native cargo, surface proteins, and their lipid-bilayer membranes, can be further engineered for various applications (Figure 1.2A). Loading of synthetic cargo is an important first engineering goal, and the most widely examined among all EV engineering efforts. To enhance targeting for specific cargo delivery, several technologies for engineering EV have been examined or can be proposed based on EV surface modification, either by expressing new or native surface proteins or by combining EVs with synthetic particles such as liposomes or polymeric nanoparticles (NPs). Finally, their native cargo (RNA, proteins, lipids) can be used for diagnostic,

discovery or therapeutic applications. Below, we summarize some of these applications.

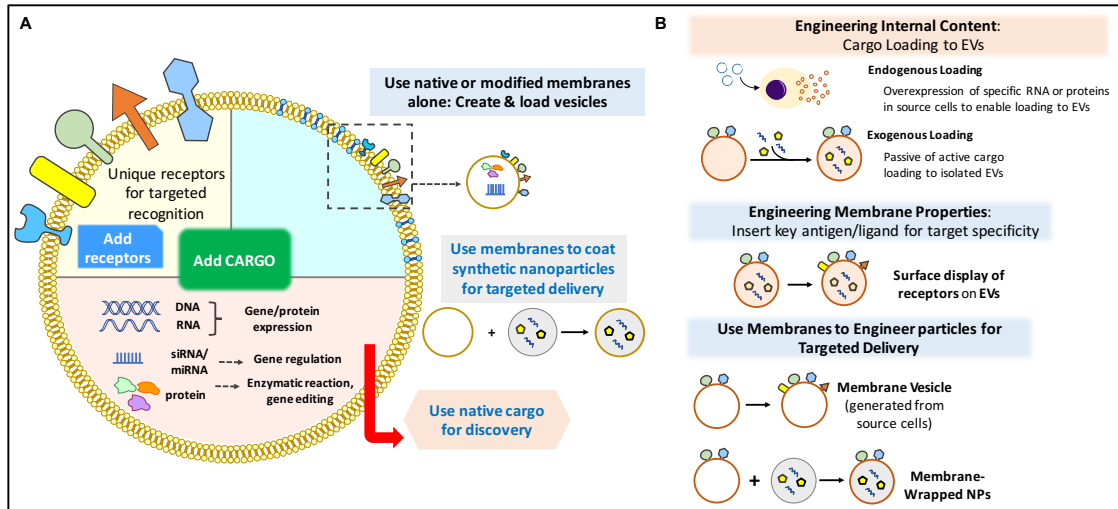


Figure 1.2 Engineering inspired by EVs and their components: together & separately. (A) The key EV components: surface proteins (receptors), lipid-based bilayer membranes, and internal cargo (DNA, RNAs, small RNAs, and proteins). It also shows possible technological applications based on EVs and/or their components. For example, native cargo can be used for discovery or diagnosis. (B) Different engineering concepts to use EVs or their membranes for targeted delivery. Target specificity is mediated by unique native surface proteins, and can be enhanced by expressing additional antigens, ligands, receptors or antibodies. Additional cargo can be loaded into EVs for delivery to specific cell targets aiming to achieve various biological effects. Endogenous loading is achieved by overexpression of specific genes (via plasmid DNA loading) or directly loaded RNAs or proteins in EV-producing cells with transfecting of DNA vector. Exogenous loading is performed by passive (mixing) or active (electroporation, sonication, or extrusion) cargo loading to isolated EVs. Cellular membrane (native or modified) can be used independently load cargo for targeted delivery. For example, membrane isolated from a specific cell type can be used to form membrane vehicles carrying specific receptors for targeting. Membrane vehicles can be used for exogenous cargo loading, or to wrap synthetic cargo-loaded nanoparticles.

1.5.1 Cargo Loading

Due to their natural ability to transfer cargo to various cell targets, EVs have the potential to be used as carriers for targeted cargo delivery. Two main approaches are used for cargo loading into EVs (Figure 1.2B). Endogenous loading was used for protein or RNA loading into EVs, whereby EV-producing cells were transfected with plasmid DNA [43] or RNA [44, 45] to overexpress specific genes and/or proteins [46], assuming that this will lead to transfer of the nucleic acids to the EVs during their biogenesis. In other cases, rather than transfection, simple incubation of drugs with cells leads to transfer of these drugs to EVs upon their biogenesis [47, 48]. More investigations have focused on *exogenous cargo loading*. Several studies used electroporation to load RNAs or drugs to EVs [47, 49-51]. The loading capacity of cargo molecules varies among different subset of EVs. Small RNAs such as miRNAs [52] or siRNAs [53] can be easily loaded into exosomes with electroporation. MVs/MPs, due to their larger size, can carry linear or plasmid DNA either loaded by direct electroporation [51, 54] or by transfecting the EV-producing cells [55]. Lamichhane *et al* showed that loading linear dsDNA larger than 1000 bp to HEK293T-derived exosomes was inefficient, while loading plasmid DNA practically impossible due to the small size of exosomes [51]. Kanada *et al* examined cargo delivery, both *in vitro* and *in vivo*, by HEK293FT-derived exosomes and MPs to show that functional protein expression was only possible from MP-mediated pDNA delivery [55]. These studies suggest that for loading practically significant amounts of large size cargo molecules, one needs to use the large MPs due to their higher cargo

capacity given the small cargo capacity of exosomes [54]. Besides electroporation, other methods such as saponin-mediate loading, extrusion or dialysis has also been used for cargo loading into EVs. Fuhrmann *et al*, compared these methods for drug-loading efficiency, with electroporation shown to be better than other methods [47].

1.5.2 Surface Modifications

A key factor for targeted delivery are the membrane properties of EVs, namely the surface proteins that essential for recognizing specific antigens on the target cells (Figure 1.1). Beyond the natural target specificity of some EVs as discussed above and also summarized in Table 1.1), one could engineer naturally-targeting and non-targeting EVs by expressing proteins or peptides on their surface of to enable or enhance target specificity (Figure 1.2B). For example, Ohno et al. developed engineered exosomes that express a peptide fusion protein (transmembrane domain of platelet-derived growth factor receptor fused to the GE11 peptide) to specifically target and deliver miRNA to breast cancer cells expressing the epidermal growth factor receptor (EGFR) [43]. Tian et al. demonstrated a drug (doxorubicin) delivery platform by engineering dendritic-cell derived exosomes expressing the exosomal membrane protein (Lamp2b) fused to a integrin-specific iRGD to target tumor cells *in vivo* [56]. In another application, using exosomes expressing Lamp2b fused to the neuron-specific RVG peptide, GAPDH-siRNA was specifically delivered to various cell types in the mouse brain [53].

1.5.3 EV-based Hybrid Technologies: Merging EV Membranes with Synthetic Membranes

Recently, another strategy was developed by fusing lipid-based particles with EVs to enable targeted delivery. PEG-mediated insertion of EGA1-PEG-micelles to A431-derived EVs resulted in EV surface decoration with EGA1 (an EGFR ligand) thus increasing the binding to EGFR-overexpressing A431 cells [57]. Liposome-exosome hybrids were first developed by Sato et al. using freeze-thaw cycles [58]. To solve the problem of losing membrane integrity during the freeze-thaw cycles, Piffoux *et al* used simple incubation of drug-loaded liposomes with MSC-derived EVs at 40 °C to create EV hybrids, and demonstrated enhanced drug delivery to CT26 colon cancer cells [59]. Fusion of HEK293FT-derived exosomes with liposomes created large size hybrids (~350 nm), which enabled encapsulation of large plasmids (dCas9 or CRISPR-Cas9 vectors) delivered to MSCs for down-regulation of Runx2 mRNA level or editing of the CTNNA1 gene [60]. The study further supports our recent study [54] that large particles are more suitable for DNA plasmid cargo loading and delivery.

1.5.4 New Technologies Based on Cellular-membrane-wrapped Nanoparticles or Loaded Membrane Vesicles

Another approach for taking advantage of the natural targeting specificity of EVs, is to use membranes of cells that generate the EVs or EV membranes, is to use these membranes to wrap preloaded synthetic nanoparticles to achieved enhanced cargo delivery (Figure 1.2B). In 2011, Hu *et al* first demonstrated coating polymeric

nanoparticles with erythrocytic membranes to achieve prolonged circulation time *in vivo* in murine model [61]. While the work used nanoparticle wrapping to evade clearance and immune recognition, the concept can be used to wrap nanoparticles with membranes from cells or EVs that recognize and target desirable cell types or tissues to deliver the cargo of the synthetic nanoparticles to the desirable targets. Nanoparticle wrapping with specific membranes can be also used for enhanced antigen presentation to trigger an immune response. For example, cancer cell-coated nanoparticles presenting tumor-associated antigens were able to trigger anti-cancer immune responses for vaccine development application, or target homotypic cancer cells for tumor treatment applications [62].

A different way of taking advantage of the natural targeting specificity of EVs, is to use membranes of cells that generate the EVs or EV membranes, is to create vesicles from these membranes and develop technology to load desirable cargo to these vesicles (Figure 1.2B) aiming to achieve enhanced cargo delivery to target cells.

1.5.5 Cargo-function Relationships as a Basis for Discovery and Diagnostic Applications

EVs have great diagnostic and discovery applications based on the relationship between their makeup (cargo and surface proteins) and function (targeting and cargo delivery outcomes). As EV content and function varies depending on the age of the parent cells and possibly the mechanism of their biogenesis, the content-function relationship can be used for diagnosis and discovery [63]. For example, RNA

sequencing of their content can identify novel small RNAs (micro RNAs, long noncoding RNAs and pi RNAs) that are important in their biological function [64], such as the ability to impart a differentiation program, promote cell growth or suppress apoptosis. As such then, specific small RNAs or mRNAs can be used for diagnostic purposes such as for applications in assessing cancer load or metastatic potential [65]. Similarly, target specificity can be used as a means to discover novel receptor-ligand interactions of importance to a specific cell type or cellular program.

1.6 Mechanisms of EV Biogenesis

A key element of the biomanufacturing process is the mechanism by which one can induce EV formation from various cell types. EVs are produced typically under physiological or pathological stress/stimulation. Biogenesis of two major type of EVs (exosomes or MPs) is quite distinct. Several mechanisms are known to and have been used to induce EV biogenesis, most of which apply to a specific cell type but some of which are more broadly applicable. For exosome generation, several stimuli such as cellular stress, irradiation, hypoxia, or starvation have been shown to increase exosome secretion. Detail mechanisms of exosomes biogenesis at a molecular level have been reviewed [66]. Currently, starvation is the only method that has been used in exosome manufacturing [67, 68].

1.6.1 Mechanisms of MP Formation

MP formation requires cytoskeleton reorganization, especially as related to actin filaments. The inhibition of actin polymerization showed different effects on MP generation. Treatment of cytochalasin D during platelet activation or neutrophil activation decreased MP formation [69, 70]. However, by using latrunculin A, Flaumenhaft *et al* showed a 2.4-fold increased MkMP generation [41]. ROCK-II (rho-associated coiled-coil-containing protein kinases 2) has been shown to mediate thrombin-mediated erythrocytic-MP generation, with Capase-2 as a ROCK-II activator [71]. Caspase-3 mediates ROCK-I cleavage, and subsequently increased phosphorylation of myosin light chain and membrane blebbing [72]. In some, but not all MP-generation cases, this is followed by flipping of phosphatidylserine (PS) from the inner to the outer leaflet of plasma membrane mediated by several enzymes including flippase, floppase and scramblase [73]. The Papoutsakis lab has have reported caspase-3 and caspase-9 activation and PS exposure in shear-induced MkMP generation [74]. Calcium is a major factor regulating many cellular responses, and appears to be involved in MP generation, as well. The calcium ionophore A23187 was shown to increase cytosolic Ca^{2+} , and to activate calpains involved in PMP formation [75].

1.6.2 Inducers of MP Formation

MP formation can be stimulated or enhanced using simple or complex chemicals, growth factors or other stimuli. For example, thrombin has been shown to induce PMP

[76] or endothelial-derived MP [71] generation. The Papoutsakis lab has previously demonstrated shear-force-induced MkMP formation *in vitro*, mediated, as discussed above, by PS exposure and caspase-9 activation [74]. Calcium ionophore A23187 has been used to increase Ca^{2+} influx and biogenesis of PMPs [77] and erythrocytic MPs [78]. TNF- α is able to stimulate neutrophil-derived microparticle formation [79]. In another study, Alexy *et al* demonstrated the formation of two distinct TNF- α induced MPs from human aortic endothelial cells. One population is ROCK-dependent, miRNA-rich MPs, and the other population is caspase-dependent, miRNA-poor MPs [80]. Lastly, lipopolysaccharide was used to stimulate MP generation from monocytes or granulocytes [81].

1.7 Biomanufacturing of EVs: Exosomes and MPs

As discussed, EVs have great therapeutic potential and several EVs has been identified and approved for clinical trials. EVs are currently pursued by several startup and larger companies for a broad range of applications, from minimally invasive diagnostic applications to therapeutic interventions, including cell therapies and cargo delivery. To achieve large-scale EV production, it is necessary to develop EV manufacturing using Good Manufacturing Practices (GMP). Currently, several approaches have been reported for GMP-grade manufacturing or exosomes either from MSCs [68, 82] or from cardiac progenitor cells [67]. The transition from bench-scale to large-scale exosome production for clinical use has been recently reviewed [83]. These exosome manufacturing protocols are all based on surface-attached

(anchorage-dependent) cells, which are generated in small or larger scale using technologies that have been developed since the 1980s to expand these cell types, and whereby exosomes are collected late in culture under some nutrient starvation protocol. However, very little has been done in GMP-manufacturing of the larger MPs (MVs) from either a systems or mechanistic point of view.

In a systems-analysis examination that applies to all EVs, as shown in Figure 1.1, the first step is to identify which cell type to target. For clinical applications, one could target tumor cells aiming to enhance cell death, or target normal cell for impart desirable positive phenotypic responses, such as promoting cell proliferation or cell differentiation or to rescue cells from injury. Next, based on known biology of EV-to-target-cell interaction, one or more specific types of EVs will be selected for initial examination based on target specificity and biological outcomes in preclinical studies before narrowing the selection to one EV type for scaling up, due to its interaction to the target cells. If there are no options among naturally targeting EVs, one could engineer the surface characteristics of EVs to enhance the uptake process from the corresponding receptors presented by target cells. These EVs can be selected from easy-to-generated EVs such as MSC-EVs [84] or HEK-derived EVs. Once the EV source cells are selected, method for EV biogenesis should be optimized. As discussed above, several mechanisms are known to and have been used to induce EV biogenesis, most of which apply to a specific cell type but some of which are more broadly applicable. One of the most general likely to be able is the application of controlled biomechanical forces. This can be executed quite readily for both suspension cultures

[85] as well as for cultures of anchorage-dependent cells [86, 87]. Scaling up the EV producing process includes: (a) manufacturing EV-producing cells in a bioreactor of suitable scale; (b) optimization of EV purification process; (c) developing assays for and testing the biological of GMP-grade EVs; and (d) developing technologies for storage and freezing of EVs and/or formulation prior to use. EV biomanufacturing will require detailed characterization of the cellular and functional product properties to enable to identify and optimize key design and operational features of the culture system for a scalable and reproducible manufacturing process. Assays for detailed characterization of EVs based on physicochemical properties (size, density), surface-protein expression, and intraparticle content, and understanding how these properties relate to biological effectiveness will be necessary for EV manufacturing. This information will be used to enable the production of a more potent EV product in terms of biological effectiveness, and devoid of contaminating smaller or larger particles. These characterization assays are to assess functional product “quality”, and thus to establish a “process” vs. “function” relationship to address the question if and how does the manufacturing process affect product quality. For example, given that mixing and agitation in cell culture bioreactors affects expression of surface proteins and RNA content [88], it is clear that scaling up will require attention to attend to the needs of EV content and surface protein expression. This issue has not yet been explored in the MP literature, but is widely recognized as important in the emerging cell-therapy industry. This is analogous to the issue to protein glycosylation of protein therapeutics that was brought to the forefront (and remains at the forefront) of

manufacturing protein therapeutics, whereby the process profoundly affects protein glycosylation and thus therapeutic efficacy.

Chapter 2

HOW DO MEGAKARYOCYTIC MICROPARTICLES TARGET AND DELIVER CARGO TO ALTER THE FATE OF HEMATOPOIETIC STEM CELLS?

The origin of idea of this work and the major experiments were performed by Dr. Jinlin Jiang. The experiments including MkMP characterization in Figure 2.1E & 2.1F, endocytic inhibitor study in Figure 2.6, MkMP activation in Figure 2.7B & 2.7C, antibody blocking assays in Figure 2.8B & 2.8C were performed by me. I did a substantial amount of writing and editing of the published paper, and work with my advisor to respond to the reviewer comments in the revisions.

2.1 Background

Cell-derived microparticles (MPs) are small membrane-enclosed vesicles (0.1 to 1.0 μm in diameter) derived from direct budding off the plasma membrane of mammalian cells and mediate inter-cellular communication in various physiological and pathophysiological processes, including coagulation, inflammation, tumorigenesis, and differentiation [89-91]. MPs are different from the smaller ($< 0.1 \mu\text{m}$) exosomes that derive from the multivesicular endosome compartment of cells and have distinct physical and biological properties [2, 4]. Platelet-derived MPs (PMPs), discovered over 40 years ago, participate in many physiological processes, including hemostasis, maintenance of vasculature, immunity and inflammatory responses [92]. The most

abundant (70% - 90%) circulating MPs express CD41 or CD61 [41]. For a long time, they were thought to originate from platelets and thus possess the biological functions of PMPs. However, it was shown that most circulating CD41+ MPs in healthy subjects derive from megakaryocytes (Mks), and these Mk-derived MPs (MkMPs) are different from PMPs [41, 93]. A role for MkMPs has not been known until our recent study, which documented a novel biological function of MkMPs, namely that they can induce differentiation of hematopoietic stem and progenitor cells (HSPCs) towards the Mk lineage without exogenous thrombopoietin (TPO) stimulation [74].

Several studies have examined mechanisms by which MPs interact with target cells. The interaction typically starts with a ligand-receptor mediated binding of MPs to target cells, and, in some cases, this initial interaction is sufficient to alter the fate of target cells [11, 12, 94-98]. Yet, in most cases, MPs exert their biological effect through transfer of signaling molecules (proteins, mRNAs, miRNAs or phospholipids), which requires uptake of MPs by the target cells [2, 99, 100]. It has been reported that two mechanisms used by target cells to integrate MPs are cell endocytosis and membrane fusion [2, 99, 100], and that cells use one of these two mechanisms to uptake MPs [15, 16]. For example, PMPs were internalized by human brain endothelial cells through active endocytosis as demonstrated by colocalization of MPs with endosomes and lysosomes [15]. Direct fusion of MPs with cells was claimed in other studies [16, 22, 101, 102], whereby, MPs were first stained with a lipid-membrane or cytosol dye and then co-cultured with target cells [16, 22, 101, 102]. The evidence to support MP-cell fusion was the observed transfer of dye or MP-

specific membrane proteins to target cells as detected by confocal or electron microscopy [16, 22, 101, 102]. Yet, it is possible that endocytosis of MPs may contribute partially, if not fully, to the observed transfer of dyes or proteins. Thus, membrane fusion remains to be firmly established as a mechanism of MP uptake by cells.

Since MkMPs can be effectively frozen without loss of their biological activity (data not shown), it is possible that they can be used in transfusion medicine to enhance thrombopoiesis or for cargo delivery to HSPCs. Also, it is possible to engineer MkMPs to carry exogenous molecules for delivery to HSPCs, and/or identify key surface molecules that mediate the recognition of HSPCs for engineering synthetic or semisynthetic macro- or nano-particles for targeted drug delivery to HSPCs. Detailed understanding of how MkMPs recognize, target and deliver cargo to various HSPCs to alter their fate would be necessary prior to exploring such applications, and this is the main goal of this report. Here we first show that MkMP target the most primitive hematopoietic stem cells (HSCs) with higher effectiveness than more differentiated HSPCs. We show that both endocytosis and membrane fusion are responsible for delivery of MkMP cargo to HSPCs, and that MkMP RNA is partially, at least, responsible for changing the fate of HSPCs. Our data support the hypothesis that the platelet activation process necessary for PMP biogenesis explains the different biological effects of MkMP vs PMPs, and that MkMPs attach to and enter HSPCs preferentially through their uropods, with CD54, CD11b, CD18 and CD43 being involved in target-cell recognition.

2.2 Materials and Methods

2.2.1 Materials and Antibodies

All chemicals and protein reagents were obtained from Sigma-Aldrich or otherwise indicated. Recombinant human interleukin 3 (rhIL-3), rhIL-6, rhIL-9, rhIL-11, stem cell factor (rhSCF), thrombopoietin (rhTPO), Granulocyte colony-stimulating factor (rhG-CSF) were purchased from PeproTech Inc. Size standard fluorescent beads (0.22, 0.45, 0.88 and 1.34 μm) and AccuCount fluorescent particles ($\sim 5.0 \mu\text{m}$) were from SpheroTech. Fluorescein isothiocyanate (FITC) - or phycoerythrin (PE)-conjugated anti-CD41 (GP α IIb), PE-conjugated anti-CD62P (P-selectin), allophycocyanin (APC)-conjugated anti-CD34, PE-conjugated anti-CD11b, APC-conjugated anti-CD235a, FITC-conjugated CD63, APC-conjugated CD81 and purified anti-CD41, anti-CD42b, anti-CD43, anti-CD50 antibodies as well as corresponding IgG isotype were all from BD Bioscience. APC-conjugated anti-CD133 antibody was obtained from Miltenyi Biotec. Purified anti-CD54 (ICAM-1) antibody was from Abcam. Anti-filamin A was from Santa Cruz Biotechnology.

2.2.2 Megakaryocytic (Mk) Culture and Kinetics of Mk Microparticle (MkMP) Formation

Frozen G-CSF mobilized human peripheral blood CD34⁺ cells were obtained from the Fred Hutchinson Cancer Research Center. CD34⁺ cells were cultured to Mks as described [103]. At d7, CD61⁺ cells (Mks) were enriched using anti-CD61 magnetic

microbeads (Miltenyi Biotec) and were cultured as described [103]. From d8 to d12, CD41 and CD62P expression and concentration of MPs in the cell culture were measured by flow cytometer (FACSAria II, BD Biosciences) using AccuCount fluorescent particles (0.88 μm and 1.34 μm) as internal control.

2.2.3 Isolation of MkMPs and MkExos

MkMPs were isolated from d12 Mk culture as described [74]. Briefly, cells were removed from d12 culture medium at $150 \times g$ centrifugation for 10 min. Next, platelet-like particles (PLPs) and cell debris were removed by centrifugation at $1000 \times g$ for 10 min [74]. Following that, MkMPs were enriched from the supernatant by ultracentrifugation at 25,000 rpm ($38000 \times g$) for 1 hour at 4°C using an Optima Max Ultracentrifuge and a TLA-55 rotor (Beckman Coulter). To isolate MkExos, we used a standard protocol [104], whereby the supernatant from previous step was filtered through 0.22 μm filters (CellTreat), and ultracentrifuged at $100,000 \times g$ for 90 min at 4°C using an Optima L-90K Ultracentrifuge and a SW41 Ti Rotor (Beckman Coulter). MkMPs or MkExos were resuspended in IMDM or PBS and stored at -80°C for further use.

2.2.4 Characterization of MkMPs and MkExos with Dynamic Light Scattering (DLS)

For these experiments, MkMPs or MkExos isolated as above were suspended in PBS that had been filtered with 0.22 μm filters twice before being used. This filtered PBS

contains no particles as confirmed by DLS measurement. DLS measurement of suspensions of MkMPs or MkExos were performed at 25 °C using a Zetasizer Nano ZS (Malvern Instruments) with 633 nm He-Ne laser, fixed angle of 173°, and automatic attenuator. Size distribution by number was collected with at least 3 measurements for each sample.

2.2.5 Characterization of MkMPs and MkExos with Flow Cytometry

To detect MkExos with flow cytometry, isolated MkExos were first captured with Dynabeads magnetic beads (4.5 µm, Thermo Fisher) coated with anti-CD63 antibody at 4 °C overnight, following the manufacturing protocol in Exosome - Human CD63 Isolation/Detection kit (Invitrogen). MkMPs or bead-bound MkExos were then incubated with isotype IgG, FITC anti-CD63, or APC anti-CD81 antibodies for 15 min at room temperature before flow cytometry analysis. The latter two antibodies target the common surface antigens of endosomal origin expressed by human exosomes [105], and which are not expressed on MkMPs.

2.2.6 Preparation of Human Platelets and PMPs

Blood for isolation of human platelets was collected by venipuncture from adult human volunteers after providing written informed consent as approved by the Institutional Review Board at the University of Delaware (IRB protocol # 622751-1). Blood was collected from healthy donors and PMPs were prepared as described [74]. Briefly, 50 mL of blood was collected into syringe with ACD buffer (trisodium citrate,

65 mM; citric acid, 70 mM; dextrose, 100 mM; pH 4.4) at a volume ratio of 1:6 (ACD:blood). Following that, blood was centrifuged at $250 \times g$ for 10 minutes and the platelet rich plasma was isolated from the supernatant. Platelets were then pelleted at $750 \times g$ for 10 minutes, followed by 1 wash with HEN buffer (10 mM HEPES, pH 6.5, 1mM EDTA, 150 mM NaCl) containing 0.05 U/ml apyrase. After that, platelets were resuspended in HEPES-Tyrode's buffer (137 mM NaCl, 20 mM HEPES, 5.6 mM glucose, 1 g/l BSA, 1 mM MgCl₂, 2.7 mM KCl, 3.3 mM NaH₂PO₄). To generate PMPs, platelets were activated by 2 U/mL human thrombin (Sigma), and removed by centrifugation at $1000 \times g$ for 10 minutes. Lastly, PMPs were isolation by ultracentrifugation at 25,000 rpm for 1 hour at 4 °C, resuspended in IMDM medium, and stored at -80 °C.

2.2.7 Human Umbilical Vascular Endothelial cells (HUVECs), Mesenchymal Stem Cells (MSCs) and Granulocytic Cultures

Primary HUVECs were obtained from ATCC and cultured according to ATCC recommendation (growth medium: vascular cell basal medium (ATCC) supplemented with endothelial cell growth kit-VEGF (ATCC)). Passages 3-5 of HUVECs were used for following co-culture experiment. Human MSCs (passages 2-4) were courtesy from Prof. Xinqiao Jia at the University of Delaware and cultured according to Lonza recommendation (growth medium: mesenchymal stem cell basal medium (Lonza) supplemented with MSCGM™ SingleQuots™ (Lonza)). Human granulocytes were differentiated from human CD34⁺ cells as previously described [106]. At d7 of

granulocytic cell culture, CD15⁺ cells were enriched using MS column (Miltenyi Biotec) and CD15 microbeads (Miltenyi Biotec).

2.2.8 Co-culture of Human CD34⁺ Lineage Negative (Lin⁻) Cells, HUVECs, Human MSCs and Human Granulocytes with MkMPs

Lin⁺ (CD2⁺, CD3⁺, CD11b⁺, CD14⁺, CD15⁺, CD16⁺, CD19⁺, CD56⁺, CD123⁺, or CD235a⁺) cells were removed from CD34⁺ cells using the Miltenyi lineage-cell depletion kit. 60,000 CD34⁺ Lin⁻ cells, cultured HUVECs, MSCs or CD15⁺ granulocytes were incubated with 10 MkMPs per cell in 50 μ L IMDM medium for 1 hour at 37°C. After that, co-cultures of MkMPs with CD34⁺ Lin⁻ cells, MSCs and granulocytes were diluted in 550 μ L IMDM supplemented with 5% BIT9500 and 50 ng/mL SCF; the co-culture of MkMPs with HUVECs was diluted in 550 μ L growth medium without any endothelial cell growth factors. Co-cultures were maintained at 37°C and 20% O₂ for 8 days before harvesting for ploidy and CD41 analyses. For some experiments, CD34⁺ Lin⁻ cells at d0 and cells from co-culture at d3, d5 and d8 were stained with anti-CD41, anti-CD34, anti-CD11b, anti-CD15 and anti-CD235a antibodies and analyzed by flow cytometry.

2.2.9 MkMP Binding and Uptake Analyses

MkMPs were stained with 20 μ M CFDA-SE dye (Life Technologies) for 20 minutes at 37°C and washed thrice with IMDM. Then, MkMPs were co-cultured with hematopoietic stem/progenitor cells (HSPCs) from d3 Mk culture at a ratio of 30

MkMPs/cell for the indicated time. For the first hour, the co-culture medium was 50 μ L IMDM and after that, the co-culture was diluted in IMDM supplemented with 5% BIT9500, 50 ng/mL SCF and 1% pen strep. Flow cytometry was used to measure binding of MkMPs to cells. Images of co-cultured cells were collected via confocal microscopy (Zeiss 5 LIVE DUO highspeed/spectral confocal microscope).

2.2.10 Cell Ploidy and CD41 Expression Analyses

Cells from various MkMP co-culture and vehicle control cultures were harvested for ploidy assay as described [107]. Measurement of CD41 expression, Mk ploidy and numbers was performed on flow cytometry at d8 of co-culture using AccuCount fluorescent particles as internal control.

2.2.11 Scanning Electron Microscopy (SEM) Analysis

HSPCs from d3 of Mk culture were co-cultured with MkMPs (30 MP/cell) in 100 μ L IMDM medium for 2 or 4 hours. Then HSPCs or MkMPs were let spread on round coverslips coated with 1 μ g/mL human fibronectin and poly-L-lysine for another hour. 2% glutaraldehyde/PBS (Electron Microscopy Sciences, EM grade) was added to fix cells for at least 1 hour at room temperature or overnight at 4°C. After that, samples were postfixed for 1.5 hours in 1% OsO₄ at room temperature. After rinsed with H₂O, samples were dehydrated in a series of ascending ethanol concentrations for 10 min in each solution. After critical-point drying in Autosamdri-815B Critical Point Dryer (Tousimis), samples were sputter-coated with gold using a Benchtop Turbo III Sputter

Coater (Denton Vacuum). The electron images were collected via Field-Emission Scanning Electron Microscope (Hitachi S4700) at a working distance of 8.5-10.5 mm and voltage of 3.0 kV.

2.2.12 Transmission Electron Microscopy (TEM) Analysis

Transmission Electron Microscopy was performed on Zeiss Libra 120 Transmission Electron Microscope and images were acquired using a Gatan Ultrascan 1000 CCD. The d3 HSPCs were incubated with MPs (30 MPs/cell) in 100 μ L medium for 5 hours and then fixed in 2% EM grade glutaraldehyde and 2% paraformaldehyde (Electron Microscopy Sciences, EM grade) in 0.2 M cacodylate buffer. Samples were then rinsed 3 times, 15 min each, in 0.1 M sodium cacodylate buffer containing 2 mM CaCl_2 and fixed for 1 hour in 1.5% potassium ferrocyanide, 2 mM CaCl_2 , 2% OsO_4 in 0.1 M sodium cacodylate buffer on ice. After 3 washes with H_2O , the samples were post-fixed in 2% OsO_4 for 1 hour at room temperature, followed by 4 washes in H_2O . Then samples were stained en bloc overnight at 4°C with filtered 1% uranyl acetate. After 3 washes in H_2O , the samples were dehydrated in a series of ascending acetone solutions. The samples were then infiltrated within n-BGE and then Quetol-NSA resin on a rotator. Samples were embedded in labeled BEEM capsules and polymerized at 60°C for 24-48 hours. The ultrathin sections were prepared using a Reichert Jung Ultracut E ultramicrotome, and were collected onto 200 mesh formvar/carbon coated copper grids. Grids were stained with 2% methanolic uranyl acetate and Reynolds' lead citrate.

2.2.13 Thrombin Treatment of MkMPs and Generation of MkMPs from Thrombin-treated Mks

MkMPs were isolated and enriched from d12 Mk culture as described above. After adding 1 mM CaCl₂, half of MkMPs were treated with 10 U/mL human thrombin for 30 min at 37°C and the other half were treated in the same way without thrombin as the control for MkMP co-culture. Mks, isolated from d12 Mk culture by centrifugation at 150 × g for 10 min, were treated with 10 U/mL human thrombin with 1 mM CaCl₂ presence for 30 min at 37°C. MkMPs were isolated and enriched from thrombin-treated Mk as described. Thrombin-treated MkMPs and MkMPs generated from thrombin-treated Mks were washed with IMDM medium thrice before co-culture with CD34⁺ cells. CD41 and CD62P expression of these MPs as well as PMPs and MkMPs were examined by flow cytometry.

2.2.14 Western Analysis

MkMPs, thrombin-treated MkMPs, MkMPs from thrombin-treated Mks and PMPs were lysed in 1X SDS lysis buffer and the proteins were separated by SDS-polyacrylamide gel electrophoresis. Primary mouse anti-N-terminal filamin A (Santa Cruz #sc-17749) antibody and secondary Alexa Fluor®488 conjugated anti-mouse IgG antibody (Life Technologies #A11017) were used for filamin A detection. Images were captured by Typhoon FLA 9500 (GE Healthcare) and quantitative analysis of blotting band intensity was performed on ImageJ.

2.2.15 Antibody Blocking Assays

At d1 and d3 of CD34⁺ cell culture, 30,000 cells were incubated with 100 µg/mL anti-CD11a, anti-CD11b, anti-CD18, anti-CD34, anti-CD43, anti-CD44, anti-CD50, anti-CD54 or anti-CD133 antibodies or isotype IgG for 15 min at room temperature. Then MkMPs (30 per cell) stained with CFDA-SE were added to cells and more antibody was added to maintain the same concentration. MkMP-cell co-cultures were incubated in the incubator for 1 hour. Cells were washed once with cold PBS before flow cytometric analysis. For some experiments, MkMP co-cultures without any antibody blocking were incubated for 3 hours and anti-CD133 antibody was added to cell culture for 15 min before confocal microscopic analysis. For other experiments, MkMPs stained with CFDA-SE were incubated with anti-CD41, anti-CD42b antibodies or Annexin V at 100 µg/mL first before co-culture with d3 HSPCs.

2.2.16 Inhibitor Studies for Interrogating Specific MkMP-uptake Mechanisms

CD34⁺ cells were cultured as described above. At d1 or d3 of Mk culture, cells were pre-treated with 5 mM methyl-β-cyclodextrin (MβCD, Sigma), 10 µM dimethylamiloride (DMA, Sigma), 20 µM chlorpromazine (CH, Sigma), or 80 µM dynasore (Sigma) for 45 min at 37 °C, which were used to inhibit lipid raft-mediated endocytosis, macropinocytosis, clathrin-dependent endocytosis, and dynamin-dependent or independent endocytosis, respectively. Cells were then co-cultured with CFDA-SE-stained MkMPs at the concentration of 30 MkMPs per cell, for 30 min at 37 °C. For other experiments, cells treated with inhibitors were co-culture with labeled

molecules known to be taken up by cells using specific mechanisms. This was to examine the impact of inhibitors on specific mechanisms and compare the impact of the inhibitors above on the uptake of these molecules (used as positive control) versus the uptake of MkMPs. Specifically, Alexa 647-conjugated cholera toxin subunit B (CT-B, Life Tech), Alexa-594-conjugated dextran 10k (Dx, Life Tech), and Alexa 647-conjugated transferrin (Tf, Life Tech) were used as positive control, since these molecules were established to be taken up by cells through lipid-raft mediated endocytosis, macropinocytosis, and clathrin-dependent endocytosis, respectively [21]. Briefly, cells treated with inhibitors were co-cultured with 10 µg/ml CT-B, 100 µg/ml Dx or 5 µg/ml Tf for 15 min at 37 °C. After being washed with cold PBS, the uptake of MkMP, CT-B, Dx or TF were analyzed by flow cytometry.

2.2.17 RNase Treatment Assay, RNA Size Distribution Measurement and Co-culture Experiments

MkMPs were isolated as above and resuspended in IMDM. For RNase treatment, MkMPs were incubated with 1 U/mL Ambion® RNase A/T1 cocktail (Life Technologies) or 10 U/mL RNase ONE™ (Promega) for 1 hour at 37°C. Following that, 1 U/mL RNase inhibitor, SUPERase-IN (Ambion) was used to stop the RNase reactions. To further remove RNase from each MkMP samples, MkMPs were washed with IMDM thrice through 25,000 rpm ultracentrifugation for 1 hour at 4 °C. The three washes result in a RNase dilution by at least 10⁶ in each sample. This dilution eliminates any impact from RNase in downstream experiments. For some

experiments, total RNA was isolated from control MkMPs (without RNase treatment) or RNase-treated MkMPs with miRNeasy micro kit (Qiagen), following the manufacturing protocol. Total RNA concentration from each sample were measured with Qubit RNA HS Assay kit (Invitrogen). Measurement of size distribution of RNA were performed by Bioanalyzer 2100 (Agilent) with RNA600 Pico kit (Agilent). For some other experiments, human CD34⁺ cells were co-cultured with control MkMPs or RNase-treated MkMPs at 10 MPs/cell for 8 days. Cells were harvested at day 8 before ploidy analysis, as described above.

2.2.18 Statistical Analysis

Paired student t test of all data was performed on Minitab 16 (Minitab).

2.3 Results

2.3.1 Characterization of MkMPs as Distinct from Mk Exosomes

We first characterized the kinetics of formation, size distribution and intracellular texture of MkMPs using a variety of techniques. CD34⁺ HSCs were differentiated into Mks as described [103]. Flow cytometric analysis showed that, from d8 to d12, most CD41⁺ MPs were CD62P⁻, indicating that these MPs were derived from Mks rather than PLPs (Figure 2.1A). Based on the concentration of CD41⁺ MPs, most MkMPs were released by mature Mks (d11 to d12) rather than immature Mks (d8 to d11) (Figure 2.1A). TEM micrographs and flow cytometric analysis suggest that these

MkMPs were a heterogeneous population with the diameter smaller than 0.88 μm (Figure 2.1B & 2.1D). MP heterogeneity is a common characteristic of all reported MPs and not unique to these MPs [108-110]. SEM micrographs show that MkMPs are not spherical and their membrane not smooth (Figure 2.1C). This information was useful for the SEM studies reported below. To further validate our MkMP isolation protocol, and to show that our MkMP preparations are not contaminated by MkExos, we examined the MkMPs and MkExos, prepared as described in our Methods, using DLS and flow cytometry. In DLS measurements (Figure 2.1E), the size distribution of our MkMP and MkExo preparations show a mean size of 340.6 nm and 48.9 nm, respectively, which are in the range of common sizes of MPs (100-1000 nm) and exosomes (<100 nm) as reported in the literature [2]. These size distributions show no population overlap between our MkMPs and MkExos. We further examined our particle preparation using two common exosomal markers, CD63 and CD81, through flow cytometry analysis [105]. As expected, MkExos expressed both CD63 and CD81, while MkMPs were CD63 and CD81 negative. Taken together, these data demonstrate that MkMPs isolated from this protocol are free from contamination from MkExos. Based on these studies, we subsequently used MkMPs from d12 Mk culture isolated through successive centrifugations.

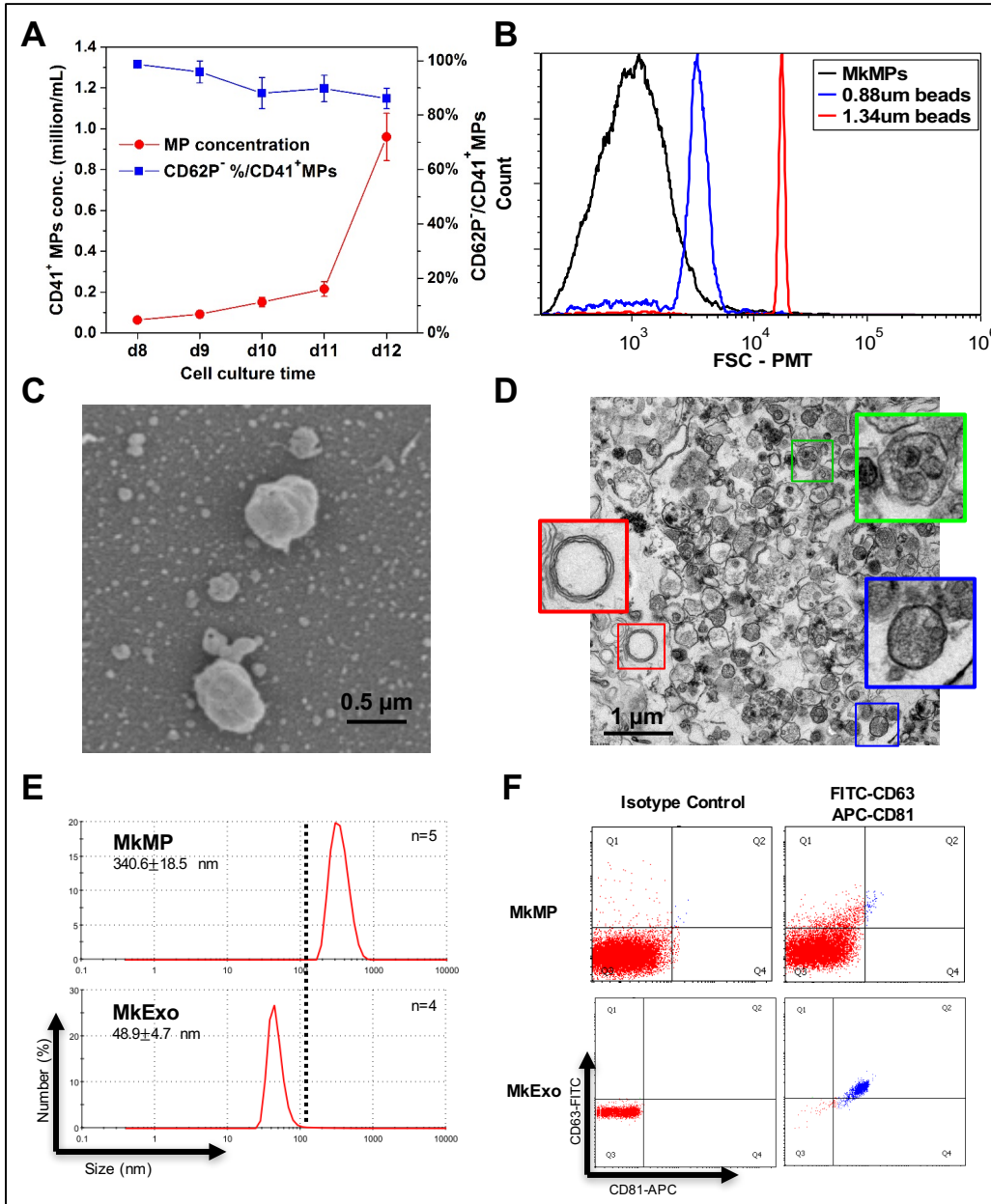


Figure 2.1 Kinetic of MkMP generation and characterization of MkMPs and MkExo. (A) CD62P expression and concentration of CD41⁺ MPs in Mk culture from d8 to d12. Mk cultures of CD34⁺ cells were enriched in Mk cells at d7 and were cultured at a concentration of 200K cell/mL. From d8 to d12, 100 μ L of cell culture medium was harvested every day for CD41 and CD62P analyses by flow cytometry. MP concentration was counted by flow cytometry using microbeads as a control. The data represent the average of three biological replicates \pm standard error of mean. (B) Representative size distribution histogram of MkMPs from d12 cells analyzed by flow cytometry using microbeads (0.88 μ m and 1.34 μ m in diameter) as internal size standards. (C-D) Representative SEM (C) and TEM (D) micrographs of MkMPs from d12 cell culture. The very small particles in the background of panel C are artifacts from sample preparation for SEM analysis as such small particles (<40 nm) cannot be collected during our MkMP preparation protocol as also shown in panel E below. Panel (D) demonstrates that MkMPs are heterogeneous in content as judged by the TEM-image texture of the MP contents, with three MPs enlarged for better examination. (E) Representative size distribution of MkMPs and MkExo measured by DLS with 2 biological replicates and 4-5 measurements. (F) Flow cytometry analysis of CD63 and CD81 expression on MkMPs and MkExos, with negative isotype IgG control.

2.3.2 MkMPs Promote Mk Differentiation and CD34⁺-cell Maintenance and Expansion of Primitive Lin-CD34⁺ Stem Cells

In order to better assess possible applications of MkMPs, we examined if MkMPs target HSPCs at all stages of differentiation. We had shown that MkMPs induce the differentiation of CD34⁺ HSPCs and partially differentiated HSPCs (d3 & d5 cells from cultures of CD34⁺ cells) towards the Mk lineage without TPO [74]. Mk cells from these MkMP co-cultures are functional in that they project proplatelets and synthesize both α - and dense-granules [74]. Here, we investigated the impact of MkMPs on more primitive, Lin- CD34⁺ cells. CD34⁺ cells were depleted of Lin⁺

(CD2+, CD3+, CD11b+, CD14+, CD15+, CD16+, CD19+, CD56+, CD123+, or CD235a+) cells before being co-cultured for 8 days with MkMPs. The co-culture contained a significant number of Mks with 2N, 4N and $\geq 8N$ ploidy classes, while very few Mks and none in higher ploidy classes were found in control cultures (Figure 2.2 A-B) (95-fold difference, $P < 0.01$).

To characterize the CD41- cells in both the MkMP co-cultures and control cultures, anti-CD34, anti-CD41, anti-CD11b, anti-CD15 and anti-CD235a antibodies were used to identify CD34+ HSPCs, Mks, granulocytes, monocytes and erythrocytes, respectively. Very few cells differentiated into granulocytes or erythrocytes in either the control culture or the MkMP co-culture, indicating that MkMPs could not induce HSPC differentiation to these two lineages (Figure A.1 of Appendix A). In addition, MkMPs significantly inhibited differentiation of HSPCs to CD15+ cells by ca. 50% (Figure S1). These data suggest that the effect of MkMPs is specific for the Mk lineage in that they do not induce differentiation to other myeloid cells, and notably the erythroid lineage, which has a common progenitor with the Mk lineage. In MkMP co-cultures, the percentage of CD41+ cells increased from 0 at d0 to ~47% at d5 and plateaued after d5 (Figure 2.2C), indicating that 5 days are sufficient for HSPCs to commit to megakaryopoiesis induced by MkMPs. Compared to control cultures, MkMP co-cultures had a higher percentage of CD34+ cells at d8 (47% vs. 28%, Figure 2.2D, $P < 0.05$) and more CD34+ cells (although not statistically significantly so: 108K vs. 27K, $P = 0.23$), thus suggesting that MkMPs can maintain a higher percentage of CD34+ cells compared to control.

We also compared the present data (Figure 2.2B) against our previous data (Figs. 5B & 5E of Ref [74]) to examine any differential impact of MkMPs on Lin-CD34+, CD34+ and d3 HSPC target cells. The number of Mks at d8 that resulted from the co-cultures of 60K Lin-CD34+, CD34+ or d3 HSPC target cells with MkMPs at 10 MkMPs/cell were ca. 90K, 52K and 38K, respectively, suggesting that MkMPs target primitive HSPCs with greater effectiveness.

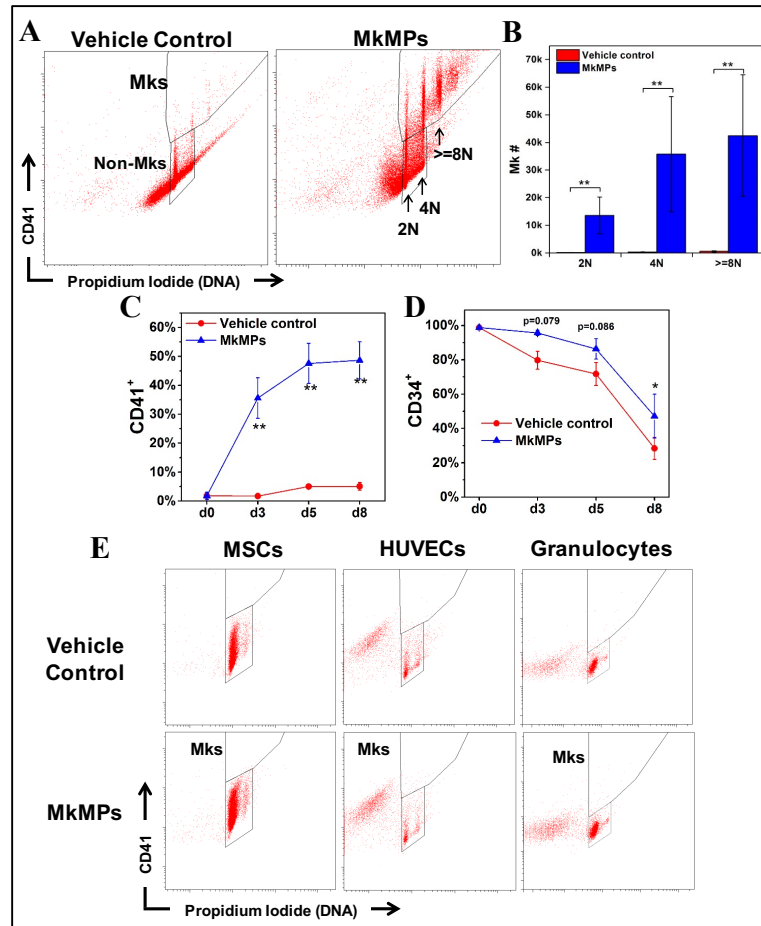


Figure 2.2 MkMPs promote Mk differentiation of primitive Lin⁻CD34⁺ stem cells and this effect is target specific for HSPCs. 60,000 primitive Lin⁻ HSPCs were enriched from CD34⁺ cells and co-cultured with MkMPs at concentration of 10 MkMPs/cell for 8 days. (A) Representative flow cytometric CD41 expression and ploidy analyses of cells from vehicle control cultures and the MkMP co-cultures at d8. (B) Numbers of Mks with different ploidy classes (2N, 4N and $\geq 8N$) in vehicle control cultures and the MkMP co-cultures at d8. Percentages of (C) CD41⁺ and (D) CD34⁺ cells in vehicle control cultures and the MkMP co-cultures at d0, d3, d5 and d8. (E) Representative CD41 expression and ploidy analyses of two sets of MkMP co-cultures with MSCs, HUVECs or granulocytes. Human MSCs (passage 2-4), HUVECs (passage 3-5) and CD34⁺ cell-derived granulocytes (d7 of culture) were co-cultured with MkMPs at the concentration of 10 MkMPs/cell for 8 days before being harvested for CD41 expression and ploidy analyses. The data in panels (B-D) are represented as the average of three biological replicates \pm standard error of mean. *, $P < 0.05$; **, $P < 0.01$.

2.3.3 Target Specificity: MkMPs Cannot Transdifferentiate Human

Granulocytes, MSCs or HUVECs into Mk Cells

Certain types of cells can transdifferentiate into other unrelated types of mature cells [111-115], and some of these events could be mediated by MPs. For example, MPs from lung endothelial cells induced transdifferentiation of bone marrow cells into endothelial cells [116]. Here, to investigate if MkMPs can induce Mk differentiation of related cell types, we co-cultured MkMPs with the ontologically or physiologically related granulocytes (that contain several related white blood cells, including neutrophils), MSCs or HUVECs, all of which are encountered by MkMPs in the bone-marrow microenvironments or in circulation. Flow cytometric analysis (Figure 2.2E) showed that no CD41+ or polyploid cells were identifiable in these co-cultures, indicating that MkMPs could not transdifferentiate these cells into Mks, and thus the action of MkMPs is specific to HSPC targets. Although MkMPs may interact with some of these cells (e.g., as neutrophils interact with platelets, they are likely to also interact with MkMPs), the interaction does not lead to fate-changing phenotype.

2.3.4 Endocytosis is a First Mechanism by which MkMPs Deliver their Cargo to

HSPCs

As discussed, the two key mechanisms by which MPs are presumed to bind to and be taken up by target cells are membrane fusion and endocytosis [100]. To inform the mechanistic investigations, we first examined the time scale of the interaction between MkMPs and HSPCs. MkMPs were stained with the cytoplasmic tracker dye CFDA-SE

and co-cultured with HSPCs from d3 Mk culture. Cells from the co-culture were analyzed by flow cytometry to examine the kinetics of MkMP-cell binding based on the mean fluorescence intensity (MFI) of cell CFDA-SE. The cell CFDA-SE MFI increased quickly within 10 min from the start of the co-culture and reached the maximum at 60 min, dropping quickly after 2 hours and reaching a basal low level after 24 hours (Figure A.2 of Appendix A). These data demonstrate that MkMPs bind to cell surface quickly to start delivering cargo to target cells. After one hour of co-culture, the decreased cell CFDA-SE MFI could be caused by dilution due to cell proliferation.

To investigate if MkMPs are just binding to cells or taken up by them, MkMP co-cultures were examined using confocal microscopy. After 3 to 5 hours of co-culture, most HSPCs contained CFDA-SE dye of variable intensity (Figs. 2.3A-C), indicating that uptake of MkMPs and/or transfer of dye (labeled cargo) from MkMPs to cells took place. Further analyses demonstrated that uptake of MkMPs took place through both endocytosis and membrane fusion. We discuss endocytosis first.

In MkMP co-culture, some cells contained variable numbers of distinct CFDA-SE fluorescence dots representing intact MkMPs, several of which were not associated with cell membranes (Figs. 2.3B-C, arrow). This suggested that these MkMPs were inside the cells, and, thus, that MkMP uptake took place through endocytosis. To confirm this, images of single cells from the MkMP co-culture at different confocal planes, 0.4 μm apart, were collected to construct a 3D image of cells interacting with MkMPs.

To identify the MkMP location (inside, out or on the surface of the cell) these images were rotated around an axis through the center of the cell to examine the distance with which the various MkMPs (concentrated green dots) “move” around this axis. Some intact MkMPs rotated around this central axis at a shorter distance than the cell surface (delineated by a dim green signal), thus indicating that these MkMPs were inside the cell rather than on the cell membrane. This can also be identified on the image slices (Figs. 2.3D-E), by focusing on MkMPs that are clearly within the image boundaries (delineated by a dim uniform green signal) of a cell: some of these MkMPs (blue arrow) disappear and others (red arrows) show up as the image slice “moves up”. These data demonstrate that intact MkMPs were internalized by cells through endocytosis, similar to what was reported for PMP internalization by endothelial cells [15].

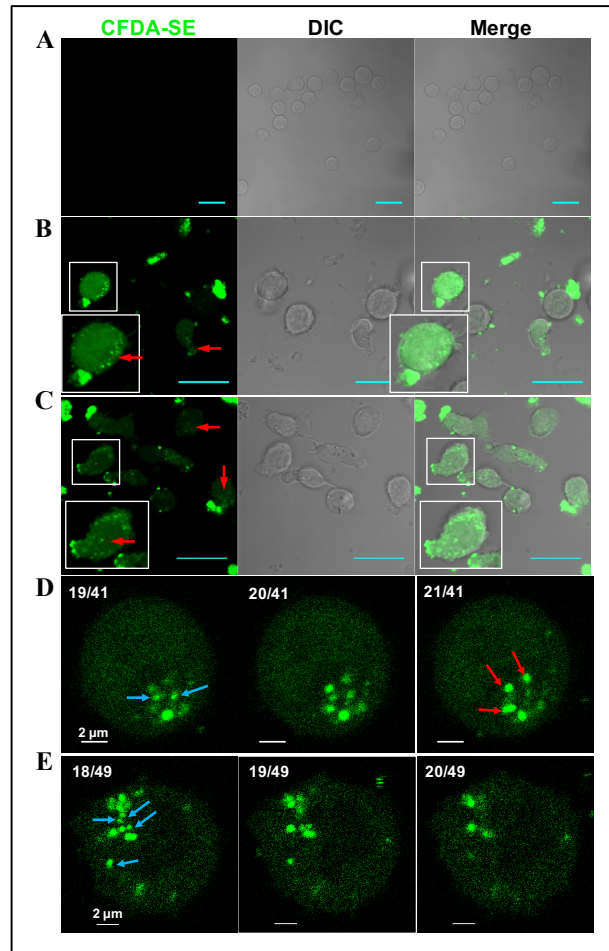


Figure 2.3 MkMPs are quickly endocytosed by HSPCs. MkMPs were stained with CFDA-SE (green) dye and then co-cultured for 3-5 hours with HSPCs from d3 of CD34⁺-cell Mk cultures. Fluorescent and Differential Interference Contrast (DIC) images were collected via confocal microscopy. (A) Vehicle control cultures without fluorescent MkMPs display no background green signal. (B-C) MkMP co-cultures (~ 4 hours) contain cells with intact fluorescence particles (MkMPs, red arrow) inside them, diffuse fluorescence staining, or fluorescent MkMPs on their surface. Inserts amplify images to show more details. Scale bar in panels (A-C) represents 20 μ m. (D-E) Fluorescent images of two cells from the MkMP co-cultures (~4 hours) at different confocal planes with 0.4 μ m apart. The numbers on the top left of each image represent (image slice number)/(total number of slices). As the image slice number increases, intact MkMPs indicated by red arrows appear while the other MkMPs indicated by blue arrow disappear, thus demonstrating that these MkMPs are inside the cell.

2.3.5 Cell Fusion is a Second Mechanism by which MkMPs Deliver Cargo to HSPCs

In addition to observing intact MkMPs inside HSPCs, we also observed gradients of CFDA-SE dye (Figs. 2.4A-B) in some cells emanating from individual MkMPs on cell membranes as indicated by the highly-concentrated dye (Figure 2.4A, red arrows). These CFDA-SE gradients appear to result from direct discharge of the dye-stained MkMP content into the HSPC cytoplasm after they fuse with cells, and not from endocytosed MkMPs. To confirm membrane fusion, cells from MkMP co-cultures were examined using SEM. Examination of a large number of SEM micrographs easily identified several events demonstrating fusion of MkMPs into HSPC membranes (Figs. 2.4C-D). We identified 4 sequential stages through which MkMPs are fused into cells based on the relative volume of MkMPs left on cell membranes (Figure 2.4C). At stage 1, following MkMP/target-cell contact and recognition, MkMPs appear to be just attached to cell surfaces, retaining their shape as an intact particle. At stage 2, less than half of the MkMP body is fused into the cell membrane. This stage is characterized by a visible bridge firmly connecting the MkMP to the HSPC membrane. At stage 3, MkMPs are half fused into cells, and this consistently results in the formation of microvilli-like membrane-ruffle structures emanating from the contact area between the MkMP and the cell (Figure 2.4C, white arrows). These membrane structures appear to be remnants of the process by which MkMPs are fused into HSPCs. At stage 4, MkMPs are almost completely fused into cells, with HSPC membranes appearing almost smooth, with just a few “wrinkles” (remnants of the

fused MkMP) on the cell surface. Note the presence of the typical microvilli on the surface of HSPCs near the location where the MkMPs interact with the HSPCs [117]. As we discuss below, these microvilli may be important in the process of how MkMPs deliver cargo to HSPCs.

We also quantified the percentage of MkMP-cell interaction events at each stage after 3 and 5 hours of co-culture (Figure 2.4D). Most (~63%) fusion events were at the 1st stage and very few at the 3rd (9.7%) and the 4th (2.8%) stages at hour 3. The fusion events at the 1st stage decreased to ~41% while the percentages at the 3rd and 4th stages increased to ~20% and ~12.9%, respectively, after 5 hours (Figure 2.4D), thus indicating that the fusion process takes place continuously in MkMP co-cultures.

TEM analysis was also used to examine interactions between MkMPs and HSPCs. As a basis for unambiguously identifying MkMPs interacting with target HSPCs, we used differences in the texture and internal structures of the particles (see also Figure 2.1D) in TEM images in relation to the texture of cells. In Figure 2.5A, one observes large texture differences between cells and the cell-emanating microvilli [117] and an MkMP (arrow) that has an electron-light texture: this image shows an MkMP interacting with an HSPC microvillus-like structure [117]. In contrast, the particles in Figure 2.5B (arrows) have the same texture as the cell, and are thus viewed as microvilli or microvilli-like membrane extensions and not MkMPs. Figure 2.5C shows an early-stage interaction of an MkMP with a HSPC near the base of a microvillus. Figure 2.5D shows a more advanced interaction (that includes a partial membrane fusion) of an MkMP with a HSPC near the base of a microvillus. In Figure

2.5E, one observes two MkMPs at different stages of fusing into a target cell: the upper, smaller MkMP is apparently only binding to the cell membrane. In contrast, for the lower, larger MkMP, the membrane (white arrow) between the MkMP and the cell body is greatly diminished, suggesting that the MkMP is partially fused into the cell. Figure 2.5F displays an image of a cluster of MkMPs near an HSPC membrane at an early stage of interaction. We should note that TEM analysis of the vehicle control culture did not identify any fusion such events, and extensive literature search displaying TEM and SEM images of HSPCs did not identify such fusion events.

These images are then uniquely associated with the co-cultures of MkMP and HSPCs, complement the fluorescence microscopy images of Figure 2.4A, support the concept that MkMPs can fuse into HSPCs, and provide evidence for the likely importance of an early interaction between cellular microvilli and MkMPs. Although the fusion process by which cells take up MkMPs or other MPs has not been yet dissected, it is known that in generic membrane fusion, lipid rafts regulate exocytosis and are present at the membrane fusion site [118]. It is possible then that lipid rafts may also play a role in MkMP uptake via membrane fusion.

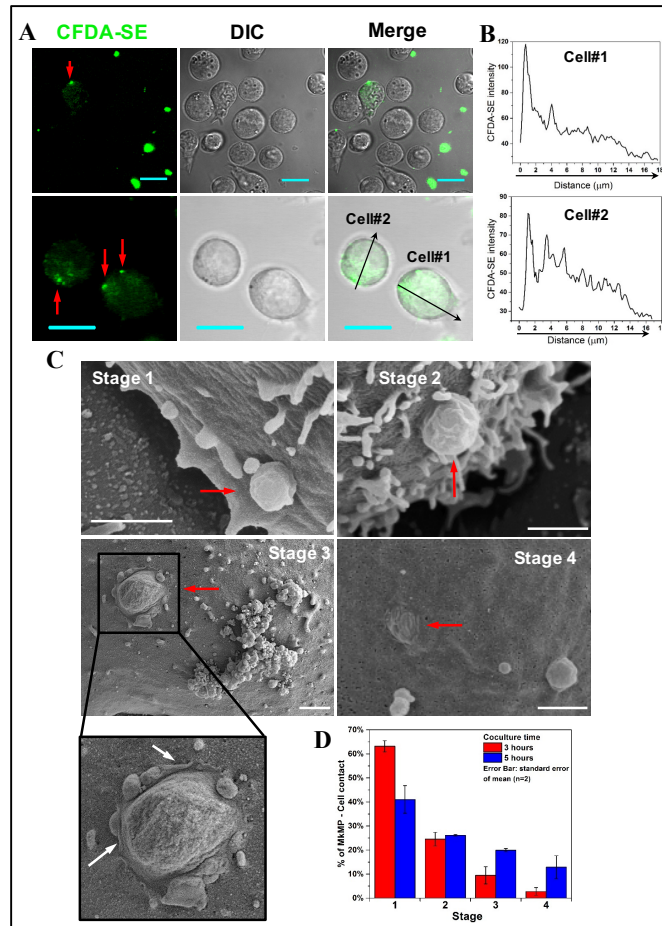


Figure 2.4 MkMPs can fuse into HSPC membranes and release their content into the target HSPCs. (A-B) MkMPs were stained with CFDA-SE (green) dye and then co-cultured with for 3-5 hours with d3 HSPCs from Mk cultures of CD34+ cells. Fluorescent and DIC images were collected via confocal microscopy. (A) Images of cells from the MkMP co-cultures demonstrate CFDA-SE dye gradients inside the cells emanating from one or few fluorescent particles (red arrow) on the cell surface; Scale bar, 20 μm . (B) CFDA-SE dye intensity profiles quantitating the dye gradient along the black arrows of cells #1 and #2 in the lower panel (A). (C-D) HSPCs as above were co-cultured with MkMPs for 3 and 5 hours and examined using SEM. (C) Representative electron micrographs demonstrate four consecutive stages through which MkMPs (red arrow) were fused into HSPC membranes; scale bar, 1 μm . (D) Percentages of MkMP-HSPC interactions at each stage after 3 and 5 hours of co-culture. The data represent the average of two biological replicates \pm standard error of mean.

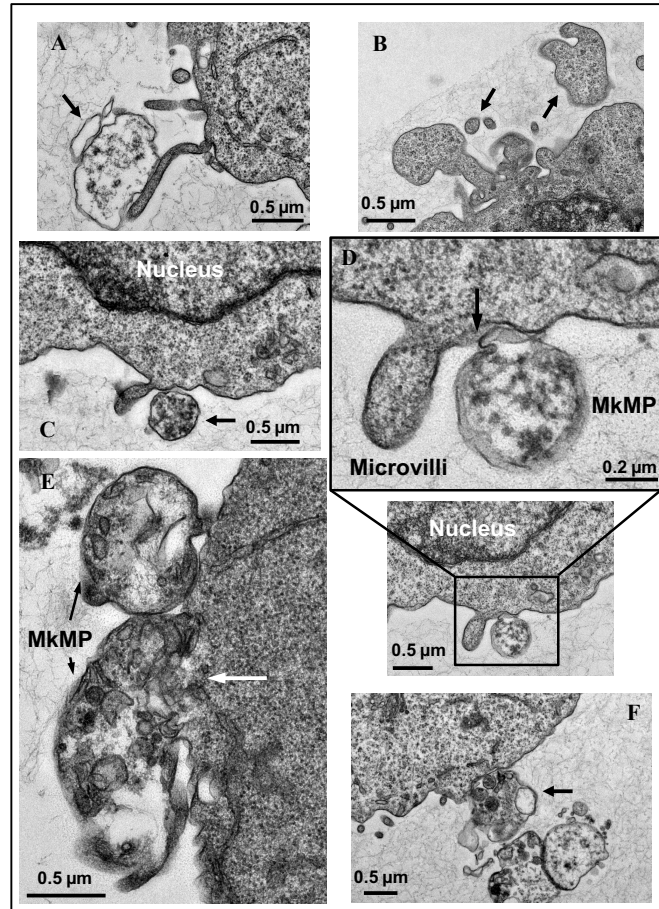


Figure 2.5 TEM details the fusion of MkMPs into HSPC membranes. d3 HSPCs from Mk cultures of CD34+ cells were co-cultured with MkMPs for 3 ~ 5 hours and examined using TEM. (A, C-F) MkMPs with different internal TEM textures bind to an HSPC. (A) An electron-light MkMP (arrow) makes contact with a microvillus emanating from the cell surface. (B) Control for image interpretation: the particles (arrow) have the same TEM texture as the cell and were thus part of the cell and not MkMPs. (C) An MkMP with electron-dense texture makes contact with the cell surface near a microvillus. (D) An MkMP interacting with the cell membrane near a microvillus displays partial membrane fusion (arrow). (E) Two MkMPs interacting with one cell display different degrees of membrane fusion; the top, smaller MkMP shows an early stage of interaction, while the interaction between the larger MkMP and the cell is at an advance stage where the membrane between the cell and the MkMP is barely visible (white arrow). (F) A cluster of MkMPs make contact with a cell via an MkMP containing small organelle-like particles.

2.3.6 Role of Macropinocytosis and Lipid Rafts in MkMP Uptake by HSPC

To investigate the uptake of MkMP by HSPCs, we treated cells with specific inhibitors before being co-cultured with MkMPs. The inhibitors were M β CD, DMA, CH and dynasore, which were used for targeting mechanisms involving lipid rafts, macropinocytosis, clathrin-dependent endocytosis and dynamin-dependent or independent endocytosis. To assess the impact of inhibitors on MkMP uptake, Alexa 647-conjugated cholera toxin subunit B (CT-B), Alexa-594-conjugated dextran 10k (Dx), and Alexa 647-conjugated transferrin (Tf) were used for positive control, since these molecules are established to be taken up by cells through lipid-raft mediated endocytosis, macropinocytosis, and clathrin-dependent endocytosis, respectively [21]. Based on the MFI from flow cytometry analysis, we found that the M β CD treatment significantly decreased MkMP uptake by 42% (Figure 2.6A), while the uptake of CT-B, a positive control for the engagement of lipid rafts, was inhibited by M β CD by 49% (Figure 2.6B). DMA, a Na⁺/H⁺ exchange inhibitor, decreased MkMP and Dx uptake by 31% and 30%, respectively (Figs. 2.6A & C). These results show that these inhibitors inhibited the uptake of known molecules (positive controls) and MkMPs to a similar extent and thus these data suggest that lipid rafts and macropinocytosis play a role in MkMP uptake. Although the treatment with the CH inhibitor significantly inhibited the clathrin-dependent uptake of Tf by 30%, it had only a small effect (16% inhibition) on MkMP uptake (Figure 2.6A, 2.6D). Thus, clathrin-dependent endocytosis is not a major player in the MkMP uptake. We also found that dynasore, a dynamin inhibitor, decreased MkMP uptake by 33% (Figure 2.6A). As detailed in the

discussion, the inhibitory effect of dynasore, combined with the lack of inhibition by CH, can be interpreted to support micropinocytosis as a mechanism of MkMP uptake. In addition to the inhibitors mentioned above, Filipin and Latrunculin B (Lat B) were also used for examine MkMP uptake, which are established-inhibitors for targeting cholesterol and inhibiting actin polymerization, respectively. Filipin showed no inhibitory effect on either MkMP or CT-B uptake (data no shown), indicating that Filipin is not an appropriate inhibitor to target cholesterol in this system. Lat B also showed no effect on MkMP uptake (data no shown), thus suggesting that actin might not be involved in early steps at least of the MkMP uptake.

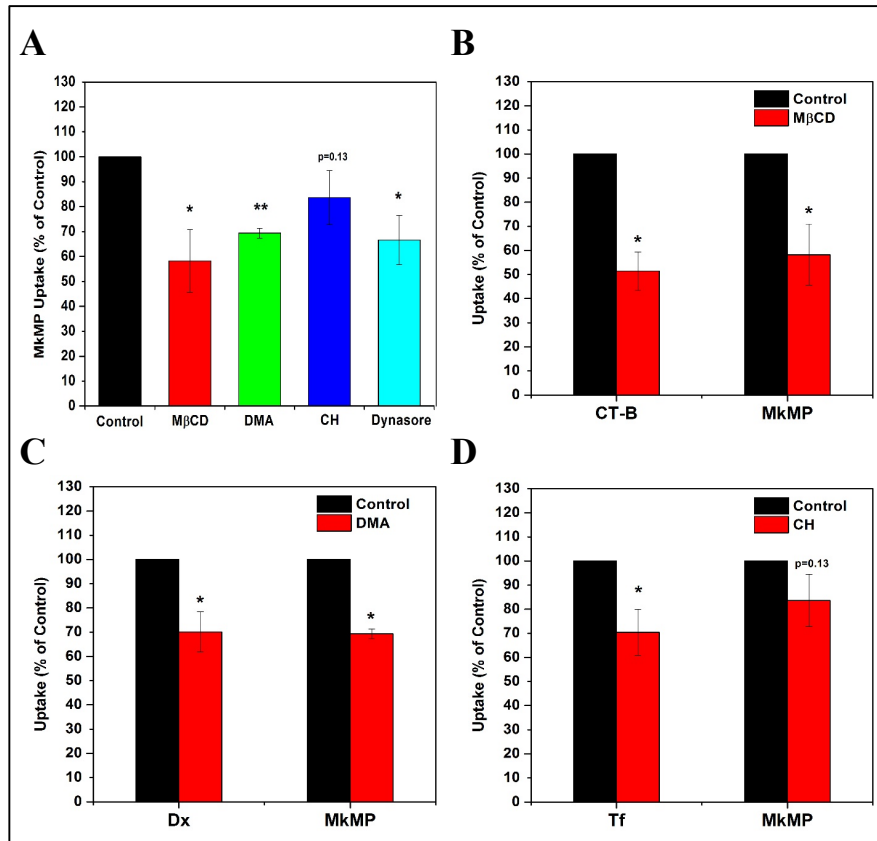


Figure 2.6 Macropinocytosis, lipid-raft and dynamin are engaged in uptake of MkMP by HSPCs. HSPCs were pre-incubated with specific inhibitors impacting MkMP uptake by HSPCs. The inhibitors used were methyl- β -cyclodextrin (M β CD), dimethylamiloride (DMA), chlorpromazine (CH), and dynasore, which target lipid raft, macropinocytosis, clathrin-dependent endocytosis and dynamin-dependent or independent endocytosis, respectively. To assess the impact of the inhibitors on MkMP uptake, we compared the outcomes from the inhibitor studies against the uptake of the following molecules (positive controls), cholera toxin subunit B (CT-B), dextran 10k (Dx), and transferrin (Tf), which are established to be taken up by lipid-raft mediated endocytosis, macropinocytosis, and clathrin-dependent endocytosis, respectively. Specifically, d3-HSPCs were pre-incubated with or without 5 mM M β CD, 10 μ M DMA, 20 μ M CH, or 80 μ M dynasore for 45 min at 37 °C, before the co-culture with (A-D) CFDA-SE-stained MkMP for 30 min, (B) CT-B, (C) Dx, or (D) Tf for 15 min at 37 °C. Uptake of MkMP, CT-B, Dx, or Tf were analyzed by flow cytometry. Data represent averages of 3 biological replicates \pm standard error of mean. *, $P < 0.05$; **, $P < 0.01$; ***, $P < 0.001$

2.3.7 PMPs Interact with and Induce Aggregation of HSPCs, but cannot Apparently Deliver Cargo to HSPCs; Thrombin-mediated Platelet-like Activation may Account for the Different Effects of MkMPs vs PMPs

Since PMPs originate from activated platelets, and platelets derive from mature Mks, PMPs are ontologically similar to MkMPs. Both PMPs and MkMPs are CD41⁺CD42b⁺ but, unlike PMPs, MkMPs are CD62P⁻ and LAMP-1⁻ [41]. PMPs promote survival, proliferation, adhesion, chemotaxis and in vivo engraftment efficiency of HSPCs [12, 94]. In our previous study [74], we reported that PMPs were unable to promote Mk differentiation of HSPCs. Here, we examined if PMPs interact with HSPCs like MkMPs do, and what might explain the aforementioned differences of the two types of MPs. PMPs were stained with CFDA-SE dye and then co-cultured with d3 HSPCs. We did not observe uptake of PMPs by HSPCs even after 24 hours of co-culture (Figure 2.7A), thus suggesting that PMPs cannot deliver, macroscopically at least, cargo to HSPCs. However, PMPs could bind to and induce aggregation of HSPCs (Figure 2.7A); MkMPs did not induce HSPC aggregation. These data suggest that although both MkMPs and PMPs can recognize HSPCs, small differences, possibly related to platelet activation which gives rise to PMPs, are responsible for these profound differences. To test this hypothesis, we used thrombin treatment aiming to achieve a platelet-like activation of Mks prior to MkMP generation and also of MkMPs. Like PMPs, most (97.3%) of MkMPs from thrombin-activated Mks were CD62P⁺ while directly thrombin treatment on MkMPs only slightly increased the percentage of CD62P⁺ MkMPs from 20.3% to 24% (Figure 2.7B). These findings

were confirmed by Western analysis (Figure 2.7C) of the characteristic activation-induced cleavage of filamin A [41, 119, 120].

Consistent with the CD62P and Western data, co-culture of MkMPs from thrombin-treated Mks with CD34⁺ cells did not generate any Mks and thrombin treatment of MkMPs reduced the numbers of Mks at all ploidy classes in the co-culture by 41% compared to co-culture with untreated MkMPs (Figure 2.7B). These results suggest that the inability of PMPs to target and induce Mk differentiation of HSPCs is caused by the changes, including changes in protein expression, brought about by thrombin activation.

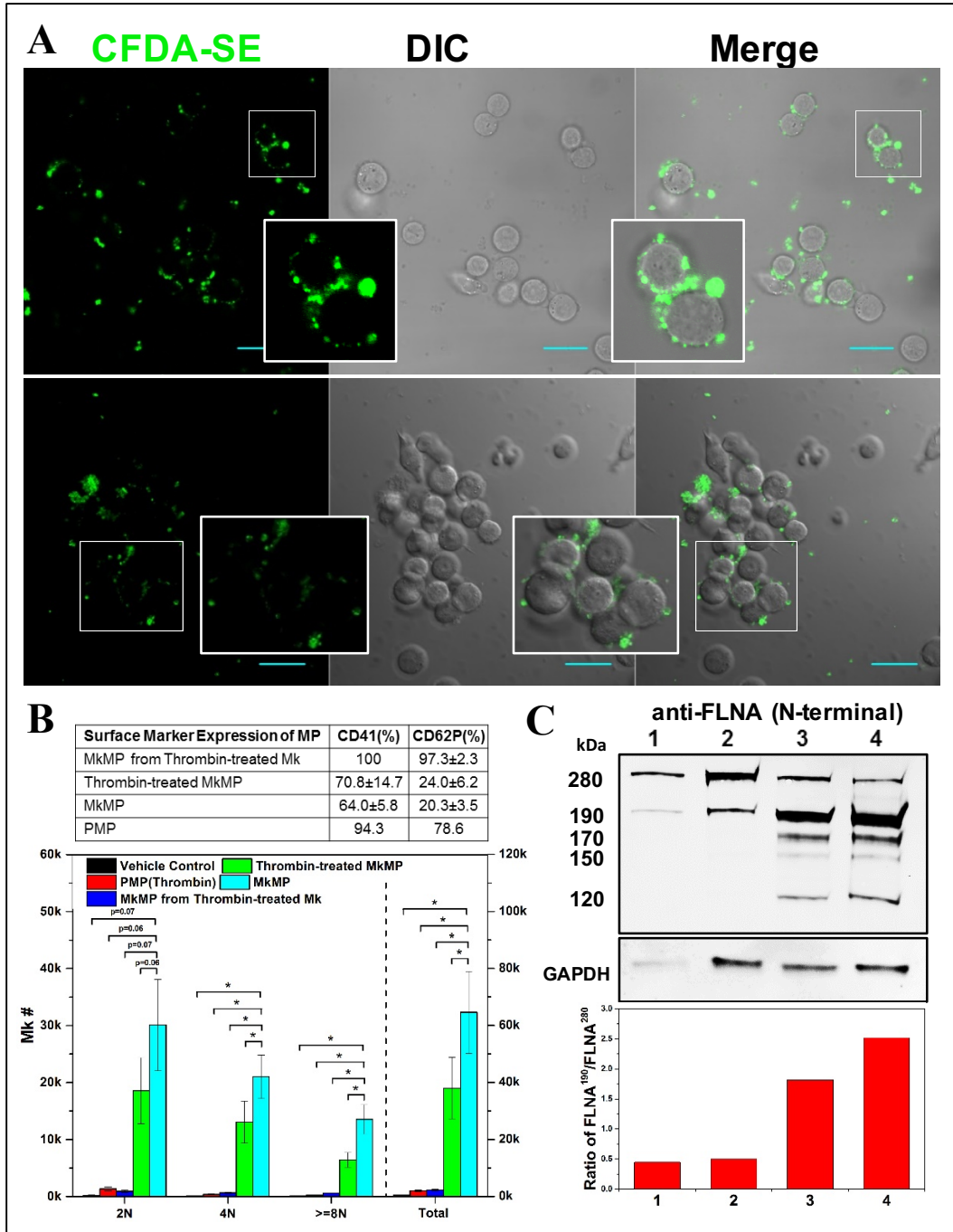


Figure 2.7 PMPs are not taken up by HSPCs and a thrombin-mediated platelet-like activation may account for the different effects of MkMPs vs PMPs. (A) PMPs were stained with CFDA-SE (green) dye and co-cultured with d3 HSPCs for 3-5 hours. Fluorescent and DIC images were collected using confocal microscopy. PMPs were not taken up by HSPCs, but induced HSPC aggregation. There was no aggregation observed in the control cultures of HSPCs without PMPs (data not shown). Inserts amplify images to show more details. Scale bar, 20 μ m. (B) Thrombin treatment activates Mk cells giving rise to MkMPs incapable of inducing Mk differentiation HSPCs, but direct MkMPs activation by thrombin is ineffective and attenuates but does not abolish the impact of MkMPs. Table displays CD41 and CD62P expression levels of various MP types to assess the impact of thrombin activation. The effect of thrombin treatment on the biological effects of MkMPs and PMPs was assessed by co-culture with CD34+ cells (10 MPs/cell) for 7 days. Ploidy distribution of Mks at d7 was analyzed by flow cytometry. Error bars: standard error of mean (n=3); * $P < 0.05$. (C) Assessment of thrombin activation via Western-blot examination of filamin A (FLNA) truncation as demonstrated by the relative amount of truncated filamin A (190 kDa; full size is 280 kDa) in MkMPs (lane 1), thrombin-treated MkMPs (lane 2), MkMPs from thrombin-treated Mks (lane 3), and PMPs (lane 4). GAPDH expression was used as loading control. The low panel displays the ratio of FLNA¹⁹⁰/FLNA²⁸⁰ estimated by quantitation of normalized band intensity of displayed Western blot and this ratio represents the level of filamin A cleavage. The majority of filamin A in MkMPs and thrombin-treated MkMPs was full-length, while most filamin A was cleaved in MkMPs from thrombin-treated Mks and PMPs. The 190 kDa N-terminal fragment of filamin A results from calpain-dependent cleavage, while the 170, 150, 120 kDa N-terminal fragments are products of caspase-3-dependent cleavage.

2.3.8 HSPC Uropods are the Preferred Area of Interaction with MkMPs, with the Uropod-enriched CD54 (ICAM-1), CD43, CD11b, and CD18 Mediating Binding and/or Uptake of MkMPs

We next investigated what surface molecules might mediate binding to and/or uptake of MkMPs by HSPCs. We first examined the characteristic surface molecules of MkMPs, including CD41, CD42b and phosphatidylserine (PS). MkMPs were stained

with CFDA-SE dye and CD41, CD42b or PS on MkMPs were blocked by either antibodies or Annexin V before the co-culture with HSPCs. Blocking did not change the CFDA-SE MFI of HSPCs (data not shown), suggesting that CD41, CD42b or PS are not involved in binding and/or uptake of MkMPs.

Examining images of cells interacting with MkMPs, we found several polarized HSPCs (e.g., three cells on the top row of Figure 2.4A), forming uropod structures at their rear edge [121], and that MkMPs preferentially bound to uropods compared to the leading side of polarized HSPCs. To investigate this observation, we identified HSPC uropods using the surface marker CD133, which is concentrated on uropods of polarized HSPCs [121]. More than 67% of CD133⁺ cells (30% of total cells) had localized CD133 expression, including all polarized HSPCs with uropods, and significantly, MkMPs only bound to the plasma membrane regions of cells, which had localized CD133 expression (Figure 2.8A). The cytoplasm near membrane regions with concentrated CD133 contained some intact MkMPs (apparently from endocytosis) and had higher overall green signal (Figure 2.8A; red arrow). These observations suggest that proteins localized on HSPC uropods may mediate MkMP binding and uptake. To investigate this hypothesis, we used antibodies to block surface proteins enriched on HSPC uropod membranes: CD43 (leukosialin), CD44 (HCAM), CD50 (ICAM-3), CD54 (ICAM-1) and CD133 [121]. CD43, a transmembrane sialoglycoprotein expressed exclusively on hematopoietic cells [122] and a potential CD54 ligand, interacts with cytoskeletal proteins and is involved in signaling regulating cell activation, proliferation and survival [123]. CD44, CD50 and

CD54 are glycoproteins with roles in cell-to-cell adhesion [124]. Blocking with either anti-CD44, anti-CD50 or anti-CD133 antibodies did not affect MkMP binding and/or uptake (data not shown). However, CD54 blocking significantly reduced CFDA-SE MFI of cells by >40% (Figure 2.8B). Potential receptors for CD54 on the MkMPs are the leukocyte function-associated antigen 1 (LFA-1, CD11a/CD18), CD43 and macrophage-1 antigen (Mac-1, CD11b/CD18). The former two are expressed on Mks and platelets [125, 126], while Mac-1 is expressed at low level on Mks [127]. Mks and platelets also express CD54 [125], thus suggesting that binding of MkMPs to HSPCs could be also mediated by CD54 on MkMPs and its receptors LFA-1, Mac-1 and CD43 on CD34+ cells [128]. To further test this hypothesis, cells from d1 or d3 CD34+ cell culture were blocked with anti-CD11a, anti-CD11b, and anti-CD18. Blocking of CD18 and CD11b significantly decreased MkMP uptake (Figure 2.8B), while blocking of CD11a showed no effect (data not shown). This suggests Mac-1 and CD54 might be the pair mediating the interaction between MkMP and HSCs/HSPCs. In contrast, CD43 blocking increased, instead of decreasing, CFDA-SE MFI of d3 HSPCs (Figure 2.8C). Moreover, we found that HSPCs aggregate when treated with anti-CD43 antibody and this was confirmed by confocal microscopy (Figure A3 in Appendix A). This and other anti-CD43 antibodies have been shown to activate CD43 [129-133]. Thus, a possible reason for the observed increased binding of MkMPs to HSPCs and HSPC aggregation is that the anti-CD43 antibody activates instead of blocking CD43. This would suggest that CD43 plays also a role in the interaction between MkMPs and HSPCs. We also blocked CD34 (hematopoietic progenitor cell

antigen), since it is the most common marker for HSC/HSPC. However, there was no significant impact of anti-CD34 antibody on MkMP uptake (Figure 2.8B)

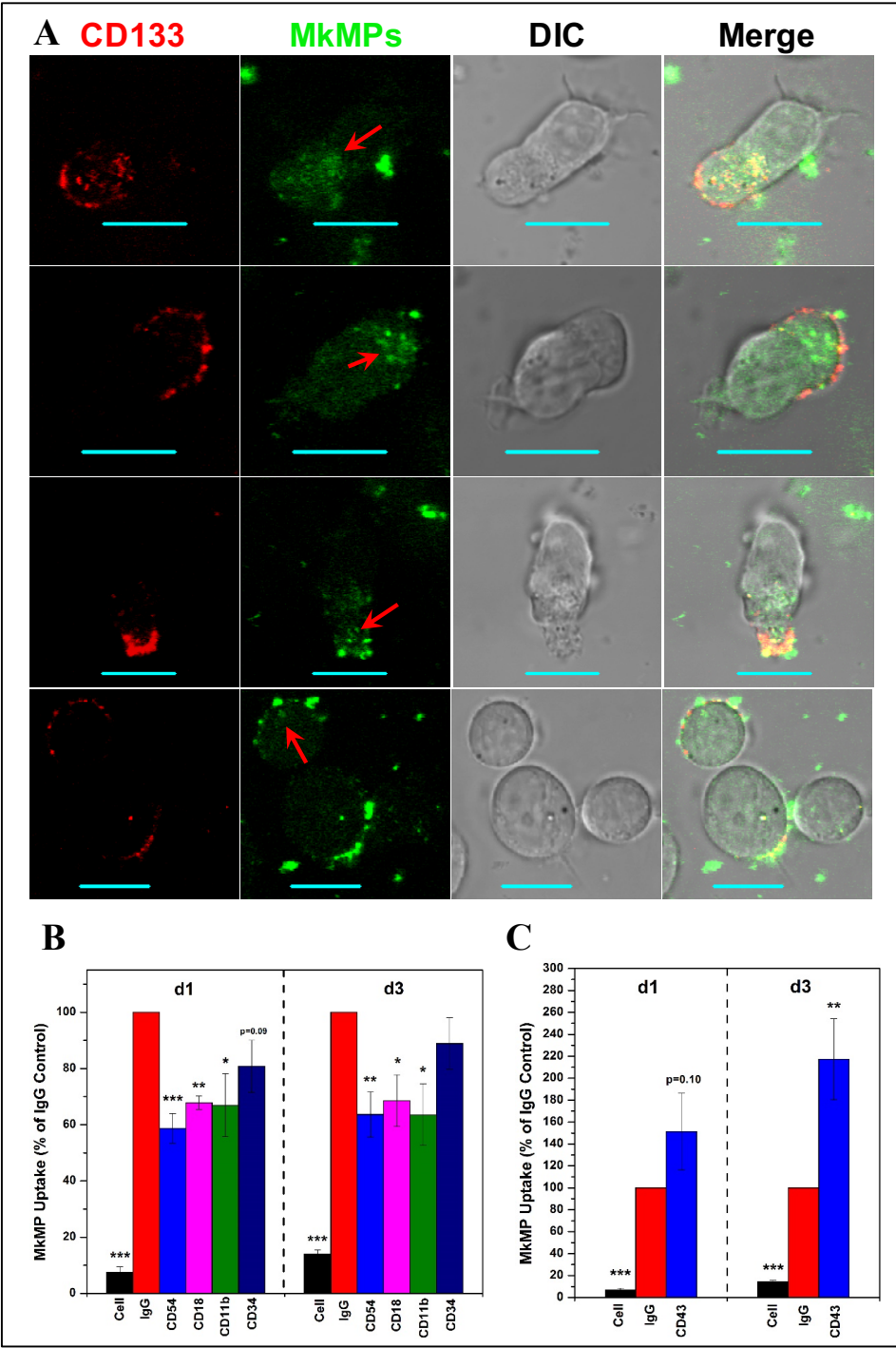


Figure 2.8 CD54 (ICAM-1), CD18/CD11b (Mac-1) and CD43 mediate the uptake of MkMPs, with the HSPC uropods being the preferred interaction area. (A) MkMPs were stained with CFDA-SE (green) dye and then co-cultured with HSPCs for 3 hours. Anti-CD133 antibody (red) was added to the co-culture before microscopic examination to identify the uropod area. Fluorescent and DIC images were collected using confocal microscopy. Internalized MkMPs in uropods are indicated by red arrows. The scale bar represents 10 μm . (B-C) d1 HSPCs and d3 HSPCs were blocked with 10 $\mu\text{g}/\text{mL}$ anti-CD54, anti-CD18, anti-CD11b, anti-CD34 antibodies or isotype IgG for 30 min before co-cultured with MkMPs stained with CFDA-SE. After 1 hour, cells were harvested for analysis of CFDA-SE MFI by flow cytometry. “Cell” represents samples without fluorescent MkMPs. The data in panels (B-C) represent averages of 3 to 6 biological replicates \pm standard error of mean. *, $P < 0.05$; **, $P < 0.01$; ***, $P < 0.001$

2.3.9 RNA Transfer Mediates the Impact of MkMPs on HSPCs

Using treatment with RNases, it has been reported that several MPs exert their biological function through RNA transfer [31, 134, 135]. Here, we used two RNases, RNase A/T1 and RNase ONETM, to examine the effect of RNase treatment of the RNA content of MkMPs and the ability of RNase treated MkMPs to induce Mk differentiation of HSPCs. First, we examined the impact of RNase treatment on the RNA content of MkMPs (Figure 2.9). As shown in Figure 2.9A, the RNA profiles of two biological replicate experiments before and after RNase treatment are remarkably reproducible. The RNA profiles of MkMPs (Figure 2.9A), when compared to the RNA profile of Mks (Figure 2.9B), show an enrichment in small RNAs and a low concentration of rRNAs; the RNA ladder of Figure 2.9C enables the identification of rRNAs and the identification of the range of small RNAs, such as RNAs <200 nts. RNase treatment degrades RNAs of all sizes, but apparently more so of small RNAs,

the range that would include miRNAs. RNase treatment degrades 65.5% of all RNA in MkMPs (Figure 2.9D). These data suggest that RNases can enter these MkMPs to degrade their RNA content. While it is firmly established that RNase A, RNase 1 and likely most RNases are actively endocytosed by mammalian cells (so much so that RNase A has been termed a “cell-penetrating protein” [136, 137]), the mechanism by which RNases enter MPs like these MkMPs remains unexplored.

Next we examined the impact of MkMP RNase treatment on their ability to program HSPCs into megakaryopoiesis. Our data show that the number of 2N, 4N and $\geq 8N$ Mks and of total Mks decreased by $\sim 50\%$ (Figure 2.10), suggesting that RNase treatment attenuates but does not abolish the effect of MkMPs. This could be due to incomplete digestion of MkMP RNA by RNases, especially of RNase-resistant miRNAs, which have been proposed as important effector molecules in other MPs [138-140]. It is also possible that some proteins carried by MkMPs are involved in inducing Mk differentiation, as in the case of ESC MPs and tumor MPs whose biological functions are dependent on both protein and RNA transfer [134, 135].

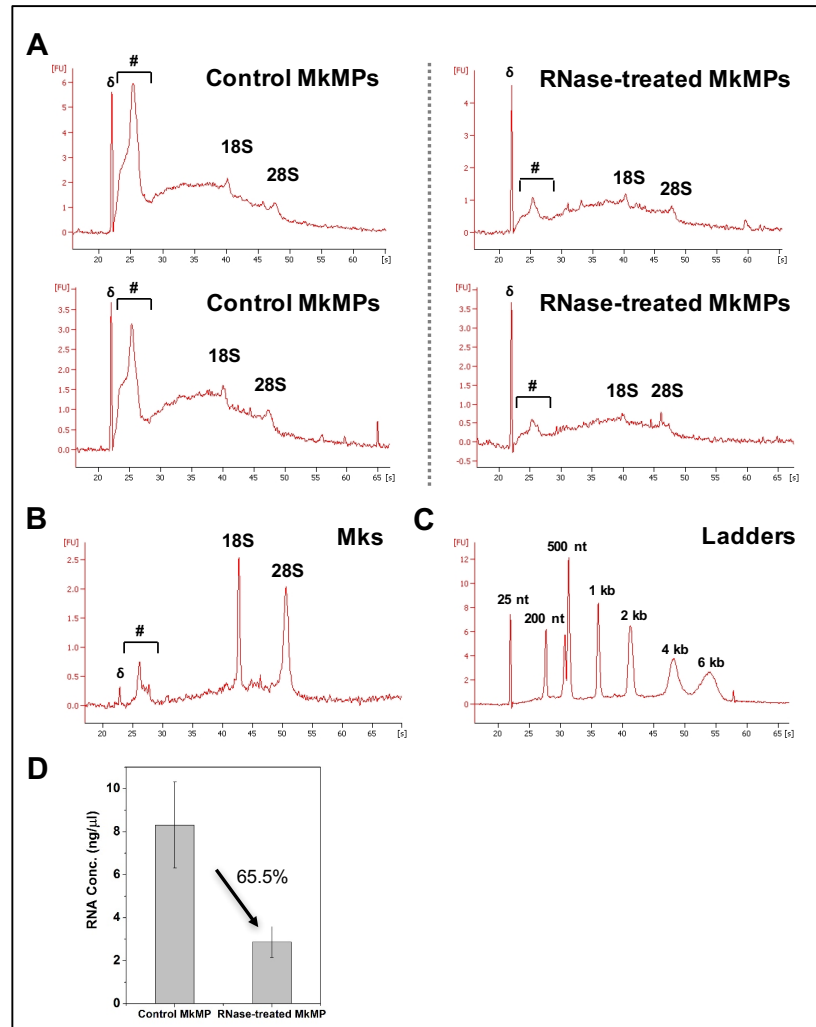


Figure 2.9 RNA profile of Mk and MkMP with or without RNase treatment. (A) MkMPs were first treated with or without RNase I for 2 hours at 37 °C. After incubated with RNase inhibitors and washed with IMDM thrice, total RNA was isolated from MkMPs and RNA profiles were analyzed by Bioanalyzer 2100. (B) RNA profile of d12 Mks. (A) presents the data from two biological replicates to demonstrate the exquisite reproducibility of the RNA profiles before and after RNase treatment. The symbol (#) in (A) and (B) marks the range of small RNAs. 18S and 28S represent rRNA, while (δ) in (A) and (B) marks the ladder of 25 nt. (C) RNA profile of ladders for size verification. (D) Total RNA concentration from MkMPs treated with or without were measured by Qubit RNA HS kit. The measurement shows 65.5% of RNA being digested after RNA treatment. The data represent two biological replicates ± standard deviation.

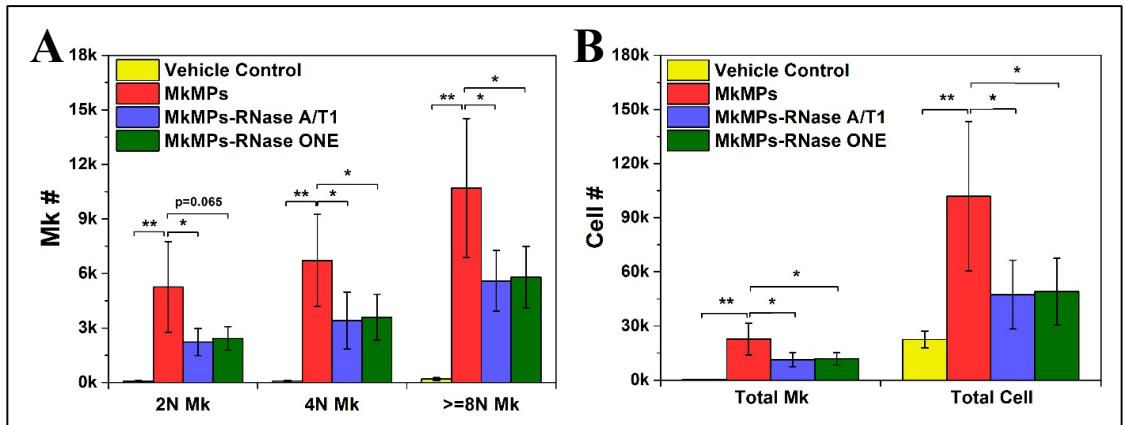


Figure 2.10 RNase treatment reduces the biological effect of MkMPs on HSPCs. Human CD34⁺ cells were co-cultured with MkMPs (10 MkMPs/cell) treated with RNase (Ambion® RNase A/T1 cocktail or RNase ONE™) for 8 days before harvested for ploidy analysis by flow cytometry. (A) Numbers of Mk cells with different ploidy classes (2N, 4N, >=8N). (B) Numbers of total Mks and total cells. The data are represented as the averages of four biological replicates ± standard error of mean. *, $P < 0.05$; **, $P < 0.01$.

2.4 Discussion

2.4.1 MkMPs Target and Induce the Megakaryocytic Differentiation of Primitive Lin-CD34⁺ and all HSPCs but not so of MSCs, HUVECs or Granulocytes

We demonstrated that MkMPs generated by mature Mks induces Mk differentiation of Lin-CD34⁺ primitive HSPCs. Combined with our previous report [74], these data show that MkMPs target all types of HSPCs. Targeting appears to be specific, as MkMPs could not transdifferentiate MSCs, HUVECs and granulocytes, three types of cells that are ontologically and physiologically related to HSPCs, and which are in contact with MkMPs in vivo. This could be either because these cells are not capable

of taking up MkMPs or and the signaling molecules in MkMPs could not transdifferentiate these cells. It will be interesting to examine if MkMPs could induce embryonic stem cells (ESCs) or induced pluripotent stem cells (iPSCs) into Mk differentiation given that both ESCs and iPSCs are capable of giving rise to all types of cells. It was also interesting that MkMPs appeared to promote better maintenance and expansion of the CD34⁺-cell compartment compared to control. These findings make a good argument for examining if ex-vivo generated MkMPs, the most abundance MPs in circulation, can be used in transfusion medicine to support enhanced thrombopoiesis and also if they can be used as a vehicle to deliver nucleic acids, proteins and organic molecules to HSPCs.

2.4.2 MkMPs are Taken up by HSPCs via Endocytosis and Cell fusion, whereby Macropinocytosis and Lipid Rafts Play an Important Role

Three mechanisms have been suggested in the literature to explain how MPs and target cells interact: receptor-mediated binding, endocytosis, and membrane fusion [2, 99, 100]. The interaction always starts from MP binding to cells, which is apparently a receptor mediated process [11], and may largely account for the MP target specificity [141]. MP binding could be unstable, leading to dissociation of MPs from cell surface, or stable, ending in uptake of MPs by the cells [2], and signaling from temporary or persistent binding could be sufficient for altering cell fate [11, 12, 94-98, 142].

Through confocal microscopy, SEM and TEM analyses, we demonstrated that both direct fusion and endocytosis are involved in the uptake of MkMPs by HSPCs. Our

SEM and TEM analyses provide the first direct observation of the membrane fusion process (as it proceeds in distinct stages), which engages microvillar-like membrane structures of the target cell (Figure 2.4C, stage 3) during the fusion process. While previous studies have provided indirect evidence for a membrane fusion process, this is the first report of direct, detailed microscopic evidence of the process.

In the studies to interrogate specific mechanisms involved in MkMP uptake by HSPCs, the level of the inhibitory effect of M β CD and DMA on MkMP uptake was similar to that of the corresponding molecules that serve as positive controls for the specific mechanisms (Figs. 2.6B & C). This strengthens the conclusion that implicates macropinocytosis and the involvement of lipid rafts (through either lipid-raft dependent endocytosis or through the role of lipid rafts in the membrane-fusion process) in the uptake of MkMPs by HSPC. We also found that MkMP uptake was inhibited by dynasore. Dynasore inhibits dynamin, a GTPase that plays an important role in the formation of clathrin-dependent vesicles via fission [143]. Dynasore also reduces cholesterol in plasma membrane to disrupt lipid-raft formation and membrane ruffling, which is a dynamin-independent mechanism [144]. Our data from the effect of CH suggest that MkMP uptake is not related to clathrin-dependent endocytosis. This then leads to the hypothesis of the dynamin-independent inhibitory effects on MkMP uptake by dynasore [144]. Preta G et al demonstrated that dynasore can target processes dependent on the use of lipid rafts [144], while Park et al. showed that dynasore can inhibit membrane ruffling, which is the essential process of

macropinocytosis [145]. Taken together, these data support our hypothesis that MkMP uptake is associated with macropinocytosis and lipid raft-mediated endocytosis.

2.4.3 MkMP RNA is in Part at least Responsible for their Biological Effects

We showed here that the ontologically similar PMPs cannot deliver cargo to or induce Mk differentiation of HSPCs, despite the fact that they express a similar set of receptors. This would argue against the possibility that the impact of MkMPs is purely receptor mediated. Furthermore, after we treated MkMPs with two different RNases to digest about 65% of the RNA carried by MkMPs, the numbers of Mks with different ploidy levels decreased by half in the co-culture with treated MkMPs compared to MkMPs without treatment. This demonstrates that horizontal transfer of RNA is in part at least responsible for the observed biological effect of MkMPs. Transfer of RNA requires uptake of MkMPs by cells following stable binding and thus the RNase treatment results provide additional evidence that MkMPs are taken up by cells.

Sequencing of the MkMP, Mk-cell, platelet and PMP RNomes shows distinct differences, and notably the enrichment of the MkMP RNA in small non-coding RNAs (miRNA, piRNAs, and long-non-coding RNAs (lncRNAs)) (data not shown), but the information cannot yet be interpreted to explain the impact of MkMPs on HSPCs. Some of these differences are also shown in the data of Figure 2.9, where the remarkably reproducible RNA profile is very distinct from the RNA profile of the parent Mk cells. While it is possible that molecules other than RNAs are responsible for the observed effects, the observed 50% reduction in the biological effect of

MkMPs by the RNase treatment could be due to the inability to completely digest the MkMP RNA (as shown in Figure 2.9), thus leaving as a distinct possibility that the impact of MkMP on HSPCs is solely RNA mediated.

2.4.4 A Role for HSPC Uropods, CD54 and CD43, and why PMPs cannot Act on HSPCs Like MkMPs Do

We have shown that MkMPs interact with HSPCs largely through their uropods, which are enriched in CD54 and CD43 surface proteins. We showed that blocking CD54, CD11b, and CD18 reduces uptake of MkMPs to HSPCs by ca. 30-40%, and also that the use of an antibody that stimulates CD43 expression promotes MkMP uptake. Since CD54 is a ligand of Mac-1 (CD11b/CD18), this would suggest an important role of pairing MkMP with HSPCs. Although blocking CD43 increased MkMP uptake, since CD54 is also a ligand for CD43 on HSPCs, this still suggests a role for CD43 in mediating the interaction between MkMP with HSPCs. Our data involving thrombin induced platelet-like activation of Mks prior to MkMP generation, which abolishes their biological effect on HSPCs, suggest that the inability of PMPs to target and induce Mk differentiation of HSPCs is caused by the thrombin activation.

Acknowledgements

I would like to acknowledge and thank Dr. Jinlin Jiang for his expertise and assistance to this project. I would also like to acknowledge and thank Dr. Jeffrey Caplan and members of Bioimaging Center (University of Delaware; UD) for assistance with

immunofluorescence and electron microscopy, and Dr. Dongjun Li (UD) and Blood Bank of Delmarva for assistance with platelet collection.

Chapter 3

ENGINEERING HUMAN MEGAKARYOCYTIC MICROPARTICLES FOR TARGETED DELIVERY OF NUCLEIC ACIDS TO HEMATOPOIETIC STEM & PROGENITOR CELLS

3.1 Background

Cell-derived microparticles (MPs) are 0.1 to 1 μm extracellular vesicles (EVs) generated by most if not all mammalian cells [1-3]. MPs bud off from cellular plasma membranes under normal physiological or pathophysiological conditions [89]. MPs and the smaller nano-size EVs, exosomes ($<0.1 \mu\text{m}$ and of different ontogeny), play an important role in cell-to-cell communication and transferring of materials such as RNA, proteins or lipids to target cells [2, 146]. EVs possess promising characteristics for RNA, DNA and protein and other cargo delivery, including: their natural capacity to transfer cargo to target cells [2]; simple and natural generation from all mammalian cells [2, 146]; stable biological activity under $-80 \text{ }^\circ\text{C}$ long-term storage [147], and, if EVs are from autologous or compatible cells, low immunogenicity and toxicity [148]. Recent studies have demonstrated mRNA [46], miRNA [44], siRNA [53]) and drug [47, 149] delivery using naturally-generated or engineered EVs.

Two main approaches for loading EVs with synthetic cargo have been investigated. Earlier studies utilized *endogenous loading*, whereby EV-producing cells were transfected with plasmid DNA or RNA to overexpress specific genes, assuming

that this will lead to encapsulation of nucleic acid in the EVs during their biogenesis [45]. More recent investigations have focused on *exogenous cargo loading*. Organic-molecule drugs can be loaded into EVs by simple incubation [149]. Several studies used electroporation to load RNAs or drugs to EVs [47, 49-51, 53]. Most studies employed cancer cell line-derived exosomes, not MPs, and very few examined DNA delivery [51, 55]. Linear dsDNA (750 bp) via HEK293T-derived 85-nm exosomes was delivered to the same cell type, but loading linear dsDNA larger than 1000 bp to these exosomes was inefficient, while loading plasmid DNA practically impossible due to the small size of exosomes [51]. Kanada *et al* examined cargo delivery, both *in vitro* and *in vivo*, by HEK293FT-derived exosomes and MPs to show that functional protein expression was only possible from MP-mediated pDNA delivery [55].

Efficient methods to deliver cargo to hematopoietic stem and progenitor cells (HSPCs) is important for fundamental studies of hematopoietic disorders and malignancies, but also for therapeutic applications. Current approaches, including viral and non-viral methods, for cargo (DNA, RNA, or protein) delivery to HSPCs have significant limitations [150-152]. Although viral gene transfer exhibits high transduction efficiency, risks such as random chromosome integration remain important challenges. Non-viral approaches are safer. Although lipofection has been used for gene transfer to various cell types *in vitro*, siRNA delivery to HSPCs is inefficient [153]. Electroporation/nucleofection is efficient for delivering cargo *in vitro* [154], but is associated with low cell viability due to thermal damage from inhomogeneous electric field distribution and high current density [153-155].

Synthetic nanoparticles (NPs) (eg, based on poly(lactic-co-glycolic acid) (PLGA)) were also examined for DNA or RNA delivery *in vitro*, but with low efficiency on gene modification and gene silencing [153, 156]. Better efficiency was achieved using triplex-forming peptide nucleic acid (PNA) technology [30, 156]. Although 99% uptake of PLGA-NPs was demonstrated based on dye fluorescence, the frequency of site-specific gene modification was less than 1% *in vitro* and even lower *in vivo*.

To overcome some of the challenges of both *in vitro* and *in vivo* cargo-delivery to HSPCs, here, we demonstrate plasmid DNA, siRNA and miRNA delivery to HSPCs using megakaryocyte-derived MPs (MkMPs). Megakaryocytes (Mks) are large polyploidy cells derived from HSPCs upon thrombopoietin (Tpo) stimulation, which upon maturation and fragmentation give rise to circulating platelets (PLTs) as well as to MkMPs, which are the most abundant MPs in circulation [41]. We have previously shown that, *in vitro*, Mks also shed MkMPs [74]. We have also demonstrated that, *in vitro*, MkMPs specifically target and are taken up by human HSPCs through fusion and/or endocytosis following specific receptor recognition [23]. MkMPs transfer cargo to HSPCs and induce potent Mk differentiation of HSPCs in the absence of Tpo, whereby RNA has been identified as a key cargo being transferred and mediating the megakaryocytic differentiation process [23]. We have also shown that human MkMPs can target murine HSPCs *in vivo* to induce *de novo* PLT biogenesis in a simple murine model [157], thus demonstrating *in vivo* target specificity and efficacy even when using a cross-species model. These findings suggest that huMkMPs may be a suitable vector system for gene and other cargo delivery to human HSPCs.

3.2 Materials and Methods

3.2.1 Experimental Design

Based on our previous studies on the role and characterization of megakaryocytic MPs, and their ability to specifically target and deliver their cargo to HSPCs [23, 74], the aim of this study was to develop a system to deliver plasmid DNA and small RNAs to HSPCs using human MkMPs. We examined functional delivery of plasmid DNA using labeled pDNA and GFP protein expression. We also evaluated the delivery of two types of small RNA, siRNA and miRNA, using functional assays. All experiments were carried out with at least three biological and multiple technical replicates for statistical significance.

3.2.2 Chemicals and Reagents

Recombinant human interleukin 3 (IL-3), IL-6, IL-9, IL-11, stem cell factor (SCF), and thrombopoietin (Tpo) were purchased from PeproTech Inc. BIT 9500 was purchased from Stemcell Tech. Anti-CD61 magnetic microbeads and MACS cell-separation tools were purchased from Miltenyi. Fluorescein isothiocyanate (FITC)-conjugated anti-CD41, allophycocyanin (APC)-conjugated anti-CD34, and IgG antibodies were purchased from BD bioscience. Anti-GFP (ab290) and corresponding isotype control (ab171870) antibodies were from Abcam. siR-MYB, siR-negative control, miR-486-5p mimics, miR-negative control, CellTracker™ CM-DiI Dye and SlowFade™ Diamond Antifade Mountant with DAPI were purchased from Thermo

Scientific. Alexa 647-conjugated AllStars Negative Control siRNA and the miRNeasy micro kit were purchased from Qiagen. All other chemicals were purchased from Sigma Aldrich.

3.2.3 Cultures of HSPCs and CHRF cells.

Frozen G-CSF-mobilized human peripheral blood CD34⁺ cells were obtained from Fred Hutchinson Cancer Research Center. Megakaryocytic cultures were set up as described [103]. Briefly, CD34 cells were cultured in Iscove modified Dulbecco medium (IMDM, Gibco) supplemented with 20% BIT 9500 (Stemcell Tech.), 100 ng/mL TPO, 100 ng/mL stem cell factor (SCF), 2.5 ng/mL interleukin-3 (IL-3), 10 ng/mL IL-6, 10 ng/mL IL-11 and human LDL under 5% O₂ for 5 days. From day 5 to 7, IL-3 was increased to 10 ng/mL and IL-6 was substituted with 10 ng/mL IL-9. At day 7, CD61⁺ cells (Mks) were enriched by anti-CD61 magnetic microbeads (Miltenyi) using MACS separation (Miltenyi). Megakaryocyte-derived microparticles (MkMPs) were isolated from culture medium from day 12 Mk culture

CHRF cells [158] were culture in growth medium (IMDM supplemented with 10% FBS (Sigma)) for 3 days to reach the concentration at 500-1000 k cells/mL. Cells were then treated with 10 ng/mL Phorbol-12-Myristate-13-Acetate (PMA) and reseeded at 200 k cells/mL in fresh medium. CHRF-derived MPs (CMPs) were isolated from culture medium at day 4 after PMA treatment.

3.2.4 Isolation of Megakaryocytic Microparticles (MkMPs) and MPs (CMPs) from CHRF cells.

MkMPs or CMPs were isolated as described [23, 74]. Briefly, cells and cell debris were removed from the culture medium by centrifugation at $2000 \times g$ for 10 min. MPs were then enriched via ultracentrifugation (Optima Max Ultracentrifuge and Rotor TLA55, Beckman Coulter) under 25,000 rpm for 30 min at 4 °C. After that, MPs were resuspended in PBS or stored at -80 °C until used.

3.2.5 Determination of Microparticle-Size Distribution.

MkMPs or CMPs resuspended in PBS were first diluted 140-fold in DI water. Their size distribution was measured by nanoparticle tracking analysis (NTA) using NanoSight NS300 (Malvern). Each analysis was carried out with 5 measurements, with the camera level set at 9-10, the detection threshold at 4, and 50-80 particles per frame with 1500 frames per measurement.

3.2.6 Exogenous loading of pDNA to CMPs or MkMPs.

The 6290-bp reporter plasmid pGFPns was a gift of Howard Gu (Addgene plasmid # 35626) [159]. The 3486-bp pmaxGFP was part of the Amaxa Nucleofection Kit (Lonza). pGFPns or pmaxGFP were first conjugated with Cy5 by Label IT® Tracker™ Cy5 (Mirus), following the manufacturer's protocol with labeling density of 4-10 label molecules per plasmid molecule. CMPs were isolated from day-4 cultured CHRF cells, and MkMPs were purified from day-12 CD34+ cell-derived Mk culture.

After washing once with 1 mL PBS by ultracentrifugation at 25,000 rpm for 30 min at 4 °C, MPs were resuspended in hypotonic buffer (Eppendorf). 5×10^6 CMPs were then mixed with Cy5-labeled pGFPns at various pGFPns/CMP ratios (5, 15, 50, 100, 250, or 500×10^3) in a total volume of 100 μ l and incubated for 15 min at 37 °C . pGFPns was loaded into CMPs by electroporation (Gene Pulser Xcell™ Electroporation System, Bio-rad) using an exponential decay pulse for 10-20 ms at 100 μ F, 37 °C in a 2-mm cuvette. Following that, 900 μ l of wash buffer (IMDM + 2% BIT + 2 mM EDTA) was added to ameliorate nucleic acid or MP aggregation, and loaded-MPs were incubated at on ice for 20 min for recovery, followed by centrifugation at $1000 \times g$ for 10 min to remove large aggregates generated due to electroporation. Loaded-MPs were collected and washed once with PBS under ultracentrifugation at 25000 rpm, 4 °C for 30 min, and resuspended in PBS or co-culture medium.

3.2.7 Exogenous Loading of Small RNAs to MkMPs.

$4-5 \times 10^6$ MkMPs were loaded with siRNA targeting *c-myb* (siR-MYB, Ambion), or Alexa 647-conjugated AllStars Negative Control siRNA (Qiagen) by electroporation in a 4 μ M siRNA solution at 150V, 100 μ F in a 4-mm cuvette at 4 °C. Similarly, $4-5 \times 10^6$ MkMPs were loaded with miR-486-5P mimic (8 μ M solution) or miRNA negative control (miR-NC) by electroporation at 150V, 100 μ F in a 2-mm cuvette at 4 °C. After loaded MkMPs were recovered in wash buffer at 4 °C for 30 min, large aggregates were isolated under $1000 \times g$ for 10 min, while small loaded MkMPs were

washed twice with PBS under ultracentrifugation at 25000 rpm, 4 °C for 30 min, and resuspended in IMDM for co-culture experiments.

3.2.8 Quantification of Plasmid-DNA Loading of CMPs or MkMPs.

Quantified by flow cytometry, Cy5^+ (%) of MP population (Eq. 1) represents the Cy5 -pDNA loading efficiency.

$$\text{Loading Efficiency (\%)} = \frac{\text{Cy5}^+ \text{ MP \#}}{\text{Total MP \#}} \quad (1)$$

pDNA (pGFPns or pmaxGFP) was purified from loaded-MPs using the QIAprep Spin Miniprep Kit (Qiagen), and its concentration quantified using the Qubit™ dsDNA HS Assay Kit (Invitrogen). To calculate the pDNA copy number per Cy5^+ -MPs, we calculated the molecular mass (M.M.) of pDNA (6290 bp of pGFPns, 3486 bp of pmaxGFP), which is 3.9×10^6 g/mol or 2.1×10^6 g/mol, respectively. Based on the pDNA concentration quantified from Qubit, the total number of pDNA copies is calculated using Eq. 2, where N_A is the Avogadro number.

$$\text{pDNA Copy \#} = \frac{\text{Loaded pDNA (ng)} \times 10^9}{\text{M.M.}} \times N_A \quad (2)$$

The pDNA copy number per Cy5^+ -MP was calculated based on the number of Cy5^+ -MPs. pGFPns purified from loaded-CMPs was confirmed through PCR amplification of the GFP sequence using a 144-bp probe, while pmaxGFP was confirmed by targeting the CMV promoter sequence using a 303-bp probe. Primers for PCR amplification were listed in Table S1. PCR amplicons were visualized by gel electrophoresis.

3.2.9 Setup of co-cultures of HSPCs with pDNA-loaded CMPs/MkMPs, or small RNA-loaded MkMPs.

Co-cultures of MPs with CD34⁺ cells were setup as described [23, 74]. Briefly, for pDNA delivery, 60,000 HSPCs from day-1 culture were co-cultured with Cy5-pmaxGFP-loaded CMPs or MkMPs with the ratio of 150 CMPs per cell or 20 MkMPs per cell under five different condition: (a, Tube) HSPCs and MPs were first co-cultured in a small volume (50-100 μ L) in Eppendorf tubes, and diluted in 1 mL co-culture medium in 24-well plate [23, 74]. (b, flow through, FT) HSPCs were first seeded onto the upper compartment of the Transwell insert (0.4 μ L pore size, Corning). After 30 min, MPs were added into the culture. (c, FT+Centri) HSPCs-MPs co-culture was set up as in (b) above in the flow-through system in a 24 well-plate. After adding the MPs, the plate was centrifuged under 600 \times g for 30 min at room temperature in order to physically enhance the contact between HSPCs and MPs. (d, FT+PB) HSPCs were pre-treated with 8 μ g/mL polybrene (PB) for 15 min at 37 $^{\circ}$ C, followed by co-culture with MPs in the flow-through system as in (b). (e, FT+PB+Centri) HSPCs were pre-treated with 8 μ g/mL polybrene for 15 min at 37 $^{\circ}$ C, followed by co-culture with MPs in the flow-through system with the centrifugation under 600 \times g for 30 min at room temperature, as the combination of (c) and (d). The % of Cy5⁺ cells at 24 hours and GFP expression at 24, 48, 72 hour of each co-culture were determined by flow cytometry.

For siRNA or miRNA delivery, 60,000 of HSPCs from day-1 culture were co-culture with MkMPs loaded with siR-Alexa 647, siR-MYB, siR-NC (non-targeting

siRNA negative control), miR-486-5p mimic, miR-NC (non-targeting miRNA negative control), unloaded MkMPs at the ratio of 30 MkMPs per cell, or without MkMPs as vehicle control, in IMDM supplemented with 10% BIT 9500, 50 ng/mL SCF, and 1X antibiotic-antimycotic at 37 °C and 20% O₂ for up to 8 days. An additional 10 pg/mL TPO was added in the siRNA delivery experiment. This minimal amount of TPO was to induce *c-myb* expression so that its down-regulation via siR-MYB can be observed. Cells from the co-culture with siR-Alexa 647-loaded MkMPs were harvested at day 1 to 5 for flow cytometry analysis to measure the % of Alexa 647⁺ cells. At days 3, 5 and 8, cells co-cultured with siR-MYB, siR-NC loaded MkMPs or unloaded MkMPs were stained with FITC-conjugated anti-CD41, and APC-conjugated anti-CD34 antibodies for flow-cytometric analysis of CD41 and CD34 expression. In miRNA delivery experiment, cells co-cultured with MkMPs loaded with miR-486-5p, miR-NC, or unloaded MkMPs were harvested at day 3, 5, and 8 for flow cytometric analysis on CD41 expression. The total cell count and Mk count were calculated at day 8.

3.2.10 Quantitative RT-PCR.

To evaluate the delivery of pDNA, at 24 hours, cells co-cultured with pGFPns-loaded CMPs were first washed with PBS, and pGFPns from cells was purified using the QIAprep Spin Miniprep Kit. A probe for the eGFP sequence was amplified through PCR, as detailed above, to confirm the delivery of pGFPns to HSPCs. At 72 hours, total RNA was isolated from the cells using the miRNeasy micro kit (Qiagen) and 0.5

µg of total RNA was reversed transcribed by the cDNA Reverse Transcription Kit (Applied Biosystems). Quantitative RT-PCR assays for *eGFP* and *GAPDH* mRNA expression were performed with iTaq Universal SYBR Green Supermix (Bio-Rad). *eGFP* and *GAPDH* expression was quantified by the Livak method. To verify the level of gene knockdown of *c-myb* expression, total RNA was isolated at day 1 of co-culture, and quantitative RT-PCR analysis were performed with iTaq Universal SYBR Green Supermix. Gene expression level of *c-myb* were calculated with the normalization to *GAPDH*. Primers used for quantitative RT-PCR were list in Table B.1 in Appendix B.

3.2.11 Super-Resolution Microscopy

To visualized the delivery of pGFPns to HSPCs, at 24 and 72 hours, HSPCs from the co-culture with Cy5-pGFPns were examined by ELYRA PS.1 Super Resolution Microscopy (SRM, Zeiss). Briefly, cells were first stained with CellTracker™ CM-DiI Dye (Invitrogen) for lipid membrane staining, and seeded onto poly-L-lysine-coated coverslip. After 10 min, cells were fixed with 4% paraformaldehyde for 10 min at room temperature. After washing with PBS thrice, samples were mounted with SlowFade™ Diamond Antifade Mountant with DAPI (Invitrogen) for imaging.

3.2.12 Nuclei Isolation

60,000 HSPCs from day-1 culture were co-cultured with Cy5-pmaxGFP-loaded CMPs or MkMPs with the ratio of 50 CMPs per cell or 20 MkMPs per cell under four

different conditions as describe above (Tube, FT+Centri, FT+PB, FT+PB+Centri.).

Isolation of nuclei was performed at 24 hours of co-culture, following the Nabii and Riabowol's protocol [160]. Briefly, cells were collected from each co-culture, washed twice with ice-cold PBS, and pelleted at 500 ×g for 4 min. After removing the supernatant, the pellet was first resuspended in 100 µl ice-cold PBS and lysed in 900 µl ice-cold PBS containing 0.1% NP-40. The sample was then pipetted 5 times, followed by centrifugation at 10,000 rpm for 10 s to collect the nuclei fraction. The supernatant containing cytoplasmic fraction was removed, and the nuclei pellet was washed again with ice-cold PBS containing 0.1% NP-40. After centrifugation at 10,000 rpm for 10 s, the nuclei pellet was resuspended in 200 µl ice-cold PBS (without NP-40). The % of Cy5⁺ and Cy5 MFI of Cy5⁺ nuclei were determined by flow cytometry.

3.2.13 Statistical Analysis

Data were presented as means ± standard error of mean from at least three replicates. Paired Student t test of all data was performed. Statistical significance is defined as $P < 0.05$.

3.3 Results and Discussion

3.3.1 Efficient Exogenous Loading of pDNA into Megakaryocytic MPs through Electroporation Demonstrates the Large Cargo Capacity of MPs Compared to that of Exosomes

Electroporation has been used as an exogenous method to load small RNAs (siRNAs or miRNAs) or small linear DNA into exosomes [43, 49-51, 53], but no reports exist for exogenous pDNA loading into MPs. Here, we developed an electroporation protocol to enable loading of plasmid DNA to megakaryocytic MPs for delivery to HSPCs. In order to optimize MP loading with plasmid DNA, we first used MPs from the model human megakaryoblastic cell line, the CHRF-288-11 cells [158]. Treatment with phorbol 12-myristate 13-acetate (PMA) differentiates CHRF cells into megakaryocytes mimicking accurately the *in vitro* differentiation of primary Mk cells [158], and at the same time giving rise to MPs, here termed CMPs. Nanoparticle tracking analysis (NTA; Figure B.1A in Appendix B) shows that CMPs have an average size of 257 nm, slightly larger than the MkMP size of 234 nm. From co-culture experiments of CMPs with CD34⁺ HSPCs, similar to those using MkMPs, more than 98% of CFSE-dye stained CMPs were recognized and taken up by HSPCs (Figs. B.2B & B.2C in Appendix B) after 30-60 mins of co-culture. Like MkMPs, CMPs program HSPCs into polyploidy Mks at day 8 of co-culture (Figure B.2D in Appendix B).

To quantify pDNA loading and delivery, we used two plasmids of different sizes and encoding an unstable and a stable GFP. We first used the larger 6290-bp pGFPns, encoding an unstable GFP [159]. pGFPns was first labeled with Cy5, and Cy5-pGFPns were loaded by electroporation at 200V into CMPs with loading ratios (pGFPns copies per MP) of 5, 15, 50, 100, 250, and 500×10^3 . The percent Cy5⁺ MPs from Eq. (1) (Methods) represents the efficiency of electroporation for Cy5-pGFPns loading. The number of pGFPns copies per Cy5⁺ CMP after electroporation was calculated as described in Methods. On an average, 40 to 50% of CMPs were Cy5⁺ over a broad range of loading ratios of 15×10^3 to 500×10^3 (Figure 3.1A). In an effort to improve the loading efficiency, we examined the impact of electroporation voltage (from 50 to 400 V) with the best loading ratio, from Figure 3.1A, of 250×10^3 . Electroporation voltage in the range examined did not affect the % of Cy5⁺ MPs, but higher voltage (200V and 400V) enabled a higher loading of pGFPns per MP (Figure 3.1B). Electroporation at 400V resulted in MP aggregation and decreased the loading efficiency. To further verify pGFPns loading, CMPs loaded with pGFPns were lysed and plasmid was extracted for a semi-quantitative PCR assay using a 144 bp probe on the GFP-coding sequence on pGFPns (Figure 3.1C). The band intensity of the amplified DNA appears proportional to the pGFPns copy # per MP (Figure 3.1B), indicating successful loading of pDNA into CMPs. The faint band of the no-electroporation control corresponds to the low Cy5⁺ fraction and the low copy # loading of Figure 3.1A and 1B indicating that plasmid DNA attaches to and perhaps some enters CMPs. Among the examined electroporation temperatures (25, 37, 45, or

55 °C), 37 °C enabled the highest loading in terms of Cy5⁺(%) of CMPs (Figure B.2), up to an average of 3455 pGFPns copies per Cy5⁺ CMP with a loading ratio of 250 ×10³ (Figure 3.1A). These data suggest that higher membrane fluidity at the physiological temperature improves pGFPns loading. Based on these findings, in all subsequent studies, we used a loading ratio of 250 ×10³ pDNA copies per MP, 200V and 37 °C.

To directly visualize the loading of Cy5-labelled pGFPns into CMPs, we used super-resolution structured illumination microscopy (SIM) [161], a method not previously employed for visualizing plasmid loading to EVs or cells. Prior to loading them through electroporation, CMPs were labelled with PKH26, a lipophilic fluorescent membrane dye. After the removal of free Cy5-pGFPns by a washing step, CMPs were added onto poly-L-lysine pre-coated coverslips for 2 hours so that they stick to the coverslip to use for SIM analysis. Our CMPs have a size range of 150-700 nm as determined by NTA (Figure B.1A in Appendix B). Here, we focused on larger CMPs to enable more definitive visualization, given that Cy5 fluorescence detection requires a large number of stained plasmid molecules based on the fact that larger CMPs can carry more plasmid molecules per the discussion above. As shown in Figure 3.1D, we identified several CMPs (represented by the red-stained circular membranes) with apparent sizes of 0.5 to 0.7 μm carrying Cy5-pGFPns (cyan). We use the term apparent because acquisition of these SIM images likely overestimates the CMP size due to the nature of the SIM signal capture. To demonstrate that Cy5-pGFPns are inside the CMPs, we show a series of images of Z-stack planes. As the

image slice number increases, the signal from Cy5-pGFPns gradually disappears, while the CMP image (red) remains intact. These images, the first ever reported of the kind, demonstrate that Cy5-pGFPns was successfully loaded into CMPs with electroporation.

Based on the CMP studies, using a pDNA loading ratio of 250×10^3 , we optimized the loading of Cy5-labeled pmaxGFP (the 3486-bp pDNA encoding of stable GFP) to MkMPs under various electroporation voltages. Over 60% of MkMPs were Cy5⁺, with up to the average of 4264 pmaxGFP copies per Cy5⁺ MkMP (Figure 3.1E). Both the loading efficiency from Figure 3.1E and the mean fluorescent intensity (MFI) of Cy5 in Figure 3.1F suggest that the best loading is obtained with 200 V. pmaxGFP loading into MkMPs was examined by PCR amplification of the CMV promoter using a 303-bp probe (Figure 3.1G).

The plasmid-loading results of Figs. 3.1A, 1B and 1E demonstrate the unique capability of MPs among EVs for high-capacity loading of large cargo molecules such as plasmid pDNA. It is quite remarkable that over 3,000 copies of a large 6290-bp plasmid, and over 4,000 copies of the smaller 3486-bp plasmid can be loaded in these vesicles for delivery to targeted cells. How does this compare to DNA content or loading of other biological particles or vesicles? Considering the size of human mitochondria (0.5-3 μm) and mitochondria DNA (16.6 kb) [162], the copy number of loaded-pDNA per MP in our study falls in the range of mitochondria-DNA copy number, which ranges from 50 to 10,000 [162]. Although no quantitative data are available, Kanada *et al* demonstrated endogenous loading of pDNA into HEK293FT-

derived EVs from transiently transfected donor cells, and only MPs were able to deliver functional pDNA to the recipient cells, but not exosomes [55].

The radius of gyration (RG) of DNA molecules (linear, open-circular, or supercoil pDNA) has been used to estimate DNA loading in vesicles [163]. RG represents the average distance between the mass center of DNA to each base pair. Latulippe *et al* showed the RG of 5.76, 9.80, or 16.80 kb pDNA are 102, 117, or 169 nm, respectively [163]. These results suggest that it is difficult to load large size pDNA into nano-size exosomes (<100nm), and is consistent to the study from Lamichhane *et al* showing a low loading capacity of 6 kb pDNA to EVs with the average size around 85 nm [51]. We estimated (Table B.2 in Appendix B) that only 1-2 copies of the 6 kb pDNA was loaded into each 85 nm-EV. A 4-fold increase (ca. 8 copies per MP) in loading capacity was obtained when using 167-nm MPs (Table B.2 in Appendix B) [51]. Based on these findings, the larger size (257 nm) of the CMPs or MkMPs (234 nm) in our study would be able to accommodate an even larger number of plasmid copies. However, our data far exceed what one would expect from any extrapolation of the data of the Latulippe *et al* [163] study: loading an average of over 3,400 copies of a 6290-bp plasmid per CMP (Figs. 3.1A & B) or over 4200 copies of a 3486-bp plasmid per MkMP (Figure 3.1E) is over two orders of magnitude higher, and represents the highest DNA loading ever reported for EVs, thus demonstrating the potential of using MPs for delivering large amounts of cargo to desirable cell targets. We also estimated the capacity of our megakaryocytic MPs for loading larger pDNAs, on the upper size range of what has been used for gene delivery, such as the

supercoiled 9.8 kb plasmid reported by Latulippe *et al* [163]. The RG of this pDNA is 117 nm, which is 14.7% larger in radius, or 50.9% larger in occupied volume than a 5.76 kb, supercoiled pDNA (RG= 102 nm). Taken together with our results (3455 or 4264 copies per MP; Figure 3.1), we estimate that the copy number of the 9.8 kb pDNA per MP will be ca. 51% smaller, or about 1700 to 2100 copies per MP (Table B.2 in Appendix B). This is still a large plasmid-loading capacity and more than sufficient for functional plasmid delivery to HSPCs.

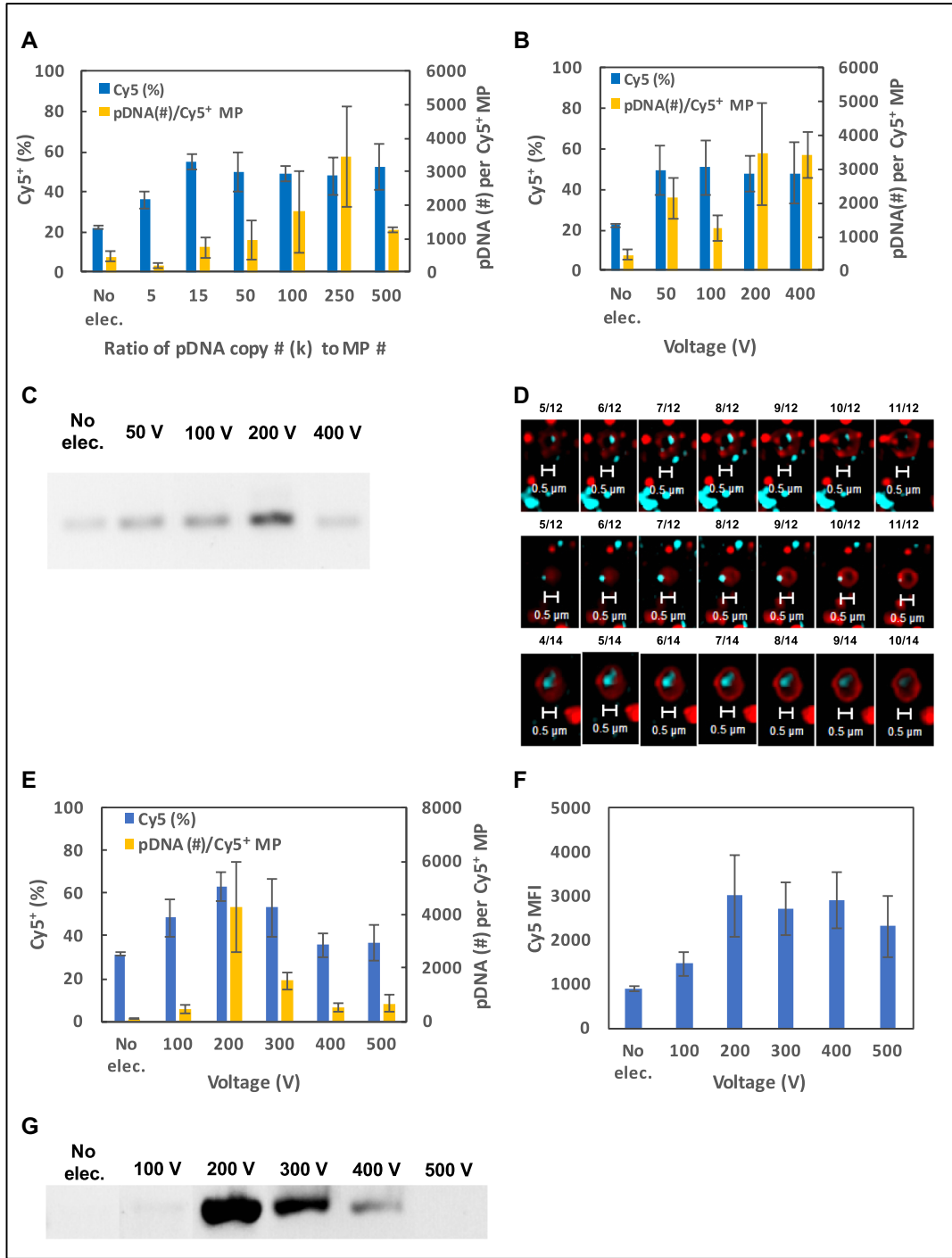


Figure 3.1 Loading of pDNA into CHRF-derived MPs (CMPs) or megakaryocyte-derived MPs (MkMPs) through electroporation. Loading of Cy5-labeled pGFPns were performed via electroporation under different (A) ratio of pDNA copy number to MP number and (B) different electroporation voltage. MPs were washed with PBS after electroporation. (A, B) The percent of Cy5⁺ MPs was measured via flow cytometry. To measure the amount of loaded-pDNA, MPs were lysed and pDNA were purified for quantification, in order to calculate the number of loaded pDNA per Cy5⁺ MP. Loading of pGFPns into CMPs was further verified by (C) PCR amplification of portion of the eGFP sequence, and (D) Super Resolution Microscopy. CMPs were first stained with PKH26 (Red) for recognition. Cyan represents Cy5-pDNA. (E-G) Similarly, MkMPs were loaded with Cy5-labeled pmaxGFP via electroporation under different electroporation voltages at the pDNA/MkMP ratio of 150×10^6 . (E) The percent of Cy5⁺ MP, number of loaded pmaxGFP per Cy5⁺ MP, and (F) the mean fluorescent intensity (MFI) of Cy5⁺ MPs were measured via flow cytometry. (G) Loading of pmaxGFP into MkMPs was further verified by PCR amplification of portion of the CMV-promoter sequence. Error bars in (A, B, E, F) represent standard error of mean of three replicates.

3.3.2 Delivery of pDNA to HSPCs using CMPs or MkMPs

CMPs were loaded with pGFPns using the optimized electroporation protocol. After electroporation, large particle aggregates due to electroporation, were separated from regular size MPs by centrifugation (Figure 3.2A). Cy5-pGFPns-loaded MPs were washed once with PBS and co-cultured with day-1-HSPCs for up to 72 hours.

Delivery of pGFPns was first confirmed through the isolation of pDNA from HSPCs harvested after 24 hours of co-culture. The eGFP encoding DNA sequence was probed by semi-quantitative PCR, and was detected only from co-culture samples with pGFPns-loaded CMPs (Figure 3.2B). We hypothesized that the gravity- or centrifugation driven, medium flow through (FT) commercial Transwell system would enhance the physical interaction between CMPs and HSPCs. Thus, we carried out co-

cultures under four different settings/conditions: (a) HSPCs/CMPs co-culture in Eppendorf tubes in small volume for 1 hour and transferred to standard 24-well plates; (b) HSPCs/CMPs seeded onto the membrane inserts of 24-well Transwell plates (Figure 3.2C, flow-through system, FT); (c) Co-culture in the FT system as above, but with enhanced medium flow using 600 ×g centrifugation of the plates for 30 minutes to further enhance the physical contact between the HSPCs and CMPs; and (d) Co-culture in the FT system with the supplemental of 8 µg/mL of polybrene (PB). The polycation polybrene [164] was used to test if it would enhance the interaction between HSPCs and CMPs. After 24 hour of co-culture, the % Cy5⁺ HSPCs were measured by flow cytometry. 47% of HSPCs were Cy5⁺ from the co-culture in Eppendorf tubes, while 65% of HSPCs were Cy5⁺ in FT system without centrifugation (Figure 3.2D). Centrifugation did not affect the % of Cy5⁺ HSPCs, but polybrene additions promoted CMP uptake to obtain 84% of detectable Cy5⁺ HSPCs (Figs. 3.2D & Figure B.3A in Appendix B).

Next, we examined the functionality, at the transcriptional level of the delivered pGFPns. Total RNA was isolated from each co-culture at 72 hours and eGFP-mRNA expression was examined by quantitative (q)-RT-PCR. Figure 3.2E shows the expression ratio of eGFP-mRNA to the reference gene GAPDH-mRNA. Both, centrifugation and polybrene addition increased the level of eGFP-mRNA by 2.93- and 3.86-fold, respectively. Unexpectedly, there was no significant difference in *eGFP* expression between the two simpler settings (tube and FT without centrifugation). Based on these results, we hypothesize that the combination of

physical and chemical enhancement will give rise to better functional pDNA delivery. To test that, we investigated GFP expression at the translation level. We examined GFP expression from both plasmids. We first show data using pmaxGFP. In addition to four co-culture methods described above, HSPCs were co-cultured with pmaxGFP-loaded CMPs or MkMPs in the FT system with the supplemental of 8 $\mu\text{g}/\text{mL}$ of polybrene and with 600 $\times\text{g}$ centrifugation of the plates for 30 minutes (FT+PB+Centri.). The percent GFP⁺ HSPCs was measured at 24, 48 and 72 hours of co-culture by flow cytometry. The results (Figure 3.2F, 2G, and Figure B.3B in Appendix B) show that centrifugation with polybrene addition promotes functional delivery of pmaxGFP, with over 8% or 5% of cells expressing GFP with the delivery by CMPs or MkMPs, respectively. These data show that our system delivers pDNA to the nucleus.

We used SIM to directly visualize pGFPns delivery and cellular localization, as well as eGFP expression. Cells co-cultured with pGFPns-loaded CMPs (we used the less stable GFP to potentially capture the dynamics of delivery) were pre-stained with DiI, a lipophilic dye, for cellular membrane staining, while pGFPns was pre-labelled with Cy5. At 24 hours (which corresponds to 0.8 cell doublings [103]), Cyan-identified Cy5-stained pGFPns were concentrated at both the cellular membranes (red staining) and the nuclear (DAPI staining) areas, but no eGFP expression was detectable (Figure 3.3). At 72 hours, which corresponds to 2.4 cell doublings, pGFPns persists on the cytoplasmic membrane, but is not visible in the nucleus. This is likely the result of the reduced stability of the GFP encoded on this plasmid. However, eGFP

expression is widespread in the two cells shown, and apparently concentrated near intracellular, red-stained membranes likely corresponding to membranes of the rough ER and various Golgi organelles. These SIM data further support the successful delivery of pGFPns to the HSPC nucleus, and capture some of the dynamics of the process: plasmid delivery to the nucleus followed by protein expression in cytoplasmic organelles. This is the first report of direct visualization via SIM of plasmid DNA delivery to the nucleus and the associated detailed localization of protein expression.

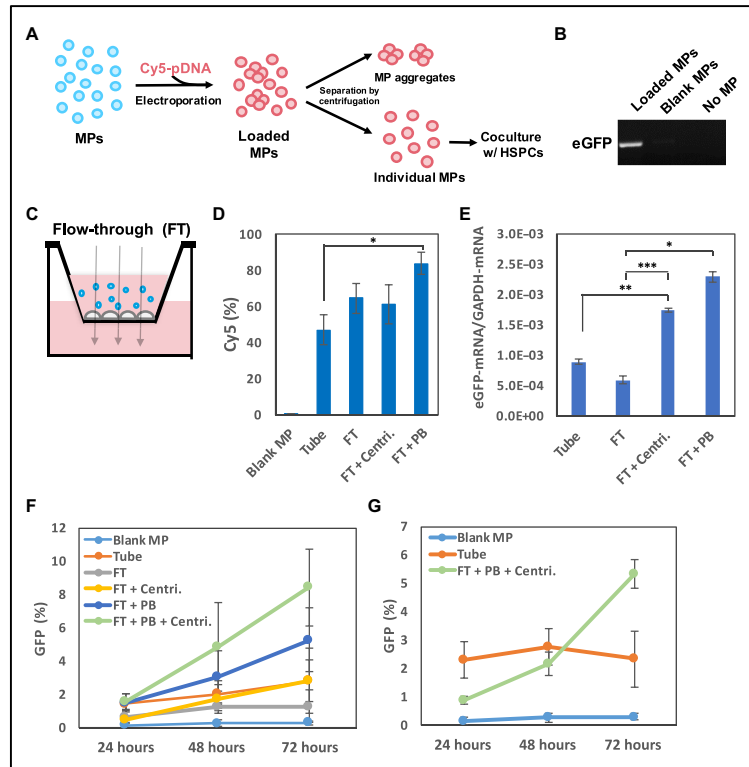


Figure 3.2 Delivery of pDNA to HSPCs via MPs. (A) Schematic showing the separation of aggregates from individual MPs after loading of pDNA via electroporation. (B) Loading of pGFPns was confirmed in day-1 cells from the co-culture of HSPCs with pGFPns-loaded CMPs via PCR amplification of portion of the eGFP sequence. (C) Schematic of Flow-Through set up with 0.4 μm membrane insert. HSPCs were first seeded onto the membrane for 30 minutes, and MPs were then added to the culture. (D, E) Day-1 HSPCs were co-cultured with Cy5-pGFPns-loaded MPs in Eppendorf tubes (Tube), the Flow-Through system (FT), the Flow-Through system with centrifugation (FT+Centri.), or the Flow-Through system but with medium supplemented with 8 $\mu\text{g}/\text{ml}$ polybrene (FT+PB). Cells were harvested for (D) flow cytometry analysis of Cy5 signal at 24 hours, and (E) eGFP-mRNA and GAPDH-mRNA quantification by qRT-PCR at 72 hours. (F, G) Day-1 HSPCs were co-culture with pmaxGFP-loaded (F) CMPs or (G) MkMPs under four co-culture conditions (Tube, FT, FT+Centri., FT+PB, and FT+PB+Centri.). Cells were harvested at 24, 48, and 72 hours for measuring GFP expression by flow cytometry. Native MPs were used as control (Blank MP). Data in (D, E) represent averages of 3 biological replicates \pm standard error of mean. *, $P < 0.05$; **, $P < 0.01$; ***, $P < 0.001$.

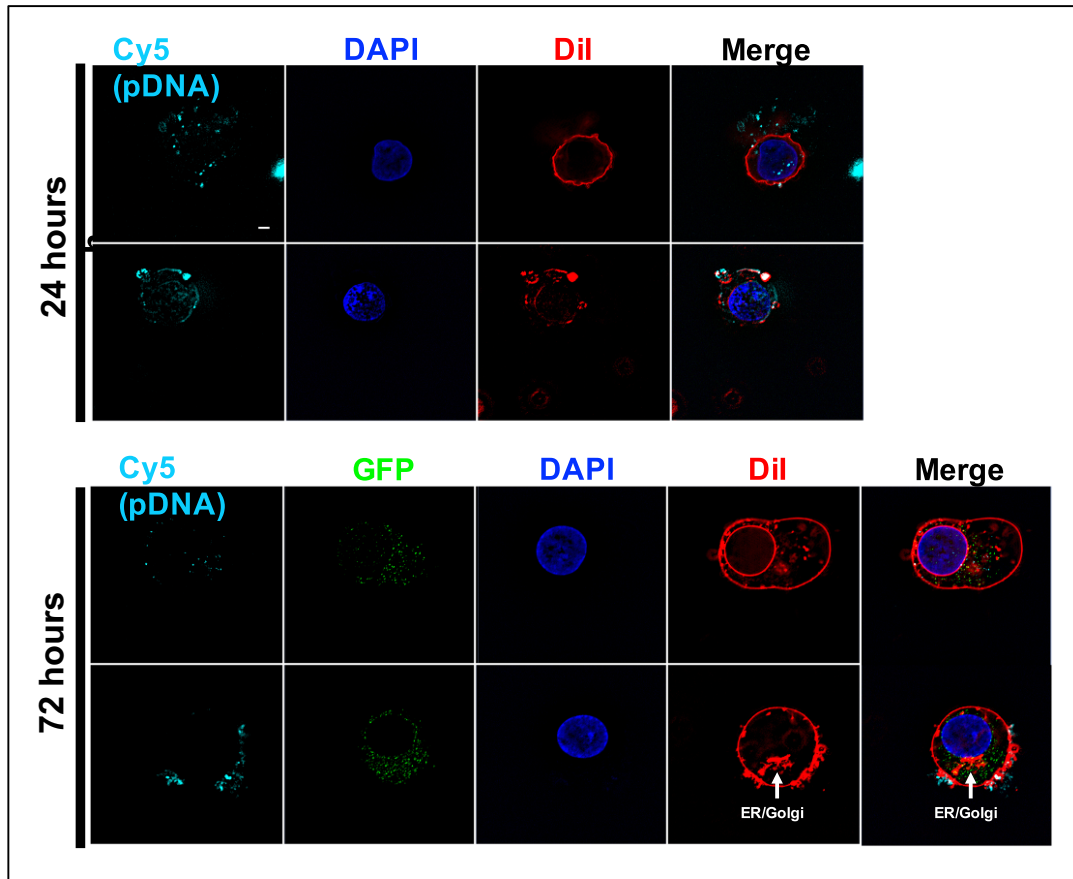


Figure 3.3 Super-resolution images of HSPCs co-cultured with Cy5-pGFPns-loaded MPs.

HSPCs co-cultured with Cy5-pGFPns-loaded MPs were harvested and fixed at 24 and 72 hour. The location of Cy5-pGFPns (cyan) and eGFP expression (green) were examined by super-resolution microscopy. Nucleus were stained with DAPI (blue) and cellular membrane was stained with DiI (Red).

3.3.3 Effective Delivery of pDNA to HSPC Nuclei

Although up to 84% of cells co-cultured with Cy5-pDNA-loaded MPs were $Cy5^+$ (Figure 3.2D), only up to 10% of cells were expressing GFP (Figure 3.2F), suggesting that flow cytometry analysis may not be capturing all the GFP-expressing cells due to detection limitations deriving from lower levels of GFP expression. We thus directly

examined the effectiveness of pDNA delivery to nuclei. Briefly, HSPCs were co-cultured with Cy5-pmaxGFP-loaded CMPs or MkMPs under various conditions as before. After 24 hours, nuclei were isolated and analyzed via flow cytometry. As shown in Figs. 3.4A and 4B, up to 81% or 75% of HSPC nuclei were Cy5⁺, which is a considerably higher fraction than for direct plasmid electroporation, indicating the effective delivery of pmaxGFP to the nuclei using either CMPs or MkMPs. Notably, addition of polybrene (PB) enhanced both the percent of Cy5⁺ nuclei, as well as their mean fluorescent intensity (MFI) by up to 2-fold (Figs. 3.4C & 4D), suggesting its role in improving pDNA transport to nucleus. This high percentage (75-81%) of delivery to nuclei was unexpected given that plasmid delivery via electroporation results in higher GFP expression (54.1% ± 2.4%). This is likely due to the different mechanisms of pDNA delivery to cell nuclei. Plasmid delivery by electroporation (known as nucleofection) is a quick process delivering pDNA to nucleus by opening pores to the nuclear envelope without the need for cell cycling, which is otherwise necessary for pDNA entry into the nucleus [165, 166]. Thus, with pDNA nucleofection, protein expression starts within 3 to 6 hour, and due to cell cycling, a fraction of the plasmid is diluted or degraded within 24 hours thus resulting in lower % of Cy5⁺ nuclei. In contrast, delivery of pDNA through MPs requires cell cycling and mitosis which is necessary for breaking down the nuclear envelope to enable pDNA entry into the nucleus [166]. We should note also that direct comparison in terms of GFP expression between electroporation and MP delivery may be affected by the fact that electroporation/nucleofection may induce non-specific changes in cell

metabolism and may alter the subcellular protein expression patterns of the transgene [167]. Taken together, these data show that MkMPs can effectively deliver pDNA to HSPCs and HSPC nuclei. Nevertheless, to achieve better protein expression, delivery of pDNA to nucleus can be further increased by (a) increasing the ratio of MkMPs per HSPC to 50-150, so that more pDNA is delivered to HSPC and HSPC nuclei; (b) using cationic polymers such as polyethylenimine (PEI), which has been shown to enhance endosomal escape [168, 169]; or (c) using pDNA complexed with nuclear localization signal (NLS) peptides such as the SV40 antigen, which can enhance plasmid nuclear import [170, 171].

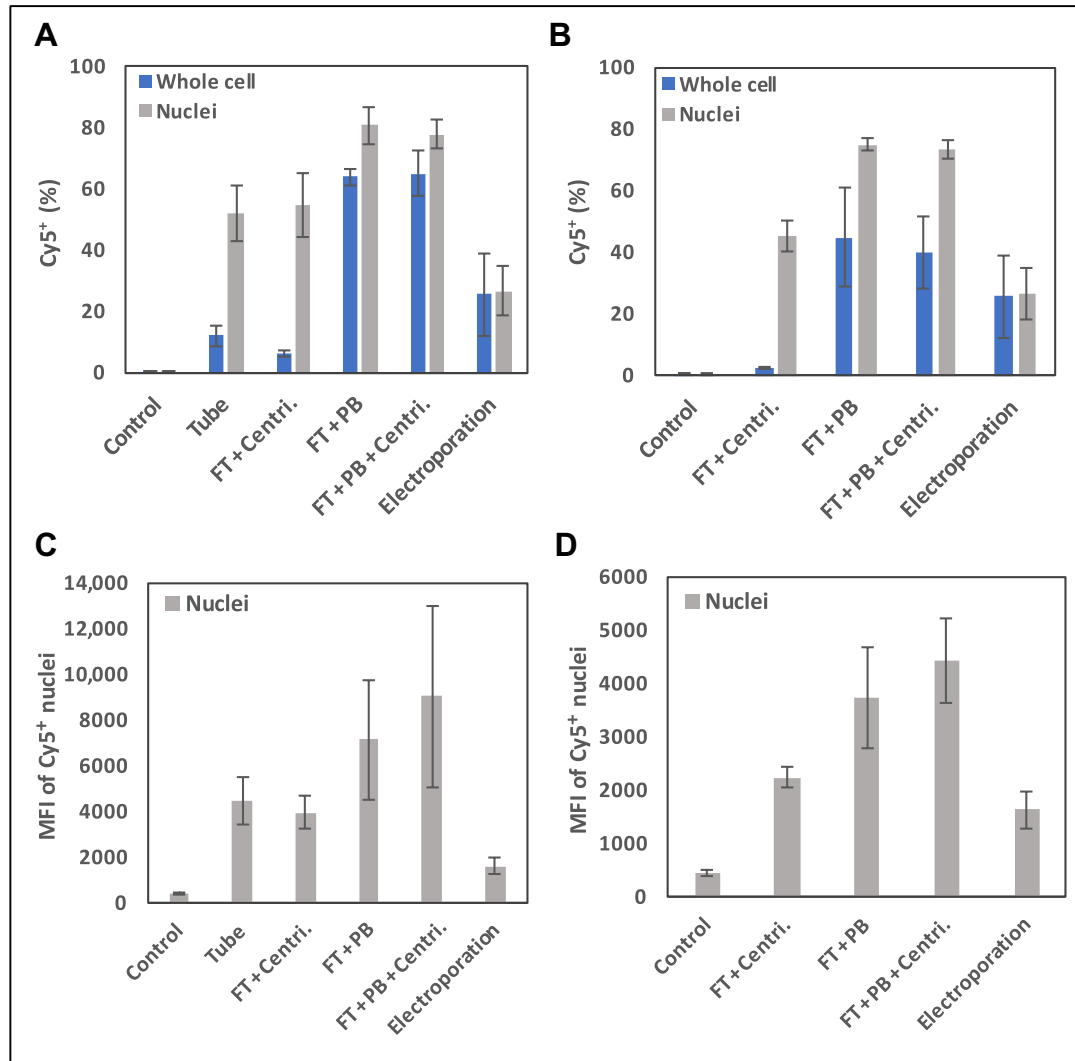


Figure 3.4 Examine the delivery of pDNA to HSPC nucleus via nuclei analysis. Day-1 HSPCs were co-culture with Cy5-pmaxGFP-loaded (A, C) CMPs or (B, D) MkMPs in Eppendorf tube (Tube), flow-through system with centrifugation (FT+Centri.), flow-through supplemented with 8 μ g/ml polybrene (FT+PB), or the combination of polybrene with centrifugation in flow-through system (FT+PB+Centri.). Both cells and isolated nuclei were harvested for flow cytometry analysis on (A, B) Cy5+ nuclei percentage or (C, D) mean fluorescent intensity (MFI) of Cy5+ nuclei at 24 hour. Data represent averages of 3 biological replicates \pm standard error of mean.

3.3.4 Functional Synthetic-RNA Delivery to HSPCs using MkMPs

Beyond plasmid DNA delivery, small RNAs (miRNAs or siRNAs) constitute an important cargo for a broad variety of therapeutic applications, especially so for delivery to HSPCs [152-154]. We have shown that the RNA content of MkMPs is responsible for megakaryocytic differentiation and PLT biogenesis of the targeted HSPCs [23, 74], thus clearly showing that RNA delivery to HSPCs is an effective process. We have also discussed that transfusion of human MkMPs in mice leads to *de novo* murine PLT biogenesis [157], thus showing that *in vivo* RNA delivery to HSPCs is effective in enabling the development of a complex biological phenotype. Here, we examined delivery of synthetic RNAs, namely an siRNA and an miRNA to HSPCs through MkMPs. While the ultimate goal is *in vivo* delivery, here we examined *in vitro* delivery as the first step to assess the efficacy of the process, assuming that *in vivo* delivery will be efficacious as our murine experiments suggest.

We modified the electroporation protocol we used for pDNA loading to CMPs to load siRNA to MkMPs in order to deliver to and silence *c-myb* expression in HSPCs. *c-myb* is a major regulator of erythropoiesis and megakaryopoiesis by restraining megakaryopoiesis at the common erythroid-megakaryocytic progenitor stage through a mechanism involving miR-486-3p [172, 173]. Bianchi *et al* silenced *c-myb* expression using siRNA (delivered directly through electroporation) to enhance Mk differentiation of CD34+ HSPCs [172]. To assess the effectiveness of siRNA delivery through MkMPs, we first loaded Alexa-647-labelled siRNA (non-specific targeting siRNA) to MkMPs by electroporation, and examined the level the loading

effectiveness by flow cytometry analysis. 24.3 ± 9.0 % of MkMPs were detected Alexa 647⁺. To assess the ability of siRNA-loaded MkMPs to deliver siRNA to HSPCs, we employed co-cultures of MkMPs with cultured, day-1 HSPCs. 35% of the cells were Alexa-647⁺ after 48 h of co-culture showing stable Alexa-647 staining up to 120 hours of co-culture, thus demonstrating effective delivery of siRNA to HSPCs (Figure 3.5A). Based on these findings, we next examined functional siRNA delivery to HSPCs. We assessed the enhancing impact of siRNA targeting *c-myb* (siR-MYB) via MkMP delivery, beyond the impact of the siRNA negative control (siR-Neg) or that of native MkMPs, which promote Mk differentiation of HSPCs by several mechanisms apparently including MYB downregulation as shown below. Briefly, siRNA-loaded MkMPs or control MkMPs were co-cultured with HSPCs, and cells were analyzed by flow cytometry for CD41 (Mk marker) or CD34 expression at days 3, 5 and 8. Delivery of siR-MYB via MkMPs increased the percentage of CD41⁺ and CD34⁻ CD41⁺ cells by up to 21 % and 19 %, respectively at day 8 of co-culture versus controls (MkMP-siR-Neg or native MkMPs) (Figs. 3.5B & 5C). These data suggest functional delivery of siR-MYB to HSPCs through MkMPs. Silencing of *c-myb* was also confirmed by quantitative-RT-PCR at day 1 of co-culture (Figure 3.5D). MYB expression decreased by 27 % from the impact of cargo contained in unmodified MkMPs versus vehicle control, and by 33 % from the delivery of MkMPs loaded with siR-MYB, indicating the silencing of *c-myb* through siR-MYB. These functional changes brought about by the delivery of siR-MYB are typical of effects observed

with most siRNAs, especially in the background of these MPs, which promote Mk differentiation.

Next, we examined functional delivery of miR-486-5p. miR-486-5p has been shown to play an important role in the regulating the proliferation, survival, and differentiation of CD34⁺ cells. Notably, it is expressed in megakaryocytic-erythroid progenitors and regulates their proliferation and survival by regulating AKT signaling and the transcription factor FOXO1 [174]. We thus hypothesized that miR-486-5p delivery will promote cell proliferation and megakaryocytic-erythroid differentiation and expansion. We loaded a miR-486-5p double-strand mimic RNA or miR-NC (non-targeting miRNA) to MkMPs via electroporation. Unmodified MkMPs or miRNA-loaded MkMPs were co-cultured with CD34⁺ HSPCs for 8 days. Due to natural response variations of CD34⁺ cells from different donors, the data from three co-culture biological replicates are presented individually in Figure 3.6. At day 8 of co-culture, miR-486-5p delivered by MkMPs significantly increased total cell numbers and Mk numbers (CD41⁺ cells) by up to 91% and 169%, respectively, compared to the co-culture of miR-NC-loaded MkMPs or unmodified MkMPs with HSPCs. Although CD41 expression varied at early culture (day 3) with different donor CD34⁺ cells, it reached similar levels at day 8 for all three donor cells. Compare to native MkMPs or miR-NC-loaded MkMPs, miR-486-5p delivery enhanced the fraction of CD41⁺ by 10 to 20 %.

HSPCs are hard-to-transfected primary stem cells [151]. Among studies using synthetic nanoparticles (NPs), only one NP form has demonstrated the ability to

deliver cargo to HSPCs [30, 156]. Mcneer *et al* demonstrated delivery to HSPCs using biodegradable PLGA NPs loaded with triplex-forming peptide nucleic acids (PNAs) and single strand donor DNA. Although presenting a great advance, the gene modification efficiency was less than 1 % *in vitro* [156], and even lower *in vivo* [30]. In our study, for the first time, we successfully demonstrated delivery of plasmid DNA for functional protein expression, and of small RNAs (miRNA and siRNA) for gene regulation/silencing in HSPCs using megakaryocytic MPs. Our study supports the potential of MkMPs for applications in gene and cell therapy targeting HSPCs. Our data also support the use of the larger MPs for delivering larger amounts and larger size-cargo to target cells.

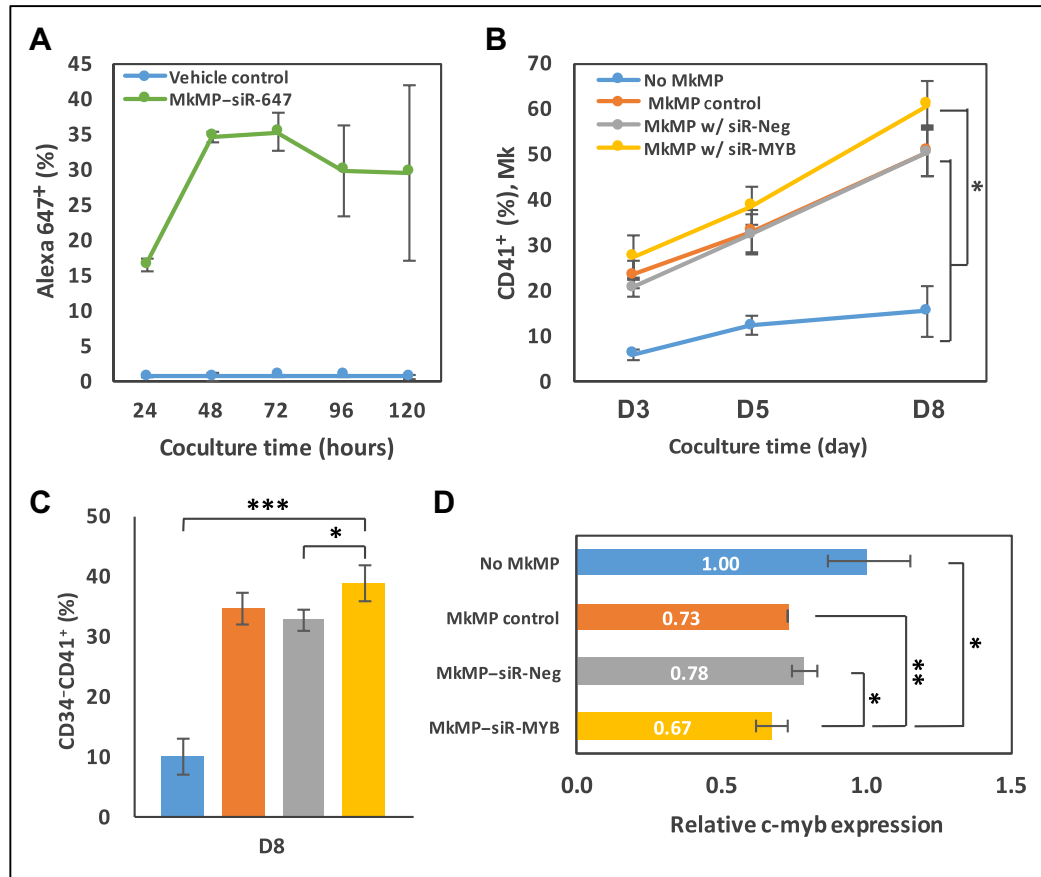


Figure 3.5 Silencing of *c-myb* through MkMP delivery of siRNA to HSPCs and enhance megakaryocytic differentiation. MkMPs were loaded with Alexa 647-labeled siRNA (green), siRNA negative control (siR-Neg, grey), or siRNA targeting MYB (siR-MYB, yellow) by electroporation. HSPCs were co-cultured with siRNA-loaded MkMPs, MkMPs without any siRNA (MkMP control, orange), or without MkMPs (No MkMP, blue). (A) Delivery efficiency of siRNA to HSPC via MkMPs were examined based on Alexa 647⁺ percentage of cells by flow cytometry analysis. (B, C) Cells from each co-culture were harvested for flow cytometry analysis on CD41⁺ (%) at day 3, 5 and 8, and CD34⁻CD41⁺ (%) at day 8. (D) Level of *c-myb* were quantified by qRT-PCR from each co-culture at 24 hour, normalized to expression of *GAPDH* as a reference gene. Data in (B-D) represent averages of 3 biological replicates \pm standard error of mean. *, $P < 0.05$; **, $P < 0.01$; ***, $P < 0.001$

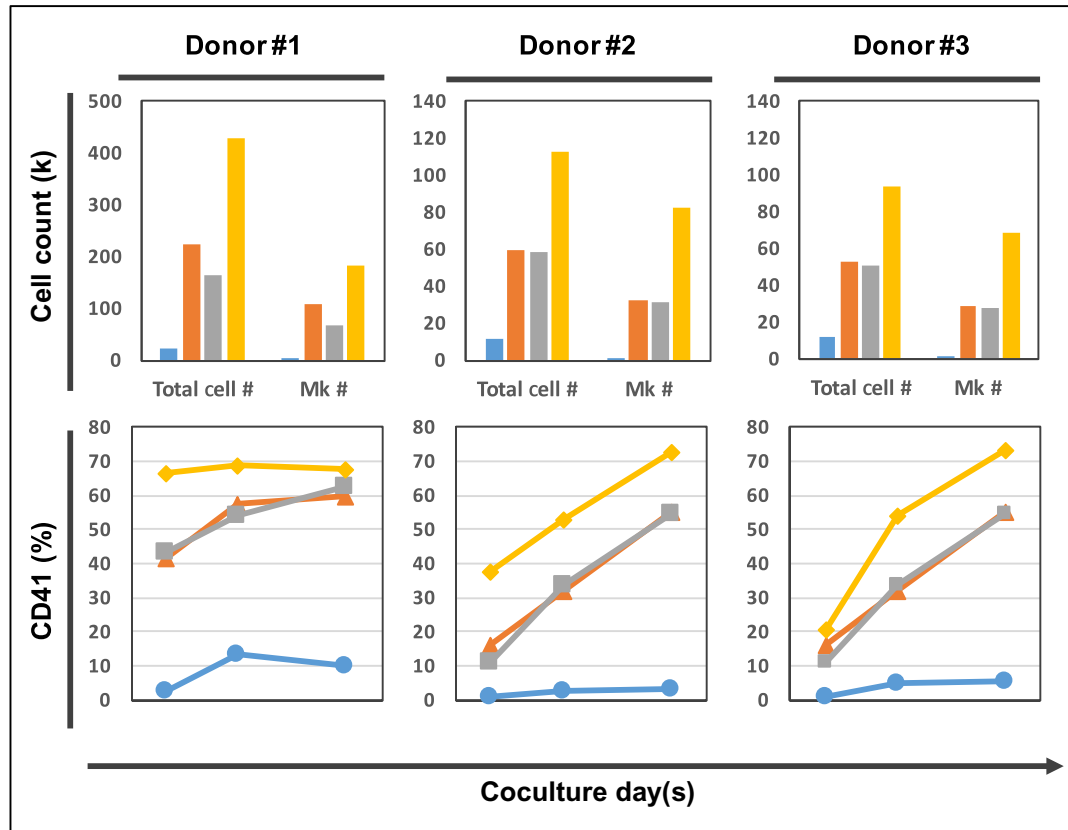


Figure 3.6 Functional delivery of miR-486-5P to HSPCs via MkMPs enhanced megakaryocytic differentiation. MkMPs were loaded with 8 μ M miRNA negative control (miR-NC), or miR-486-5P mimics by electroporation. 60,000 CD34+ HSPCs were co-cultured with vehicle control (blue, circle), MkMPs control (orange, triangle), miR-NC-loaded MkMPs (gray, square), or miR-486-5P-loaded MkMPs (gold, diamond) for up to 8 days. (Upper Panel) Number of total cells or megakaryocytes were counted at day 8 of co-culture. (Lower Panel) CD41 (Mk marker) expression were examined at day 3, 5, and 8 of co-culture by flow cytometry analysis. Three biological replicates of co-culture were shown.

Acknowledgements

I would like to acknowledge and thank thank Dr. Jeffrey Caplan and members of Bioimaging Center (University of Delaware; UD) for assistance with

immunofluorescence microscopy, and Eric Muñoz and Dr. Brittany Wilson in Dr. Mathew Hudson's lab for assistance with NTA analysis.

Chapter 4

ROLE OF MICRORNAS FROM MEGAKARYOCYTIC MICROPARTICLES (MKMPS) IN MKMP-INDUCED MEGAKARYOCYTIC DIFFERENTIATION OF HEMATOPOIETIC STEM/PROGENITOR CELLS

4.1 Background

Cell-derived microparticles (MPs) are sub-micron size (0.1-1.0 μm) membrane vesicles of extracellular vesicles (EVs) that play an important role in cell-to-cell communication by carrying and transferring various material including proteins, lipids, short DNA, or RNAs (mRNAs, miRNAs and other small RNAs like pRNAs and lcrRNAs) to target cells [2, 89]. Delivered cargo contains signaling molecules and triggers various biological programs and the development of complex developmental phenotypes. For example, endothelial-progenitor-cell derived MPs triggered angiogenesis by transferring of mRNA to endothelial cells [29]. Activated-platelet-derived MPs (PMPs) were shown to target endothelial cells and transfer an Argonaute 2 (Ago2)-miR-233 complex to regulate gene expression in endothelial cells [175]. In another example, MPs derived from human bone-marrow mesenchymal stem cells stimulated proliferation of tubular epithelial cells and protected cells from apoptosis through RNA delivery [31]. These studies demonstrate the importance of RNA (mRNA and miRNA) being transferred by MPs in triggering complex biological phenotypes in target cells.

MicroRNAs (miRNAs) are small non-coding RNAs (20-22 nt in size) that have been shown to regulate gene expression at the post-transcriptional level by targeting specific mRNAs leading to mRNA degradation or inhibition of translation [176]. EV-mediated transfer of miRNAs between cells has been studied in various cell types or disease phenotypes, such as in cardiovascular [177] or lung disease [178]. RNA sequencing (RNAseq) has been used in order to identify the RNA molecules involved in EV-triggered biological phenotypes of target cells [64]. Morhayim *et al.* used next-generation RNAseq to identify miR-29a, a highly abundant and enriched miRNA in osteoblast-derived EVs, as playing a critical role in hematopoietic proliferation [64]. Similarly, using RNAseq, Vinãs *et al* demonstrated that miR-486-5p was enriched in human cord-blood endothelial colony-forming cell-derived EVs, and have shown that it has a protective role against kidney ischemic injury, both *in vitro* and *in vivo* [179].

As previously shown in Chapter 2, megakaryocytic microparticles (MkMPs) can induce Mk differentiation of CD34+ HSPCs [23, 74]. RNase treatment demonstrated the importance of RNA in MkMPs as being important in the development of this phenotype since degradation of MkMP-RNA attenuated the ability of MkMPs to trigger the Mk differentiation of HSPCs (Figure 2.10). The specific miRNAs and the associated mechanisms by which they trigger or mediate the differentiation process of HSPCs is not known. In this study, we aim to identify miRNA(s) from MkMPs involved in MkMP-induced differentiation of HSPCs.

4.2 Materials and Methods

4.2.1 Chemicals and Reagents

Recombinant human interleukin 3 (IL-3), IL-6, IL-9, IL-11, stem cell factor (SCF), and thrombopoietin (TPO) were purchased from PeproTech Inc. BIT 9500 was purchased from Stemcell Tech. Anti-CD61 magnetic microbeads and MACS cell-separation tools were purchased from Miltenyi. Fluorescein isothiocyanate (FITC)-conjugated anti-CD41, Phycoerythrin (PE)-conjugated anti-CD42b, allophycocyanin (APC)-conjugated anti-CD34, and IgG antibodies were purchased from BD bioscience. Signaling inhibitors, miRNA mimics, miRNA inhibitors, and miR-negative control were purchased from Sigma Aldrich.

4.2.2 Megakaryocyte (Mk) Culture from CD34⁺ HSPCs

Frozen G-CSF-mobilized human peripheral blood CD34⁺ cells were obtained from Fred Hutchinson Cancer Research Center. Megakaryocytic cultures were set up as described [103]. Briefly, CD34⁺ cells were cultured in Iscove modified Dulbecco medium (IMDM, Gibco) supplemented with 20% BIT 9500 (Stemcell Tech.), 100 ng/mL TPO, 100 ng/mL stem cell factor (SCF), 2.5 ng/mL interleukin-3 (IL-3), 10 ng/mL IL-6, 10 ng/mL IL-11 and human LDL under 5% O₂ for 5 days. From day 5 to 7, IL-3 was increased to 10 ng/mL and IL-6 was substituted with 10 ng/mL IL-9. At day 7, CD61⁺ cells (Mks) were enriched by anti-CD61 magnetic microbeads

(Miltenyi) using MACS separation (Miltenyi). Megakaryocyte-derived microparticles (MkMPs) were isolated from culture medium from day 12 Mk culture.

4.2.3 Isolation of Megakaryocytic Microparticles (MkMPs)

MkMPs were isolated as described [23, 74]. Briefly, cells and cell debris were removed from the culture medium by centrifugation at $2000 \times g$ for 10 min. MPs were then enriched via ultracentrifugation (Optima Max Ultracentrifuge and Rotor TLA55, Beckman Coulter) under 25,000 rpm for 30 min at 4 °C. After that, MPs were resuspended in PBS or stored at -80 °C until used.

4.2.4 Isolation of Platelet-like Particles (PLPs) and Mk-derived Microparticles (MkMPs)

Large Mk cells were excluded from cell culture by centrifugation at $150 \times g$ for 10 minutes and PLPs were pelleted from supernatant by centrifugation at $1000 \times g$ for 10 minutes. MkMPs were enriched from supernatant by ultracentrifugation at 25,000 rpm (Beckman Coulter Optima Max Ultracentrifuge) for 1 hour at 4°C.

4.2.5 MiRNA Transfection into CD34+ HSPCs

200,000 CD34+ cells were freshly thawed and cultured in Iscove modified Dulbecco medium (IMDM) supplemented with 20% BIT 9500, and 100 ng/mL SCF. After 3 hours, cells were transfected with 8 μ M of miRNA mimics, non-targeting miRNA (miR-NC), miRNA combination, or without miRNA (No miRNA) by nucleofection

via Amaxa Nucleofector II with program U-08, following the manufacturer protocol. After transfection, cells were cultured in IMDM supplemented with 10% BIT 9500, and 50 ng/mL SCF, and 1 ng/mL IL-3 for up to 13 days. Medium was replaced at day 1 post-transfection. At day 7, 10 and 13, cells were harvested for flow cytometric analysis on CD41, CD42b expression, and total cell count measurements.

4.2.6 Signaling Inhibitor Study

Co-cultures of MkMPs with CD34⁺ cells were setup as described [23, 74]. Briefly, 60,000 fresh CD34⁺ HSPCs were pretreated with signaling inhibitors for 30 minutes. After that, these cells were co-cultured with MkMPs at the concentration of 30 MPs per cell in IMDM supplemented with 10% BIT 9500, and 50 ng/mL SCF for up to 8 days. At day 3, 5 and 8, cells were harvested for flow cytometric analysis on CD41, CD42b, and CD34 expression. Total cell count and Mk count were measured at day 8.

4.2.7 Preparation of Human Platelets and PMPs

Blood for isolation of human platelets was collected by venipuncture from adult human volunteers after providing written informed consent as approved by the Institutional Review Board at the University of Delaware (IRB protocol # 622751-1). Blood was collected from healthy donors and PMPs were prepared as described [74]. Briefly, 50 mL of blood was collected into syringe with ACD buffer (trisodium citrate, 65 mM; citric acid, 70 mM; dextrose, 100 mM; pH 4.4) at a volume ratio of 1:6 (ACD: blood). Following that, blood was centrifuged at $250 \times g$ for 10 minutes and the

platelet rich plasma was isolated from the supernatant. Platelets were then pelleted at $750 \times g$ for 10 minutes, followed by 1 wash with HEN buffer (10 mM HEPES, pH 6.5, 1mM EDTA, 150 mM NaCl) containing 0.05 U/ml apyrase. After that, platelets were resuspended in HEPES-Tyrode's buffer (137 mM NaCl, 20 mM HEPES, 5.6 mM glucose, 1 g/l BSA, 1 mM MgCl₂, 2.7 mM KCl, 3.3 mM NaH₂PO₄). To generate PMPs, platelets were activated by 2 U/mL human thrombin (Sigma), and removed by centrifugation at $1000 \times g$ for 10 minutes. Lastly, PMPs were isolation by ultracentrifugation at 25,000 rpm for 1 hour at 4 °C, resuspended in IMDM medium, and stored at -80 °C.

4.2.8 RNA Extraction and Library Preparation

Total RNA was isolated from 3 biological samples of MkMPs, 2 biological samples of platelet-derived MP (PMPs) and 3 biological samples of platelet like particles (PLPs) by using the miRNeasy micro kit (Qiagen) following by the manufacturer's protocol. RNA concentration was measured by NanoDrop (Thermo Scientific, ND1000) and size distribution of total RNA was analyzed using an ABI Prism 3130XL Genetic Analyzer at the University of Delaware Sequencing & Genotyping Center at Delaware Biotechnology Institute. 2.0~5.0 µg, 1.0~1.5 µg and ~0.5 µg total RNA from PLPs, MkMPs and PMPs, respectively, were used for small RNA library preparation. 8 Small RNA libraries were prepared as described [180] without the step of low molecular mass RNA separation. RNA with 18-40 nt and 40-150 nt was purified by 15% polyacrylamide/urea gels and eluted from gels for library construction using

Illumina TruSeq Small RNA Sample Prep kit according to the manufacturer's protocol. Briefly, RNA was sequentially ligated with 3' and 5' adaptors, reverse transcribed to cDNA using SuperScript III reverse transcriptase (Invitrogen) and cDNA libraries were amplified by PCR (18-40 nt RNA: 14 cycles, 98°C for 10 s, 60°C for 30 s, 72°C for 15 s; 40-150 nt RNA: 16 cycles, 98°C for 10 s, 60°C for 30 s, 72°C for 45 s). Following that, a 6% polyacrylamide hydrogel was used to purify cDNAs with size ranges of 140-160 base pairs (bp) and 160-275 bp derived from 18-40 nt and 40-150 nt input RNA, respectively. Library was pooled together and 20 µL of pooled libraries at a final concentration of 10 nM was sequenced at the University of Delaware Sequencing & Genotyping Center at Delaware Biotechnology Institute using 51 cycles on the Illumina HiSeq2500 DNA sequence analyzer. Small RNA (18-40 nt) was sequenced using 2 lanes.

4.2.9 RNA Sequencing Data Analysis

Sequencing data analysis was provided by Dr. Shawn Polson and Jaysheel Bhavsar from Center for Bioinformatics & Computational Biology at University of Delaware. For small RNA (18-40 nt) sequencing data, a custom bioinformatics pipeline was used to end-trim raw reads to obtain an average Q>30, and to partition the data into miRNA and piRNA size fractions. Only reads where flanking adapter sequence was detected at the 3' end were retained for analysis as they represent full-length sequencing of the molecule. Trimmed and filtered reads were then clustered by identical sequence and each cluster was aligned against human miRNA sequences downloaded from the

miRBase (Release 21) [181]. MiRNA reads were normalized by the number of counted reads per 1,000,000 total reads. Differential expression analysis was performed using the edgeR Bioconductor Package [182]. MiRNA was considered as differentially expressed in MkMPs, PMPs and PLPs when False Discovery Rate (FDR) $P < 0.01$.

4.3 Results

4.3.1 MicroRNAs (miRNAs) in Human Megakaryocyte-derived Microparticles (MkMPs)

We have previously shown that MkMPs were enriched with small RNAs but not ribosomal RNA (rRNA) [23], and these small RNAs play an important role in triggering Mk differentiation of HSPCs [23, 74]. We hypothesize that miRNAs are key components of MkMPs in inducing and/or promoting Mk differentiation. To characterize the miRNA profile, total RNA was extracted from Mks, MkMPs generated from Mks, or platelet-like particles (PLPs) generated from Mks, that were derived from CD34⁺ cells of 3 different donors, or human platelets (PLTs), PLT-derived MPs (PMPs), and small RNA libraries were prepared for next-generation sequencing. 514 and 609, 484, 589, or 530 human miRNAs were identified in Mks, MkMPs, PLPs, PLTs, or PMPs, respectively, as the average expression level of miRNAs (Count Per Million, CPM) was ≥ 1 , while only 154 (out of 609) miRNAs were highly abundant in MkMPs (CPM ≥ 100). The Venn diagram (Figure 4.1) shows

that Mks and MkMPs shared most of the miRNAs (491 miRNAs), while 23 and 118 miRNAs were distinctly expressed in Mks and MkMPs, respectively. Similarly, MkMPs shared 446 or 481 miRNAs with PLTs and their MPs (PMPs), respectively. Notably, PLPs possessed the closest miRNA profile to MkMPs, with 550 shared miRNAs, which could be perhaps explained from the fact that they have a common origin, namely Mk cells.

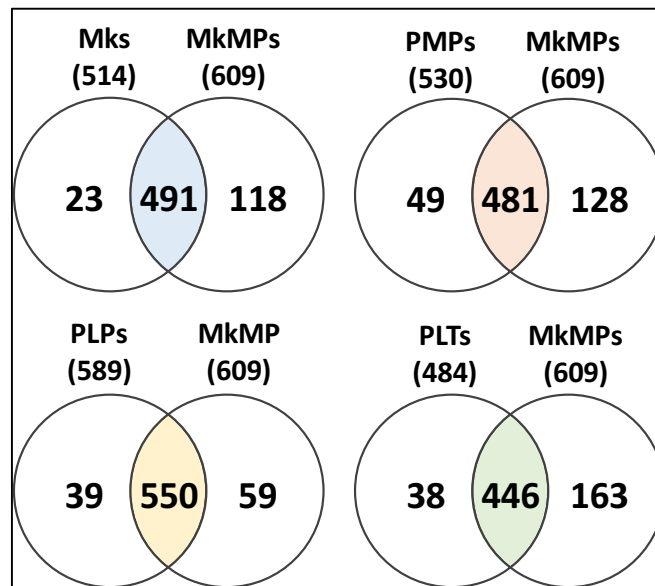


Figure 4.1 Venn diagram showing the number of miRNAs detected (CPM \geq 1) in Mks, MkMPs, PLPs, PLTs, and PMPs, and the number of miRNA shared between MkMPs with others.

To examine the enrichment of miRNA from Mks to MkMPs, we further performed a differential expression analysis, shown in Figure 4.2. The hypothesis for that analysis was that perhaps differential expression against miRNAs in Mk cells or platelets or PMPs would be one possible way to identify miRNAs that might mediate the observed phenotype (ability of MkMPs to induce Mk differentiation of HSPCs),

assuming that some of those differentially expressed miRNAs were also in abundant concentrations in MkMPs. 58 miRNAs were found significantly ($p < 0.01$) and highly (\geq two folds) enriched from Mks into MkMPs, while 90 miRNAs were significantly downregulated (fold changes ≤ 0.5) in MkMPs. Table 4.1 lists the 18 miRNAs which were highly abundant (CPM ≥ 100) and highly enriched in MkMPs. However, only 2 of the miRNAs (mir-19b-1//mir-19b-2_3p (No.46), and miR-181b-1//miR-181b-2 (No.49)) were within top 50 most abundant miRNAs in MkMPs. As the purpose of this study was to identify the miRNA(s) in MkMPs that regulate or mediate Mk differentiation of CD34⁺ HSPCs, and since each of the highly-enriched miRNA listed in Table 4.1 only accounts for less than 0.2% of total miRNA in MkMPs, we hypothesized that these miRNAs are not the most likely mediators of the observed phenotype.

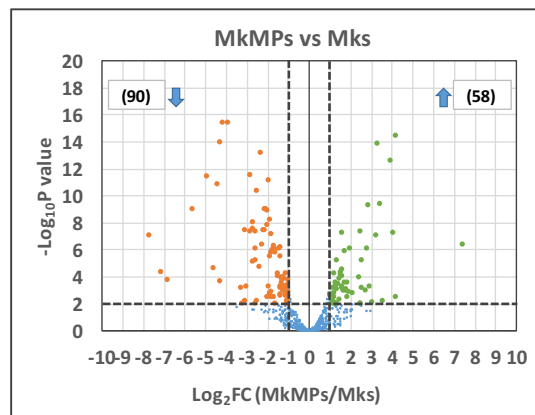


Figure 4.2 Volcano plot showing the results from the differential expression analysis of miRNAs in MkMPs vs. Mk cells. 58 miRNAs were significantly ($p < 0.01$) enriched (fold change ≥ 2) in MkMPs, while the expression level of 90 MkMP miRNAs were significantly lower (fold changes ≤ 0.5) than in Mk cells.

Table 4.1 Highly abundant (CPM >100), significantly enriched ($p < 0.01$; differential expression \geq two-fold) miRNAs in MkMPs compared to Mks.

| miRNA (Gene ID) | MkMPs (CPM) | Mks (CPM) | Fold Change | FDR |
|----------------------------------|--------------------|------------------|--------------------|------------|
| mir-19b-1//mir-19b-2_3P | 1999.33 | 378.86 | 2.43 | 0.00025 |
| mir-181b-1//mir-181b-2 | 1869.99 | 363.50 | 2.37 | 0.00051 |
| mir-378a_3P | 1766.13 | 281.71 | 2.92 | 0.00009 |
| mir-19a_3P | 986.87 | 170.89 | 2.66 | 0.00012 |
| mir-30b | 873.83 | 129.73 | 2.99 | 0.00000 |
| mir-17 | 452.59 | 101.47 | 2.01 | 0.00172 |
| mir-335 | 394.39 | 44.40 | 3.93 | 0.00000 |
| mir-106b | 388.20 | 70.16 | 2.47 | 0.00001 |
| mir-345 | 361.60 | 66.55 | 2.49 | 0.00081 |
| mir-155 | 343.28 | 54.40 | 2.91 | 0.00003 |
| mir-181c | 324.84 | 64.18 | 2.29 | 0.00005 |
| mir-20a | 288.40 | 60.84 | 2.15 | 0.00059 |
| mir-320b-1//mir-320b-2_3P | 266.37 | 47.07 | 2.57 | 0.00027 |
| mir-451a | 190.90 | 27.36 | 3.18 | 0.00000 |
| mir-151b_3P | 152.06 | 23.24 | 2.89 | 0.00006 |
| mir-494_3P | 135.02 | 28.49 | 2.13 | 0.00177 |
| mir-369_3P | 121.11 | 23.72 | 2.23 | 0.00539 |
| mir-376c_3P | 118.30 | 25.94 | 2.03 | 0.00204 |

Next, we hypothesized that miRNAs with high levels of expression (abundance) would be more likely to achieve the observed biological phenotype. Therefore, we listed the top 10 most abundant miRNAs in MkMPs, Mks, PLTs, and PMPs in Table 4.2, and calculated the miRNA profile in MkMPs in terms of their abundance (percent of the total miRNA). The top most abundant 20 miRNAs in MkMPs account for 81.8% of total miRNA, while the top 7 miRNAs account for more than 57% of total miRNA. Figure 4.3 shows the pie chart of these top 7 abundant miRNAs and their percent abundance in MkMPs.

Table 4.2 The top 10 most abundant miRNAs in MkMPs, Mk cells, PLTs, or PMPs

| Mks | | | | MkMPs | | |
|-------------|-------------------------|------------|----------|-------------------------|------------|----------|
| Rank | miRNA (Gene ID) | CPM | % | miRNA (Gene ID) | CPM | % |
| 1 | mir-191 | 231441.16 | 23.1 | mir-486-1//mir-486-2 | 164086.52 | 16.4 |
| 2 | mir-486-1//mir-486-2 | 195802.95 | 19.6 | mir-191 | 117782.38 | 11.8 |
| 3 | mir-99b | 164314.59 | 16.4 | mir-26a-1//mir-26a-2 | 91773.92 | 9.2 |
| 4 | mir-146b | 65671.04 | 6.6 | let-7f-1//let-7f-2 | 68251.10 | 6.8 |
| 5 | mir-26a-1//mir-26a-2 | 39624.87 | 4.0 | mir-92a-1//mir-92a-2_3P | 44479.75 | 4.4 |
| 6 | let-7f-1//let-7f-2 | 23623.34 | 2.4 | mir-126 | 44217.90 | 4.4 |
| 7 | mir-126 | 22642.37 | 2.3 | mir-22_3P | 43151.58 | 4.3 |
| 8 | mir-146a | 21993.07 | 2.2 | mir-21 | 38616.69 | 3.9 |
| 9 | mir-21 | 20196.65 | 2.0 | mir-146b | 34454.68 | 3.4 |
| 10 | mir-148a_3P | 17053.54 | 1.7 | mir-181a-2//mir-181a-1 | 33752.36 | 3.4 |
| | Other miRNAs | | 19.8 | Other miRNAs | | 31.9 |
| PLTs | | | | PMPs | | |
| Rank | miRNA (Gene ID) | CPM | % | miRNA (Gene ID) | CPM | % |
| 1 | mir-191 | 263870.96 | 26.4 | mir-191 | 206137.79 | 20.6 |
| 2 | mir-486-1//mir-486-2 | 80545.84 | 8.1 | mir-486-1//mir-486-2 | 103923.47 | 10.4 |
| 3 | let-7f-1//let-7f-2 | 76283.37 | 7.6 | let-7f-1//let-7f-2 | 94944.80 | 9.5 |
| 4 | mir-99b | 71050.29 | 7.1 | mir-26a-1//mir-26a-2 | 92167.99 | 9.2 |
| 5 | mir-10a | 54138.85 | 5.4 | mir-92a-1//mir-92a-2_3P | 46188.65 | 4.6 |
| 6 | mir-26a-1//mir-26a-2 | 51712.20 | 5.2 | mir-10a | 34589.82 | 3.5 |
| 7 | mir-146a | 43647.11 | 4.4 | mir-181a-2//mir-181a-1 | 31379.42 | 3.1 |
| 8 | mir-92a-1//mir-92a-2_3P | 43032.19 | 4.3 | mir-22_3P | 30645.32 | 3.1 |
| 9 | mir-146b | 25103.57 | 2.5 | mir-21 | 30506.50 | 3.1 |
| 10 | mir-181a-2//mir-181a-1 | 23931.88 | 2.4 | mir-146a | 26543.95 | 2.7 |
| | Other miRNAs | | 26.7 | Other miRNAs | | 30.3 |

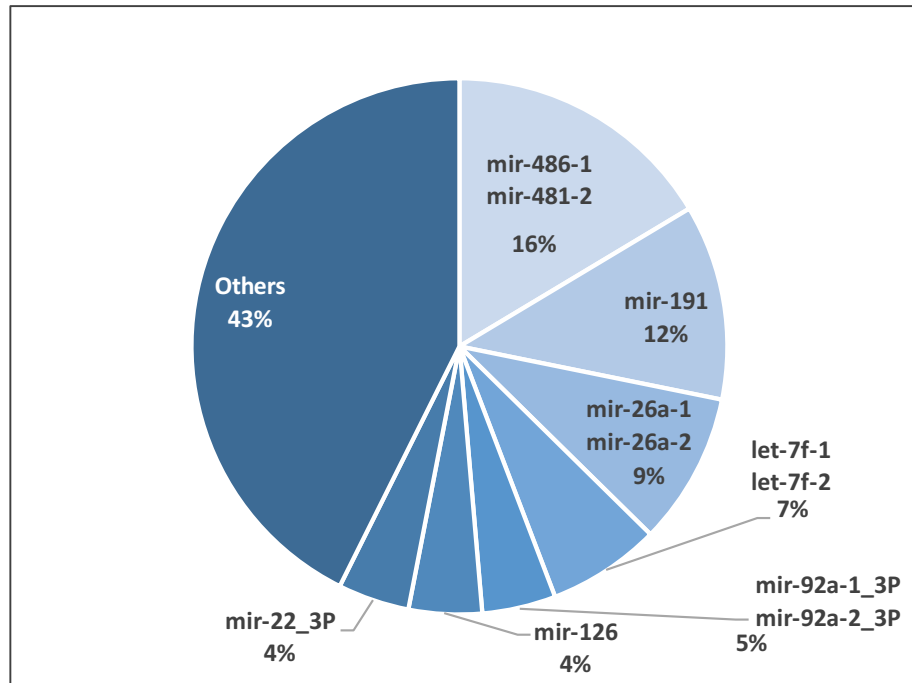


Figure 4.3 Pie chart showing the miRNA distribution in MkMPs. The top seven miRNAs are shown in detail.

4.3.2 Effect of Individual, Most-abundant in MkMPs, miRNAs on Mk Differentiation and Expansion of CD34⁺ HSPCs

From the results shown above, we then investigated the top 7 abundant miRNAs individually, by performing direct transfection of each miRNA mimic into CD34⁺ HSPCs. Briefly, 8 μ M of each miRNA mimic were electroporated into 200,000 CD34⁺ HSPCs, and transfected cells were cultured in minimal medium (IMDM supplemented with 10% BIT and 50 ng/ml SCF, but without thrombopoietin).

Expression of CD34 (an HSPC marker), CD41 (an Mk marker), and CD42b (a mature Mk marker), and cell counts were examined at days 7, 10 and 13. In general, based on the published literature, miRNA concentrations from 1 nanomolar and up to 3.6

micromolar have been used to directly transfect HSPCs for achieving a desirable phenotype [173, 183, 184]. In this study, since the seven miRNAs from MkMP we choose are highly abundant in MkMPs, and due to the fact that multiple MkMPs are taken up by one recipient HSPC, we hypothesized that higher concentrations of these seven miRNAs are delivered to HSPC via MkMPs. In a pilot study, using a miR-486-5p mimic, based on the fact that we had demonstrated the role of miR-486-5p in Mk differentiation of HSPCs [23], we investigated if there is a dose effect of miRNA mimics on the Mk differentiation (CD41 expression) of HSPCs. High (8 μ M) or low (2 μ M) concentrations of miR-486-5p mimic were transfected into CD34⁺ HSPCs. At day 10 post-transfection, 29.4% of cell transfected with 8 μ M miR-486-5p were CD41⁺, while only 21.7% were CD41⁺ from the 2 μ M miR-486-5p transfection, indicating the dose effect of miRNA mimics transfected into HSPCs (Figure C1 in Appendix C). Therefore, we chose 8 μ M of miRNA mimics for the following experiments. As shown in Figs. 4.4A & 4B, transfection of miRNA mimics of miR-486-5p and miR-92a-3p significantly induced and promoted Mk differentiation of CD34⁺ HSPCs, resulting in 38.8% and 36.6% of the cells expressing CD41 at day 13, respectively. Moreover, the Mk number at day 13 was significantly increased upon transfection of miR-486-5p or miR-92a-3p mimics compared to “No miRNA” control (Figure 4.4C). However, miR-22-3p (Figure 4.4B) and the other four miRNA mimics (miR-191-5p, miR-26a-5p, let-7f-5p, and miR-126-5p, data not shown) showed no statistically significant effect on Mk differentiation. Notably, compared to the positive control (CD34⁺ HSPC cultures supplemented with Tpo), which resulted in 56.6% of

the cells expressing CD41 by day 13, the miR-486-5p mimic alone achieved more than 50% of Tpo's effect in terms of percent CD41 expression. Next, we examined the effect of each miRNA mimic on cell expansion. As shown in Figure 4.4D, miR-22-3p significantly increased the total cell number by 78.0% and 49.2%, compared to "No miRNA" and "miR-NC" controls, respectively. Together, these results suggest that miR-486-5p and miR-92a-3p play a role in Mk differentiation, while miR-22-3p promotes total cell expansion deriving from HSPCs.

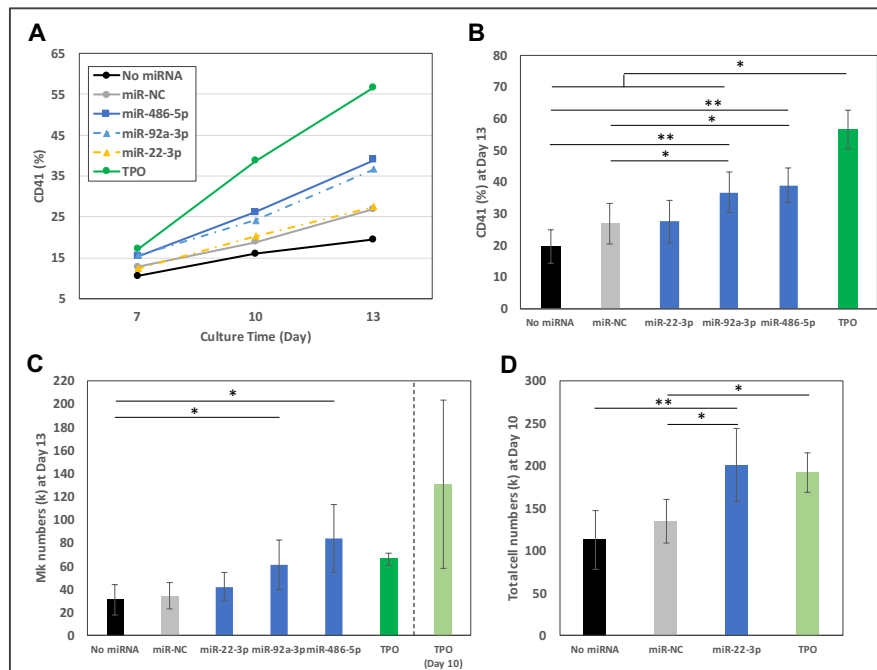


Figure 4.4 The effect of single miRNAs on Mk differentiation. CD34⁺ HSPCs were transfected with miRNA mimics, miRNA negative control (miR-NC), or without miRNAs (No miRNA), and cells were cultured in minimal medium (IMDM supplemented with 10% BIT and 50 ng/ml SCF) without Tpo. Cells cultured in Tpo-supplemented medium (100 ng/ml) served as positive control (TPO). Cells were harvested for flow cytometric analysis for (A, B) CD41 expression at days 7, 10 and 13. (C) Mk numbers, or (D) total cells numbers were measured at day 13 or day 10, respectively. Error bars in (B), (C), and (D) represent the SEM of six biological replicates. * $p < 0.05$, ** $p < 0.01$.

4.3.3 Effect of Combinations of the Most-abundant in MkMPs miRNAs on Mk Differentiation and Expansion of CD34+ HSPCs

Combinations of small RNAs (including siRNAs or miRNAs) have been shown to improve cell proliferation [185], and alter cell phenotypes [186]. Here, we hypothesized that combinations of miRNAs enriched in MkMPs would induce and promote Mk differentiation of CD34+ HSPCs. Table 4.3 list the combinations of the top 7 most abundant miRNAs in MkMPs (shown in Figure 4.3). The level of each miRNA was based on the relative abundance in MkMPs. For example, C1 contains all 7 miRNAs, while C2 is comprised of 6 miRNAs (without mir-486-5p), similarly for C3 to C8. Similar to the study of individual miRNAs, the pre-made miRNA combinations were then transfected into 200,000 CD34+ HSPCs, and the culture was maintained for 13 days in minimal medium (IMDM supplemented with 10% BIT and 50 ng/ml SCF) without Tpo. As shown in Figure 4.5A & 5B, two miRNA combinations (C2 and C7) significantly enhanced Mk differentiation of CD34+ HSPCs with 40% and 42% of the cells being CD41+ at day 13, respectively. The number of Mk cells at day 13 increased by up to 116% from the effect of miRNA combination C2, and 95.0% from C7 (Figure 4.3.5C). Moreover, C2 also significantly increased total-cell expansion by 33% and 37% compared to the “No miRNA” and “miR-NC” controls at day 13, respectively. Surprisingly, the combination of all 7 top miRNAs (combination C1) did not promote Mk differentiation or cell expansion, and neither did the miRNA combinations C3, C4, C5, C6, or C8.

Table 4.3 List of the combination of miRNA mimics

| Candidates | C1 | C2 | C3 | C4 | C5 | C6 | C7 | C8 |
|------------|----|----|----|----|----|----|----|----|
| miR-486-5p | | | | | | | | |
| miR-191-5p | | | | | | | | |
| miR-26a-5p | | | | | | | | |
| let-7f-5p | | | | | | | | |
| miR-92a-3p | | | | | | | | |
| miR-126-5p | | | | | | | | |
| miR-22-3p | | | | | | | | |

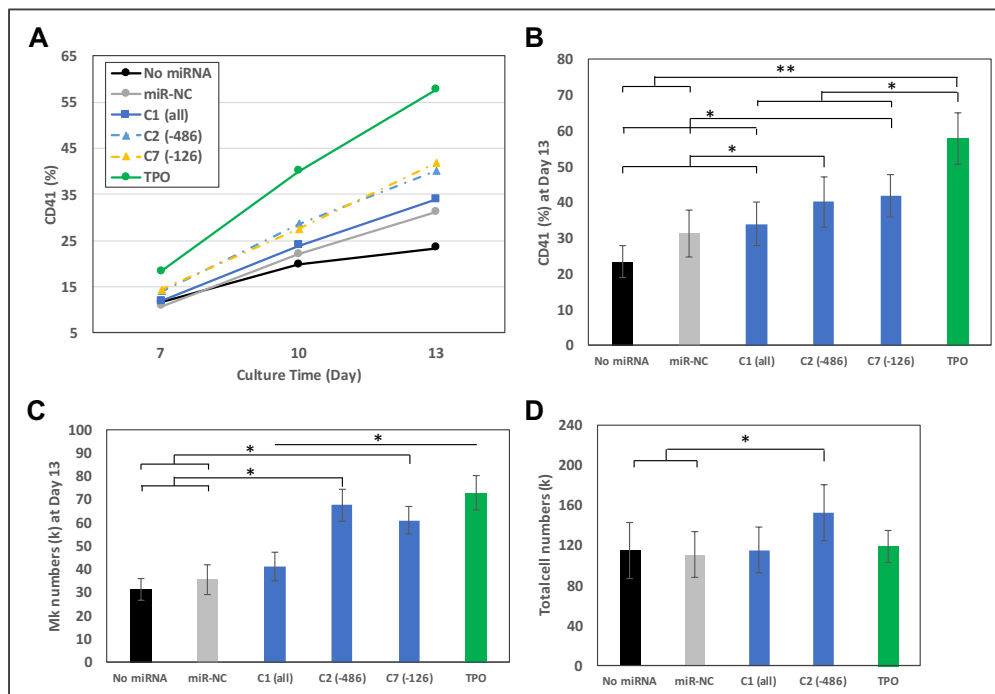


Figure 4.5 Effect of miRNA combinations on Mk differentiation. CD34⁺ HSPCs were transfected with the miRNA combination listed in Table 4.3.3, or miRNA negative control (miR-NC), or without miRNAs (No miRNA), and cells were cultured in minimal medium (IMDM supplemented with 10% BIT and 50 ng/ml SCF) without Tpo. Cells cultured in Tpo-supplemented medium served as positive control (TPO). Cells were harvested for flow cytometric analysis for (A, B) CD41 expression at day 7, 10 and 13. (C) Mk numbers, or (D) total cells numbers were measured at day 13. Error bars in (B), (C), and (D) represent the SEM of six biological replicates. * $p < 0.05$, ** $p < 0.01$

4.3.4 Outcomes from Using of Specific Pathway Inhibitors Suggest that JNK, p38, PI3K, and mTOR Signaling Regulates MkMP-induced Mk

Differentiation of HSPCs

Multiple signaling pathways have been proposed and identified as being involved in Tpo-induced signaling [187, 188], and notably signaling through as Jak/STAT [189] and PI3K/Akt/mTOR [190] signaling. Within the mitogen-activated protein kinase (MAPKs) family, the MEK-ERK1/2 (extracellular signal-related kinases 1 and 2) signaling pathway has been shown to play an important role in Tpo-induced Mk development [191], while p38-MAPK was shown to be involved in TPO-mediated HSC expansion [192] and erythropoiesis [193]. The role of JNK-MAPK in Tpo-induced megakaryopoiesis remains unknown [194]. Here, we aimed to probe the signaling pathway(s) engaged by MkMPs to enable Mk differentiation of CD34⁺ HSPCs. Briefly, CD34⁺ HSPCs were pretreated with various inhibitors of chosen signaling pathways (JNK, p38, MEK, Jak2, STAT3, PI3K, Akt and mTOR inhibitors, Table 4.4) for 30 minutes before they were co-cultured with MkMPs at the ratio of 10 MkMPs/cell. CD41, CD42b, CD34 expression, and cell counts were measured at days 3, 5, 7, and 12. The concentration of inhibitors and treatment times were chosen based on published studies [195, 196]. As shown in Figure 4.6A, SP600125 (JNK inhibitor) or rapamycin (mTOR inhibitor) significantly suppressed Mk differentiation and decreased CD41 expression at day 7 from 46.7% (MkMP) to 36.2% (JNK) and 31.2% (mTOR), respectively, while SB203580 (p38 inhibitor) significantly suppressed CD41 expression from 55.1% (MkMP) to 48.6% (p38) at day 12, compared to MkMP

control. Moreover, SP600125 resulted in a higher fraction of cells expressing CD34 compared to MkMP or vehicle controls (Figure 4.6B). LY-294002 (PI3K inhibitor) and rapamycin suppressed Mk maturation by decreasing CD42b expression from 35.6% (MkMP) to 12.5% (PI3K) and 13.8 % (mTOR) at day 12, respectively, compared to the MkMP control (Figure 4.3.6C). Furthermore, treatment with SP600125, LY-294002 or rapamycin significantly inhibited cell growth and decreased total cell numbers by 88.4%, 85.4%, or 83.3% at day 7 of culture, respectively (Figure 4.6D). AG-490 (Jak2 inhibitor) and WP1066 (STAT3 inhibitor) were toxic to HSPCs and induced cell apoptosis. Taken together, these results suggest that MkMP induced Mk differentiation of HSPCs through multiple signaling pathway including JNK-MAPK, p38-MAPK, PI3K, and/or mTOR signaling pathways (Figure 4.7).

Table 4.4 List of signaling inhibitors, their targets, and concentrations used [194-196]

| Signaling Inhibitor | Target | Pathway | Concentration |
|----------------------------|--------------------|----------------|----------------------|
| SP600125 | JNK | MAPK | 10 uM |
| SB203580 | p38 | | 10 uM |
| PD98059 | p44/p42-MEK-ERK1/2 | | 10 uM |
| AG-490 | Jak2 | Jak/STAT | 1 uM |
| WP1066 | STAT3 | | 0.1 uM |
| LY-294002 | PI3K | PI3K/Akt/mTOR | 10 uM |
| Wortmannin | Akt | | 10 uM |
| Rapamycin | mTOR | | 10 uM |

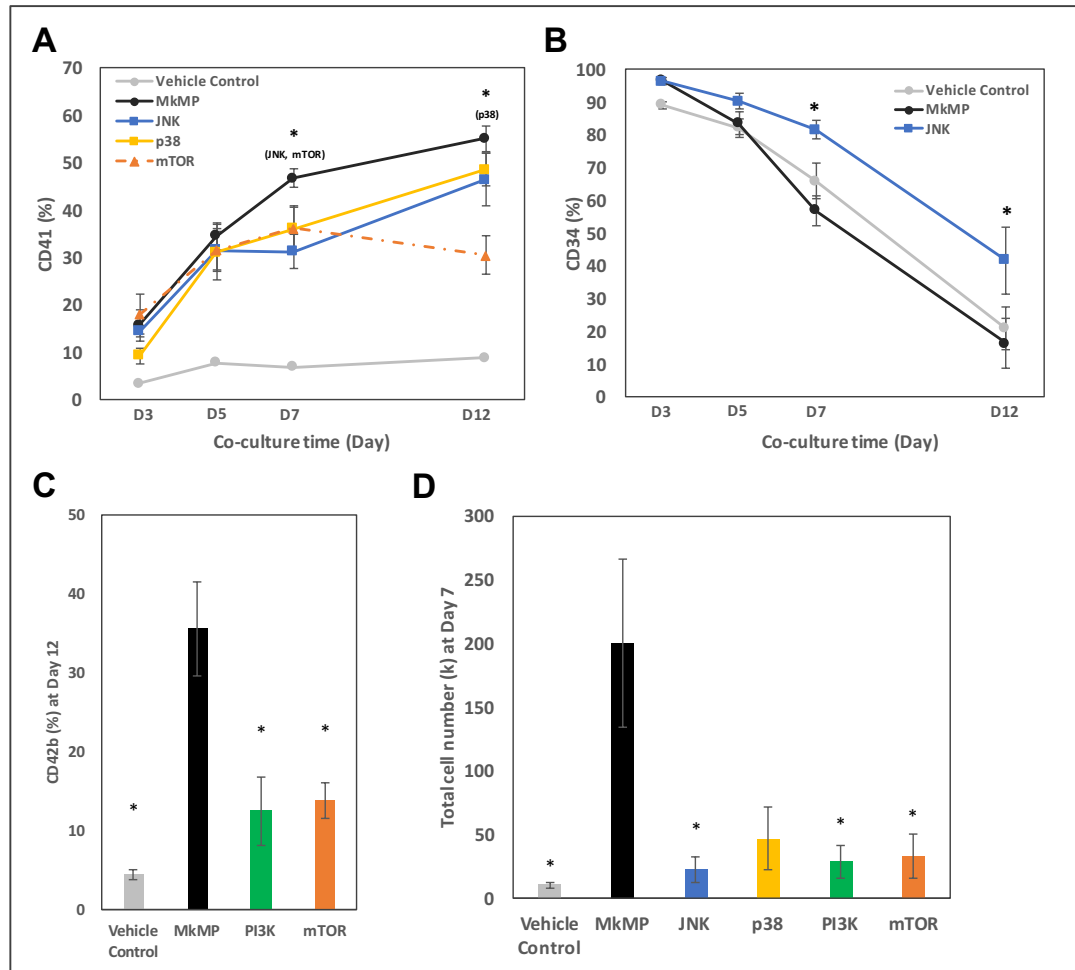


Figure 4.6 Impact of signaling inhibitor on MkMP-induced Mk differentiation. CD34⁺ HSPCs were pretreated with a signaling inhibitor, or solution without an inhibitor (MkMP control), and were co-cultured with MkMPs or vehicle control. Cells were harvested for flow cytometric analysis for (A, B) CD41 or CD34 expression at days 3, 5, 7, or 12, or (C) CD42b expression at day 12. (D) Total cell numbers were measured at day 7. Error bars in (C), and (D) represent the SEM of 3-4 biological replicates. * $p < 0.05$ (compared to MkMP control unless specified.)

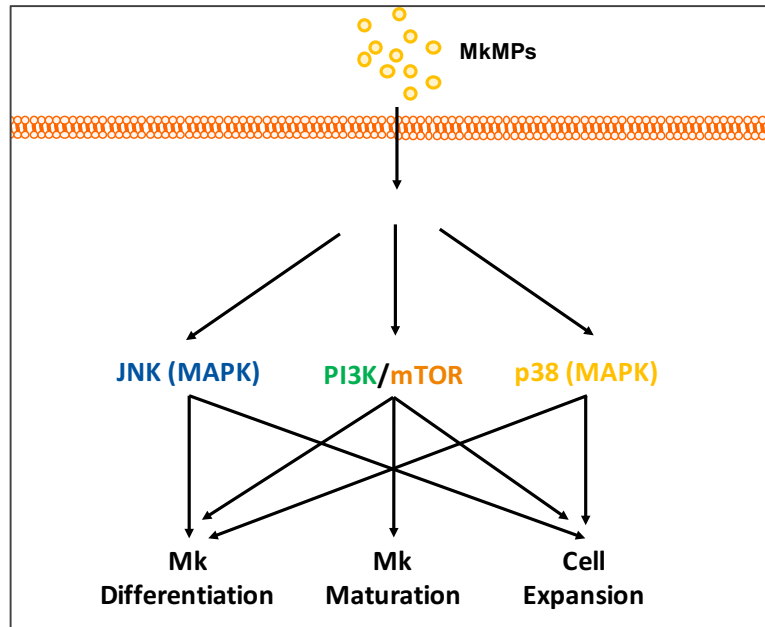


Figure 4.7 Proposed signaling pathways in MkMP-induced Mk differentiation.

4.3.5 MiR-486-5p Inhibitor Suppressed MkMP-induced Mk Differentiation of CD34+ HSPCs

We have shown above that transfection of CD34+ cell with the miR-486-5p mimic induced Mk differentiation of CD34+ HSPCs. We have also demonstrated MkMPs loaded with additional exogenous miR-486-5p mimic enhanced CD41 expression after 8 days of co-culture with CD34+ HSPCs (Figure 3.6 & Ref.[54]). To further pursue the role of miR-486-5p in its ability to induce Mk differentiation of CD34+ cells, we performed a loss-of-function experiment by loading of a miR-486-5p inhibitor into MkMPs. Briefly, MkMPs were loaded with 4 μ M of a miR-486-5p inhibitor by electroporation and were co-cultured with CD34+ HSPCs for 8 days. CD41 expression was measured by flow cytometry at days 3, 5, and 8. As shown in Figure 4.8, CD41

expression were significantly suppressed by 6.2% and 5.3% at day 5 and 8 with miR-486-5p-inhibitor-loaded MkMPs, respectively. However, the delivery of the miR-486-5p inhibitor had minimal effects on the total cell number or Mk number (data now shown). These results further support the role of the native, in MkMPs, miR-486-5p in inducing Mk differentiation of CD34+ HSPCs.

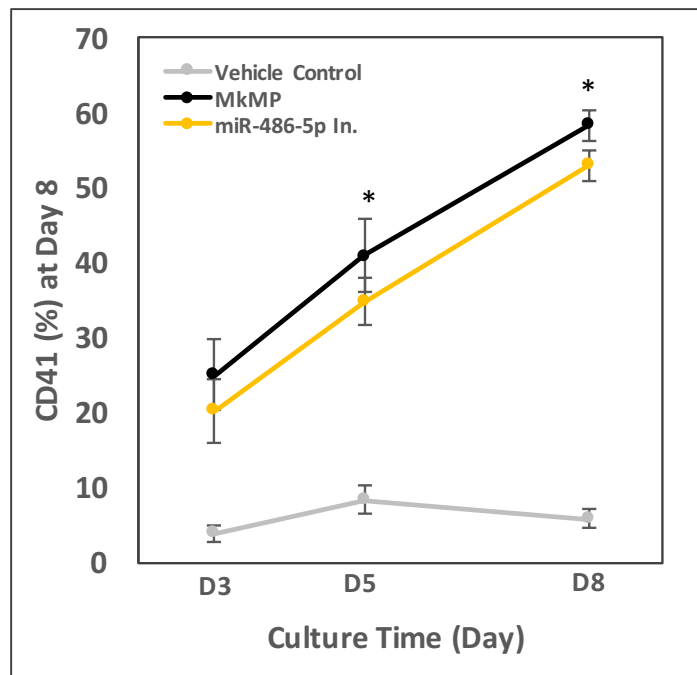


Figure 4.8 Co-culture of miR-486-5p inhibitor-loaded MkMPs with CD34+ HSPCs. The fraction of cells expressing CD41 was measured by flow cytometry on days 3, 5, and 8. Error bars represent SEM of six biological replicates. * $p < 0.05$ (compared between MkMP and miR-486-5p In.)

Acknowledgements

I would like to acknowledge and thank Jinlin Jiang of the Papoutsakis lab for his expertise and assistance with the RNA sequencing preparation and analysis performed in this study.

Chapter 5

ROLE OF P53 AND TRANSCRIPTION-INDEPENDENT P53-INDUCED APOPTOSIS IN SHEAR-STIMULATED MEGAKARYOCYTIC MATURATION, PARTICLE GENERATION, AND PLATELET BIOGENESIS

The origin of idea of this work and the major experiments were performed by Dr. Stephanie Luff. The experiments including ELISA assay in Figure 5.1 and Figure 5.2, immunoblotting in Figure 5.3A, qRT-PCR in Figure 5.4E, microparticle (MP) analysis in Figure 5.5B and co-culture assay in Figure 6 were performed by me. I did a substantial amount of writing and editing of the published paper, and work with my advisor to respond to the reviewer comments in the two rounds of revisions.

5.1 Background

Megakaryocytes (Mks) are large, polyploid cells that reside in the bone marrow (BM) and differentiate from CD34⁺ hematopoietic stem and progenitor cells (HSPCs). As they mature, Mks migrate to the endothelial lining of BM sinusoids where, through gaps of the endothelium, they extend proplatelets (PPTs) into circulation [197, 198]. PPTs mature in circulation, form platelet-like particles (PLPs) leading eventually to the production of platelets, the small anuclear blood cells that regulate thrombosis, vascular repair, and immune responses [199, 200]. Understanding Mk differentiation and platelet biogenesis is important for creating safe and effective therapies for

thrombocytopenic diseases, as well as for developing efficient production of platelets *ex vivo*. The demand for donor-derived platelets for transfusion continues to grow [201]. Platelet-like particles (PLPs) produced *ex vivo* would bypass the dependency on blood donors, significantly decrease the risk of contamination with blood-borne pathogens, and prevent alloimmunization to transfused platelets. Current *ex vivo* PLP production methods have low yield, which would make generating platelet doses for transfusion prohibitively expensive [202]. Understanding how Mks produce platelets *in vivo* could help to replicate the process for affordable, high-yield *ex vivo* PLP generation.

It is now firmly established that biomechanical forces are an important physiological factor in platelet biogenesis [74, 203, 204]. Notably, Mks experience complex biomechanical forces as they deform to penetrate gaps of the BM-sinusoid wall, and shear stresses upon exposure to blood flow as they extend PPTs into circulation. We have shown [74] that shear forces of physiological level accelerate DNA synthesis of immature Mks, promote phosphatidylserine (PS) externalization and caspase-3 activation, and dramatically enhance the generation of PPTs, PLPs, and Mk microparticles (MkMPs), thus promoting the overall process of thrombopoiesis. MkMPs are the most abundant microparticles (MPs) in circulation [41], and have been found to target HSPCs to induce them into Mk differentiation [23, 74]. Thus, MkMPs may potentially serve as platelet substitutes [23, 74]. Therefore, understanding the process of shear-induced thrombopoiesis and MkMP biogenesis is of both practical and fundamental importance.

In our previous report published by Dr. Luff and Papoutsakis, it was shown that Mk maturation in response to shear is mediated by transcription factor AP-1 via mitogen-activated protein kinase (MAPK) mechanotransduction [205]. However, it is not yet known what regulates the cellular, apoptotic-like processes leading to Mk fragmentation in response to shear [74]. This is the focus of this present study: to examine the role of transcription factor p53 in the response of Mks to shear as it affects Mk maturation and the associated apoptotic-like processes. We discuss next why we chose to focus on p53 in this response.

Our lab has previously demonstrated that the p53 is an important regulator of megakaryopoiesis, the differentiation of HPSCs into Mks leading to mature Mks. Specifically, Furhken, *et al.* determined that p53 is responsible for controlling polyploidization and the transition to endomitosis (mitotic cycle without cytokinesis) in the megakaryocytic CHRF cell line by preventing cell cycling and stimulating apoptosis [206]. Apostolidis, *et al.* confirmed these findings *in vivo* in p53 knock out (KO) mice [207], and, in a subsequent study proposed a transcriptional regulon (including the cell cycle-regulator p21 and the apoptosis inducer Bax) to explain how p53 controls these processes [208]. The mechanism by which p53 selects the promoters of genes for either cell cycle arrest or apoptosis depends on specific post-translational modifications, and notably acetylation [209]. Acetylation at K320 drives p53 to bind to the promoters of genes for cell cycle arrest, while acetylation at K373 leads to the binding of p53 at apoptotic promoters. Acetylation at these two Lysine residues, in addition to K382, has been linked to the shear stress response of

endothelial cells (ECs) [210]. K320 and K373 were deacetylated in response to shear flow in ECs, while there was increased acetylation at K382 [210]. Therefore, we hypothesized that acetylation of p53 at these sites may also occur in the Mk shear stress response.

During Mk maturation, several apoptotic regulators are engaged, altering cellular processes and structures including the plasma membrane, cytoskeleton, and nucleus [211] by activating a set of cysteine proteases known as caspases. Caspases can be activated by both intrinsic and extrinsic apoptotic pathways [212], both of which are regulated by p53 in either a transcription-dependent or -independent manner [213, 214]. Chipuk, *et al.* demonstrated that p53 induces transcription-independent p53-induced apoptosis (TIPA) by directly binding to Bax and activating it, leading to its accumulation in the mitochondria membrane and subsequent initiation of the intrinsic apoptotic pathway [214]. The main factor determining whether p53 is nuclear or cytoplasmic is its acetylation status [215]. Not only is p53 acetylation important for its nuclear export, but also for its interaction with Bax [216, 217]. Yamaguchi, *et al.* found that acetylation at K320, K373, and K382 is necessary for p53 to elicit TIPA [216]. Given that TIPA is linked to Caspase 3 activity [216] and that our lab has previously demonstrated that Caspase 3 is important in the shear-stimulated biogenesis of PPTs, PLPs, and MkMPs, we hypothesized that TIPA may be directly involved in this process. Additionally, as Caspase 9 mediates Caspase 3 activation, we hypothesized that Caspase 9 is the intermediary that links TIPA to the Mk shear stress phenotype. For the first time, we show that shear flow stimulates Bax-p53 binding,

cytochrome c release, and Caspase 9 activation in Mks, and that cytoplasmic p53 plays a role in the biogenesis of Mk particles.

5.2 Materials and Methods

5.2.1 Megakaryocytic Culture of CD34+ Hematopoietic Stem Cells and the CHRF-288-11 Megakaryoblastic Cell Line

Wild-type and p53-KD CHRF-288-11 (“CHRF”) cells were cultured as previously described [158, 207] for either 3 or 4 days following PMA stimulation. We confirmed that the KD CHRF cells had undetectable levels of p53 through western blot analysis (Figure D1 in Appendix D.). Primary stem cell-derived Frozen human G-SCF mobilized peripheral blood CD34+ cells (Fred Hutchinson Cancer Research Center) were cultured as described [103, 205].

5.2.2 Shear Stress Experiments

For primary stem-cell derived Mks, cells were seeded into flow slides (μ -Slide I^{0.6} Luer, Ibidi) coated with vWF (Haematologic Technologies) at 250,000 cells per slide at either day 8 or 11 [74, 205]. On day 9 or 12, cells were subjected to shear flow that resulted in shear stress levels of either 1.0 dyn/cm² for 2 hours (for acetyl-p53 experiments) or 2.5 dyn/cm² for 30 min (for all other experiments) using a syringe pump system established by Jiang, *et al* [74] and described in our previous study [205]. These shear levels and exposure times were examined in our previous study and

are within the physiological ranges of shear Mks likely experience in the BM and lung vasculature [74]. The longer time point for probing p53 acetylation levels was chosen to ensure that entire acetylation pattern was captured, given that removal from MDM2 and phosphorylation are prerequisites to acetylation [218]. 30 min represents the time needed for trans-sinusoidal migration of murine Mk fragments into circulation [203] and is sufficient for platelet biogenesis [74]. Therefore, we performed most experiments for this duration. The respective shear flow rates for either 30 or 120 min were chosen based on previous work from our lab [74]. For all CHRF experiments, cells were seeded into the fluidic chambers one day prior to shear flow without the vWF coating (due to their increased adherence to plastic surfaces compared to primary Mks). At day 3 or 4, cells were subjected to shear flow that resulted in shear stress levels of 2.5 dyn/cm^2 for 30 min.

5.2.3 Immunofluorescence Assays

Immunofluorescence staining was used for protein quantification in place of Western Blot analysis due to the low numbers of Mks retrieved after shear flow that result in sub-microgram total protein lysate, and scaling up the system was not practical. Thus, immunofluorescence coupled to MFI (mean fluorescent intensity) quantification was chosen for quantitating the levels of several proteins. Immunofluorescence staining was performed as previously described [205, 219]. Cells were fixed and stained within the flow chamber to retain morphological structures. Primary antibodies used were: anti-acetyl-p53 K320 (EMD Millipore #06-1283), anti-acetyl-p53 K373 (EMD

Millipore #04-1137 or 06-916), anti-acetyl-p53 K382 (EMD Millipore #04-1146), anti-active Caspase 9 (Santa Cruz #22182), normal mouse IgG (Santa Cruz #sc-3879), normal rabbit IgG (Santa Cruz #sc-3888), and normal goat IgG (Santa Cruz #sc-2028). Secondary antibodies were anti-mouse Alexa Fluor 488 (Life Technologies #A11017), anti-rabbit Alexa Fluor 647 (Life Technologies #A21245), and anti-mouse Alexa Fluor 647 (Life Technologies #A21235). Quantification was performed within the cell perimeter only; to delineate the cell borders, 5 μ M of Syto13 (Life Technologies #S7575) or Syto40 (Life Technologies #S11351) was used. Fluidic chambers were visualized using a Zeiss LSM 780 confocal microscope with Plan-Apochromat 40x/1.4 oil DIC objective and Zeiss Zen software. Immunofluorescence was quantified using Velocity software (PerkinElmer). For cells harvested from the fluidic chambers, analysis for protein quantification was performed on the FACS Aria II flow cytometer.

5.2.4 Western Blot Analysis

Mks from day 9 and day 12 culture under static or shear-exposed condition were lysed and total protein were isolated. SDS-Polyacrylamide gel electrophoresis was performed using ExpressPlus 4-20% Bis-Tris polyacrylamide gels (Genscript #M42012) and the Mini-PROTEAN Tetra Vertical Electrophoresis Cell (Bio-Rad #1658004), followed by transfer onto nitrocellulose membrane (Genscript #L00224A60) via the Owl VEP-2 Mini Tank Electroblotting System (ThermoFisher). Membranes were blocked using 5% milk (w/v) in TBST for 1 hr at room temperature. Immunoblotting for Caspase 9 with GAPDH as a reference protein was performed

using anti-caspase 9 (Abcam #ab185719), and anti-GAPDH (Santa Cruz #sc-47724) primary antibodies, and anti-rabbit Alexa Fluor 647 (Life Technologies #A21245) and anti-mouse Alexa Fluor 488 (Life Technologies #11017) secondary antibodies.

5.2.5 Transfection of Primary Stem Cell-derived Mks

Overexpression of wild-type p53 was achieved through nucleofection using protocol T-003 on the Amaxa Nucleofector II (Lonza). “pCMV-Neo-Bam p53 wt” was a gift from Bert Vogelstein (Addgene plasmid #16434). The p53 insert was sequenced using Sanger sequencing (University of Delaware Sequencing and Genotyping Center). The S46A amino acid substitution was achieved by introducing a T136G nucleotide mutation using the Agilent QuikChange Lightning kit (#210518) with Forward (5'-TCAATATCGTCCGGGGCCAGCATCAAATCATCCAT-3') and Reverse (5'-ATGGATGATTTGATGCTGGCCCCGGACGATATTGA-3') mutagenic primers. Knock down of p53 in primary Mks at day 12 was achieved by transfecting CD61+ Mks at day 9 with the InvivoGen psiRNA-p53 plasmid (#psirna42-hp53) that expresses siRNA targeting p53 mRNA. Day 9 was chosen because the manufacturer suggested it takes 2 days for sufficient expression. We determined that transfection of day 11 primary stem-cell derived Mks with a control GFP plasmid achieves 70% GFP+ on day 12 (Figure D2 in Appendix D.). Since the psiRNA-p53 plasmid does not contain a selectable marker for human cells, we performed the experiments with the assumption that a majority of Mks were successfully transfected given the 70% efficiency we can achieve. Transfected primary stem cell-derived Mks will be referred

to as “p53-KD Mk”, while the previously-establish KD CHRF cells [206] will be referred to as “p53-KD CHRF”.

5.2.6 Sandwich ELISAs

We performed an ELISA to confirm that p53 protein decreased following transfection of the psiRNA-p53 plasmid and that p53 protein increased following transfection of the “pCMV-Neo-Bam p53 wt” plasmid. Briefly, monoclonal mouse anti-p53 (DO-1) antibody (Santa Cruz #sc-126) was immobilized to the surface of a well in a 96-well plate (CELLTREAT #229196) in PBS buffer at room temperature (“capture antibody”). Following two washes with PBS, blocking of the remaining protein-binding sites was achieved using 5% milk (w/v) in TBST. The lysates from each sample were then incubated in each well at 37C for 90 min. Polyclonal rabbit anti-p53 (Santa Cruz #sc-6243) was then incubated in each well at room temperature for 2 hr (“probing antibody”). Following 4 washes with PBS, goat anti-rabbit Alexa Fluor 488 (Life Technologies #A11070) was incubated in each well for 1 hr. Fluorescent signal was measured using the PerkinElmer Victor 3V plate reader using an excitation/emission configuration for GFP. We also performed an ELISA to confirm that the p53-S46A mutant had decreased Bax binding. We cultured PMA-treated CHRF for 4 days and following shear-flow exposure (2.5dyn/cm^2 for 30 min), cells were harvested and lysed in the Co-IP buffer described above. We the set up three samples to measure p53-Bax interaction: Bax capture followed by p53 probing (“Bax-p53”), p53 capture followed by Bax probing (“p53-Bax”), and p53 capture followed

by p53 probing (“p53-p53”). The first two samples were designed to measure how much p53 and Bax were bound to one another while the third was to measure the total levels of p53 in the lysate. For the Bax-p53: anti-Bax antibody (Santa Cruz #sc-7480) was immobilized to the well surface, followed by incubation with the lysate, then incubation with polyclonal rabbit anti-p53 antibody (Santa Cruz #sc-6243) and goat anti-rabbit Alexa Fluor 488 secondary antibody (Life Technologies #A11070). For p53-Bax: monoclonal mouse anti-p53 antibody (Santa Cruz #sc-126) was immobilized to the well surface, followed by incubation with the lysate, then incubation with anti-Bax antibody (Santa Cruz #sc-7480) and goat anti-mouse Alexa Fluor 488 secondary antibody (Life Technologies #A11017). For p53-p53: 4% SDS (w/v) was added an aliquot of lysate to dissociate any complexes to allow for easier measurement of total p53. Monoclonal mouse anti-p53 antibody (Santa Cruz #sc-126) was immobilized to the well surface, followed by incubation with the lysate, then incubation with polyclonal rabbit anti-p53 antibody (Santa Cruz #sc-6243) and goat anti-rabbit Alexa Fluor 488 secondary antibody (Life Technologies #A11070).

In other experiments, we performed an ELISA to confirm the expression of HDAC1, p300, PCAF, and acetyl-p53. Capture antibodies include: anti-HDAC1 (Santa Cruz #sc-6299), anti-p300 (Santa Cruz #sc-32244), anti-PCAF (Sigma Aldrich #SAB1404637), and anti-p53 (Santa Cruz #sc-126). Probing antibodies include: anti-HDAC1 (Santa Cruz #sc-7872), anti-p300 (Santa Cruz #sc-584), anti-PCAF (Santa Cruz #sc-8999), anti-acetyl-p53 K320 (EMD Millipore #06-1283), anti-acetyl-p53 K373 (EMD Millipore #06-916), and anti-acetyl-p53 K382 (Cell Signaling

Technology #2525). Secondary antibody used for all sandwiches was goat anti-rabbit Alexa Fluor 488 secondary antibody (Life Technologies #A11070).

5.2.7 qRT-PCR Assay on MDM2 Expression

To examine the effect of overexpression of wild-type p53 or mutant p53 (“p53-S46A”) on the transcriptional activity of p53, 10⁶ d11 Mks were transfected with both plasmids individually with program T-003 of the Amaxa Nucleofector II (Lonza). Transfection without any additional plasmids was used as negative control (“WT”). After 24 h, total RNA was isolated from each culture with the Qiagen miRNeasy Kit following the manufacturer’s specification. After RNA extraction, 1 µg of total RNA from each group were reversed transcribed via the cDNA Reverse Transcription Kit (Applied Biosystems). qPCR assays for *MDM2* and *GAPDH* expression were performed with iTaq Universal SYBR Green Supermix (Bio-Rad) and the following primers: Forward (5’-GAGCAGGCAAATGTGCAATAC-3’), Reverse (5’-TGGTCTAACCAGGGTCTCTT-3’) for *MDM2*, and Forward (5’-CCCTTCATTGACCTCAACTACA-3’), Reverse (5’-ATGACAAGCTTCCCGTTCTC-3’) for *GAPDH*. The *MDM2* expression levels were quantified using the Livak method with normalization to the expression of *GAPDH* as a reference gene.

5.2.8 Annexin V Binding Assay

Following shear-flow exposure, Mks were harvested from the fluidic slides using Accutase (ThermoFisher #A1110501) for 10 min at 37°C. Cells were washed twice in Annexin Binding Buffer (10 mM HEPES, 140 mM NaCl, 2.5 mM CaCl₂, pH 7.4). Cells were then stained with anti-annexin V-PE (BD #560930) at 4°C for 15 min and analyzed by flow cytometry (FACS Aria II, BD Biosciences).

5.2.9 Mk Particle Assays and Co-culture with Hematopoietic Stem Cells

PPTs, PLPs, and MkMPs were harvested as previously described [74, 205]. PLP quality was measured by Fibrinogen binding, as previously described [74, 205]. To assess MkMP quality, co-culture experiments were performed as previously described [74]. We chose to use CHRf-derived MPs (CMPs) because of the significant reduction of p53 (to undetectable levels) in the p53-KD CHRf strain. Following 3 days of PMA treatment, CMPs were harvested from static culture using ultracentrifugation at 25000 rpm for 30 min at 4°C and co-cultured with HSCs for 8 days. Cells were co-cultured in IMDM, 10% (v/v) BIT9500 (Stemcell #09500), 50ng/mL SCF (Peprotech), and 1X antibiotic antimycotic (ThermoFisher). At day 8, a ploidy assay was performed as previously described [206].

5.3 Results

5.3.1 Shear-forces Induce Increased Acetylation of Transcription Factor p53 in Immature and Mature Mks

To examine whether p53 is differentially acetylated following exposure to shear flow and how it compares to what is currently known about p53 acetylation in response to shear in ECs (i.e. increased acetylation at K382 and decreased acetylation at K320 and K373) [210], we performed quantitative immunofluorescent confocal microscopy to measure the expression of acetylated p53 and determine its subcellular localization. In immature (day 9) Mks, we found significantly more acetylation of p53 at K320, K373, and K382 following shear-flow exposure by both quantitative confocal microscopy and an ELISA (Figure 5.1A). At both time points, Acetyl-p53 K320 was mostly localized in the nucleus (Figure 5.1B), under both static and shear flow conditions. A higher fraction of K373 is localized in the cytoplasm (Figure 5.1B), and upon shear flow, more K373 moves to the cytoplasm (less co-localization with DNA; Figure 5.1C). K382 was equally distributed between the nucleus and the cytoplasm (Figure 5.1B).

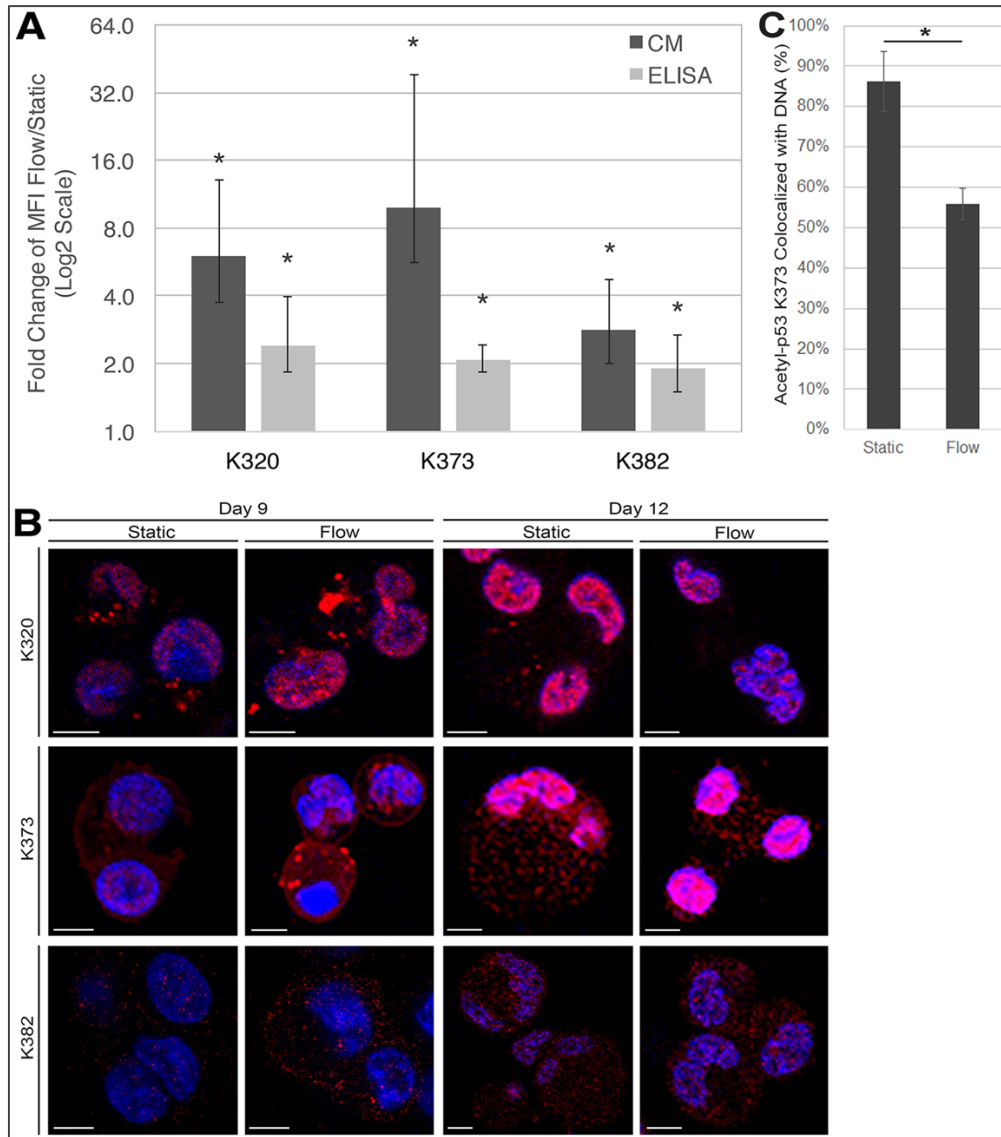


Figure 5.1 Shear flow alters p53 acetylation and sub-cellular localization in Mks. **A**, Fold change of mean fluorescence intensity (MFI) of acetyl-p53 expression for Lysine (K) 320, K373, and K382 in static and flow d9 Mks. Quantification was achieved using quantitative confocal microscopy (dark gray) and ELISA (light gray). One sample t-test, $*p < 0.05$, $n = 3$ (biological replicates) for CM, $n = 4$ for K373/K382 ELISA, $n = 5$ for K320 ELISA; error bars: SEM. **B**, Confocal microscopy of d9 and d12 Mks with immunofluorescent staining probing for acetyl-p53 (red), DAPI (blue), and co-localization (pink). Scale bar: 5 μ m. **C**, Co-localization analysis from **B** on K372-acetyl-p53 (red) with nucleus (blue, DAPI) of d12 Mks under static or shear flow condition.

We were interested in examining the deacetylase and acetyltransferases effecting p53 to investigate potential mechanisms by which p53 acetylation is altered in response to shear flow. There is only one deacetylase, HDAC1, that removes acetyl groups from p53, but several enzymes can acetylate p53 at different residues [220]. Tip60 acetylates K120, PCAF acetylates K320, and p300 acetylates K164, K305, K370, K372, K373, K381, K382, and K386 [220]. Since K320, K373, and K382 were differentially acetylated here in response to shear, we probed the expression of PCAF and p300 acetyltransferases. As Zeng, *et al.* demonstrated that HDAC1 deacetylates p53 in the EC shear-stress response [210], we also probed the expression of HDAC1. Since differential acetylation of p53 in response to shear was substantial in day 9 Mks, we chose these cells to examine the expression of acetyl-modifying enzymes. In response to shear-flow, we found significant downregulation of HDAC1 from ELISA quantification (Figure 5.2), which could explain the increased acetylation at all three shear-sensitive p53 residues. In addition, there was upregulation of p300 (Figure 5.2), which could be responsible for the increased acetylation at K373 and K382. There was also a significant increase in PCAF expression (Figure 5.2), which could account for some of the K320 acetylation.

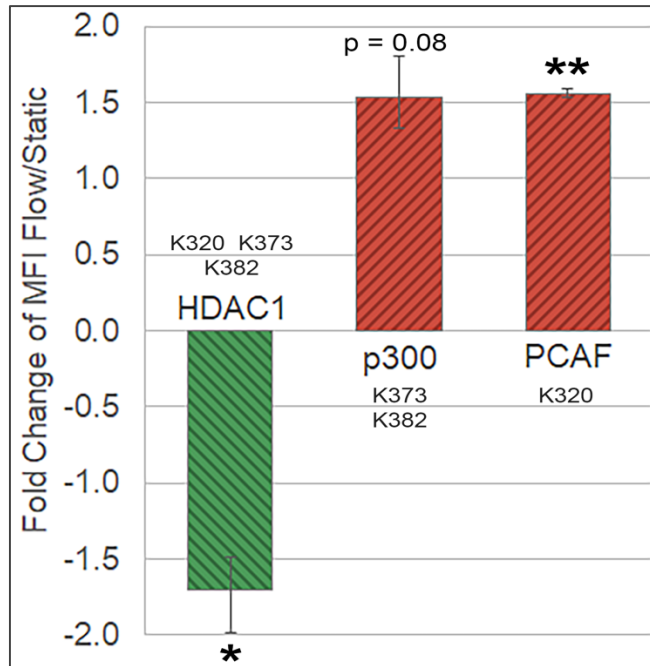


Figure 5.2 Shear flow exposure modulates expression of acetyl-modifying enzymes. Fold change of mean fluorescence intensity (MFI) in d9 Mks before and after shear-flow exposure for p53 deacetylase (HDAC1) and acetyltransferases (p300/PCAF). Quantification was achieved using an ELISA. One sample t-test, * $p < 0.05$, ** $p < 0.01$. $n = 3$ (biological replicates), error bars: SEM.

5.3.2 Shear Flow Stimulates Activation of Caspase 9 in Both Immature and Mature Mks, which Occurs Concurrently with PS Externalization

Our lab has previously shown that shear flow stimulates Caspase 3 activation in Mks and that as the percentage of PPT-producing Mks increased, so did the expression of active Caspase 3 [74]. Additionally, pan-Caspase and Caspase 3 inhibition during Mk maturation significantly decreases PLP/PPT production [74]. In order to determine if transcription-independent p53-induced apoptosis (TIPA) is involved in shear-induced Caspase 3 activation, we examined the activation of Caspase 9, which is upstream of

Caspase 3 activation [212]. To do this, we examined the expression of active Caspase 9 in immature (day 9) and mature (day 12) Mks using Western-blot analysis (Figure 5.3A) and confocal microscopy (Figure 5.3B) and found that following shear-flow exposure, active Caspase 9 (cleaved Caspase 9) expression increased at both days.

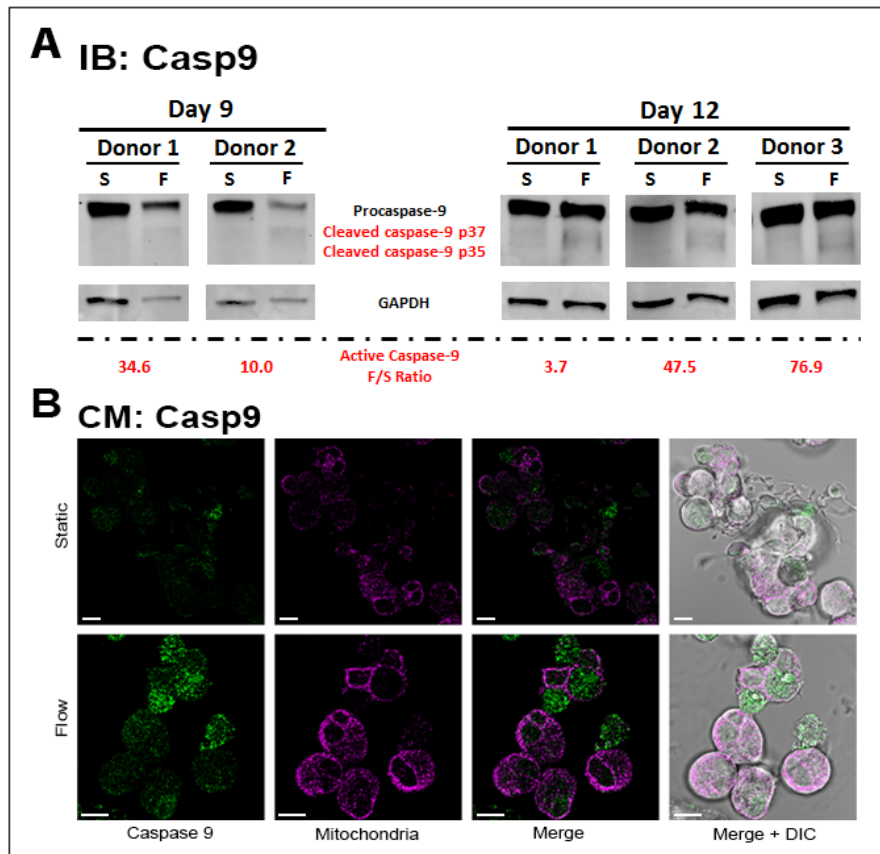


Figure 5.3 Caspase 9 activation in Mks is enhanced upon shear-flow exposure. A, Quantitative analysis of active (cleaved) and inactive (full length) caspase 9 expression from d9 (n=2) and d12 (n=3) Mks via immunoblot (Western-blot) analysis (Figure S4). Quantification was performed by Image J with normalization to GAPDH expression. B, Confocal microscopy of representative d12 Mks before (top row) and after (bottom row) shear-flow exposure. Green: active Caspase 9, Pink: MitoTracker. Scale bar: 10 μ m.

To examine the impact of p53 on Caspase 9 activation, we knocked down (KD) and overexpressed wild-type (WT) p53, and also expressed a mutant form of p53 (see below) in primary Mk cells. As probed by an ELISA assay, p53 KD reduced the level of p53 protein by 21% while p53 overexpression resulted in 36% increase in p53 protein (Figure 5.4A). p53 overexpression was optimized to increase the levels of p53 protein without extensive cell death (Figure D3 in Appendix D). Dr. Luff have shown that acetyl-p53 protein binds to Bax in cytoplasm [221]. To determine the role of p53/Bax interaction on Caspase 9 activation, we designed a mutant form of p53 (“p53-S46A”) that does not bind Bax as detailed below. The mutation was achieved using site-directed mutagenesis using the same method others have used for mutating cytoplasmic p53 [216, 217, 222, 223]. The mutant p53 was created by a Serine-to-Alanine substitution using site-directed mutagenesis against Serine 46 of the wild-type p53 plasmid used for overexpression [224]. We chose S46 based on the structural modeling work by Follis, *et al.* that demonstrated the importance of this residue in Bax binding [225]. We performed an ELISA to validate the functions of p53-S46A and confirmed that the mutation severely impaired the ability of Bax to bind p53 (Figure 5.4B).

We used these different Mk populations (WT, p53-overexpression, and p53-S46A-expressing) to determine whether TIPA is involved in Caspase 9 activation. We assume that the expression of p53-S46A will generate a discernible phenotype even in the presence of the WT p53. We wanted to understand how the three cell populations differed, so we used the same immunofluorescence protocol for staining active

Caspase 9 but measured on the flow cytometer instead. We chose to examine day 12 Mks because our goal was to understand TIPA in the context of Mk-particle biogenesis, which is not found at day 9. Expression of p53-S46A and p53-KD decreased, in a statistically significant way, Caspase 9 activation compared to WT and p53-overexpression Mks (Figure 5.4C), although the difference between p53-S46A and control was not as large possibly because of the presence of the WT p53 as discussed above. These findings further implicate p53 in Caspase 9 activation.

We also wanted to elucidate whether PS externalization is modulated by TIPA and if it occurs concurrently with Caspase 9 activation. Consistent with previous findings by Jiang, *et al.* [74], we confirmed that shear flow exposure increased PS externalization in immature and mature WT Mks (Figure 5.4D). Overexpression of WT p53 significantly increased PS expression in both statically-grown Mks and Mks exposed to shear flow at day 12. Also, the phenotype in which shear flow stimulates PS externalization was conserved upon p53 overexpression (Figure 5.4D). This is consistent with previous findings from our lab that found p53 modulates PS externalization in CHRF cells and primary murine Mks [206, 226]. While these data demonstrate that PS externalization is p53-dependent, we also wanted to examine the role of TIPA in this process. To do this, we used the p53-S46A mutant protein that does not bind Bax. Given the effects of p53-S46A on Caspase 9 activation and that overexpressing p53 increased PS externalization, we hypothesized that expressing p53-S46A would negate PS externalization. However, we unexpectedly found that expressing p53-S46A did not decreased PS externalization in static Mks or Mks

subjected to shear flow as compared to the p53-overexpressing Mks (Figure 5.4D). In fact, expression of p53-S46A enhanced PS externalization under both static and shear conditions similar to that of the p53 overexpression thus suggesting that PS externalization is affected by p53 but not by TIPPA.

In order to confirm that these effects were caused by non-transcriptional events, we examined the mRNA levels of *MDM2*, which is regulated by p53. Others have shown that the p53-S46A mutation can increase the expression of *MDM2* [227]. We observed a slight increase (30%) in *MDM2* expression in the Mks with p53-S46A compared to Mks overexpressed with WT p53 (Figure 5.4E). In contrast, Mayo, *et. al* found significantly greater expression of *MDM2* (estimated 3-fold increase), with a negligible change in *MDM2* protein expression and a limited cellular response (20% increase in cellular survival) following transfection with p53-S46A [227]. Given how small is the change in *MDM2* expression here in comparison, it likely has no or very little impact on the responses we see in the Mks with p53-S46A.

For the first time, these data suggest that TIPPA is necessary for shear-induced Caspase 9 activation and that PS externalization occurs concurrently with TIPPA but is not directly regulated by it. The only other study to examine Caspase 9 activation in the context of TIPPA showed no direct involvement of p53, but instead an indirect link, and examined these processes in cells not relevant to primary Mks, namely the HCT116 human colorectal carcinoma cell line [228]. Our data presented here lead us to conclude that shear flow stimulates Caspase 9 activation in a TIPPA-dependent manner but that shear-induced PS externalization is TIPPA-independent.

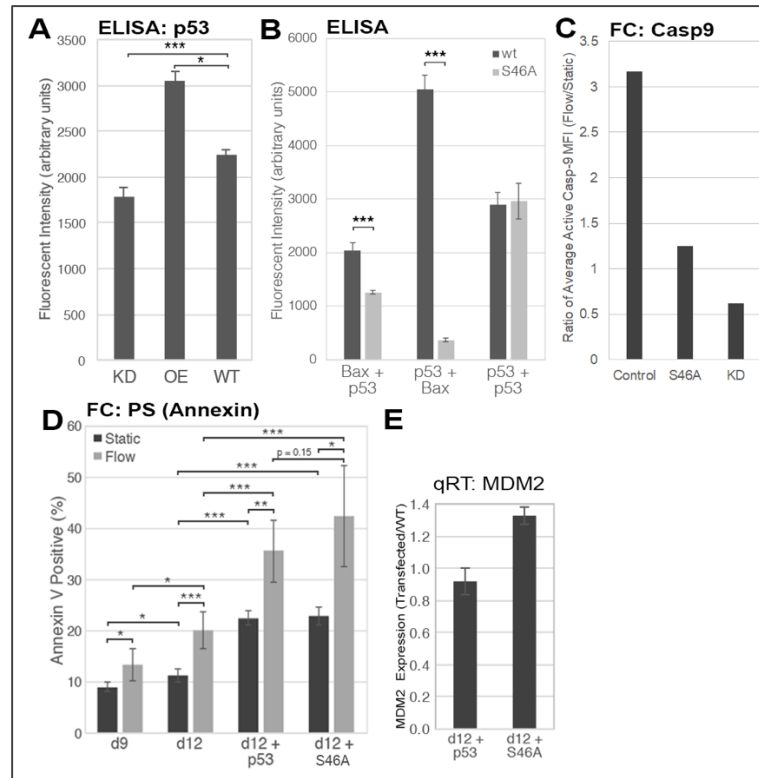


Figure 5.4 Shear-induced Caspase 9 activation in Mks is TIPA-dependent while Shear-induced PS externalization is p53-dependent, TIPA-independent. A, ELISA measuring total p53 levels in p53-KD, p53-overexpression, and wild-type Mks and normalized to basal lysate fluorescence. Unpaired t-test, $n = 3$ (biological replicates), $*p < 0.05$, $***p < 0.001$, error bars: SD. B, ELISA measuring the amount of p53 bound to Bax (left), Bax bound to p53 (center), and total p53 in the sample (right) in wild-type CHRF cells (black) and CHRF cells expression p53-S46A (gray) following shear flow exposure at d4 post-PMA treatment. Fluorescence values were normalized to basal lysate fluorescence. Unpaired t-test, $n = 3$ (biological replicates), $***p < 0.001$, error bars: SD. C, Ratio of average active Caspase 9 mean fluorescent intensity (MFI) before and after shear-flow exposure from wild-type, p53-overexpression, p53-S46A-expressing, or p53-KD d12 Mks were measured by flow cytometry, $n = 3$ (biological replicates). D, Percent of cells expressing PS on their plasma membrane (Annexin+) in wild-type d9 and d12 Mks, Mks with wild-type p53 overexpression, and Mks expressing mutant p53-S46A before (black) or after (gray) shear-flow exposure. Unpaired t-test, $n = 3$ (biological replicates), $*p < 0.05$, $**p < 0.01$, $***p < 0.001$, error bars: SD. E, Expression levels of MDM2 following overexpression of wt-p53 or expression of mutant p53-S46A quantified by qRT-PCR.

5.3.3 Transcription-independent p53-induced Apoptosis is Important in the Shear-stimulated Mk-particle Generation and the Biological Effectiveness of these Particles

To determine the importance of shear-stimulated TIPA on Mk maturation, we examined how modulating its activity affected the biogenesis of Mk particles (PPTs, PLPs, and MkMPs) from day 12 Mks. Our lab has previously shown that shear flow stimulates Mk particle generation in a caspase-dependent manner [74]. Given the data we present here that links cytoplasmic p53-bax interaction with Caspase 9 activation, we hypothesized that TIPA may have a direct role in the biogenesis of these particles. To test this hypothesis, we overexpressed WT p53 and expressed the p53-S46A mutant to examine whether shear-stimulated particle biogenesis was impacted. Overexpression of wild-type p53 increased the number of PPTs and MkMPs generated by shear-flow exposure (Figure 5.5A & 5.5B), indicating that the level of p53 expression may play a role in Mk particle generation under shear-flow. Expression of p53-S46A decreased the number of PPTs generated by shear flow to the level of WT Mks (Figure 5.5A), while for MkMPs it decreased the number significantly lower than those generated by WT Mks. Since the mutant p53 was unable to bind to Bax, this result confirmed the importance of the interaction between p53 and Bax, indicating that TIPA was involved in mediating Mk particle biogenesis. While the number of PLPs generated by mature Mks was not affected by the p53 modulation (Figure 5.5A), their ability to bind fibrinogen (FGN) increased in p53-overexpression Mks and decreased to that of wild-type in Mks expressing p53-S46A (Figure 5.5C). FGN

binding is an important functional feature of platelets and PLPs and indicates the likely effectiveness of platelets and PLPs in an *in vivo* setting. To examine the role of p53 acetylation in shear-induced Mk particle biogenesis, inhibition of p53 acetyltransferases resulted in decreased shear-induced PLP generation by 19% and 27% with 1 μM and 10 μM of acetyltransferase inhibitor, respectively. From these data, we conclude that TIPA is directly involved in the production of these Mk particles mediated by p53 acetylation. The data from the study by Dr. Luff that p53 acetylation enhanced p53-bax interaction [221], combined with the data in Figure 5.5, that p53-bax interactions play a role in shear-stimulated Mk particle biogenesis, these results demonstrate the importance of p53 acetylation in TIPA-induced Mk particles biogenesis after shear flow exposure.

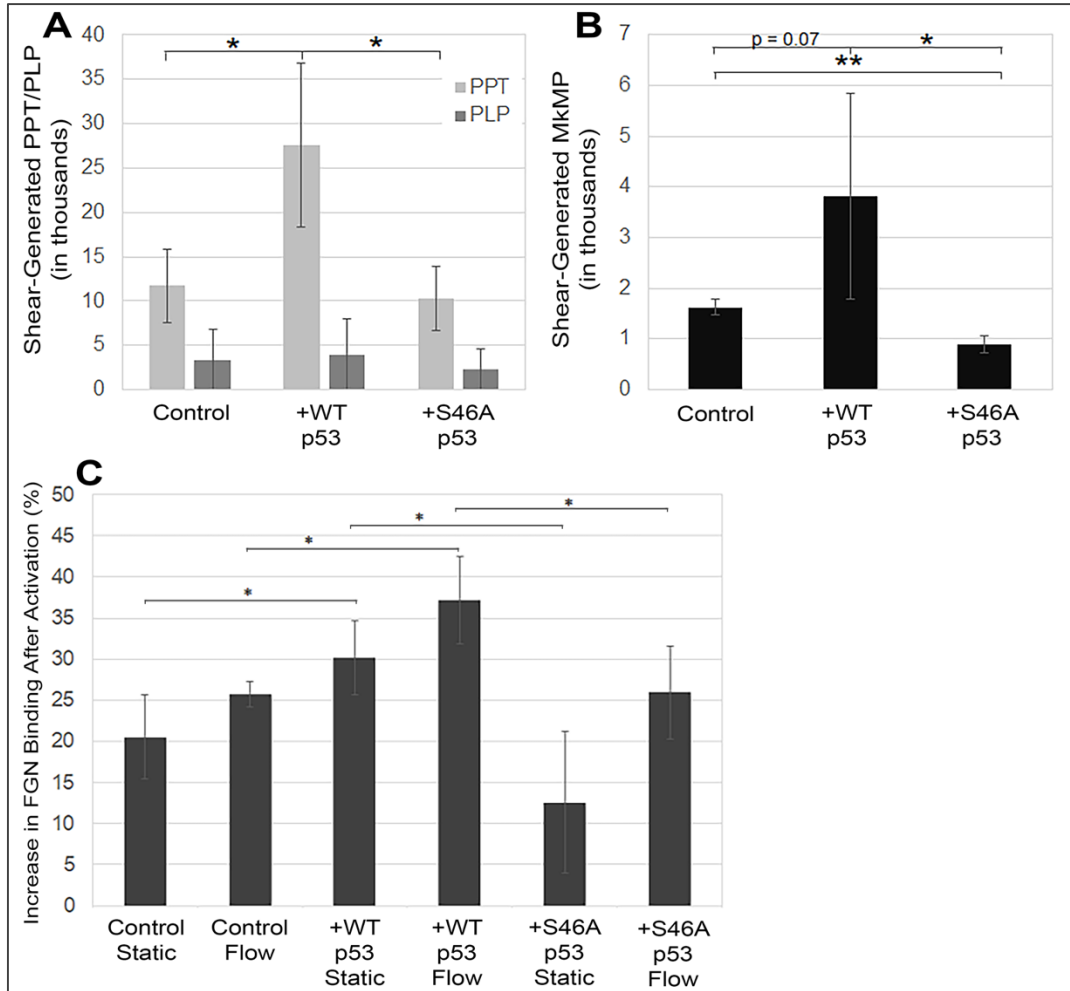


Figure 5.5 Shear-stimulated Mk particle biogenesis is dependent upon transcription-independent p53-induced apoptosis.

A, Number of PPTs and PLPs generated by shear-flow exposure from wild-type, p53-overexpression, and p53-S46A Mks. Particle numbers were normalized per 100,000 Mks. Unpaired t-test, * $p < 0.05$, $n = 3$ (biological replicates), error bars: SD. B, Number of MkMPs generated following shear-flow exposure by wild-type, p53-overexpression, and p53-S46A Mks. MkMP numbers were normalized per 100,000 Mks. Unpaired t-test, * $p < 0.05$, *** $p < 0.001$, $n = 3$ (biological replicates), error bars: SD. C, Percent of PLPs from wild-type (WT), p53-overexpression (OE), and p53-S46A (d46) Mks that are bound to fibrinogen (FGN) following activation with 3 units of thrombin. Unpaired t-test, * $p < 0.05$, $n = 3$ (biological replicates), error bars: SD.

Previous studies from our lab have demonstrated the target specificity of MkMPs for HSPCs and their biological impact on inducing Mk differentiation of HSPCs [23, 74]. Since we determined that TIPA is involved in MkMP biogenesis, we hypothesized that TIPA might also play a role in the quality of MkMPs in terms of their ability to program HSPCs. To examine this, we co-cultured CD34⁺ HSPCs with CHRF-derived MPs (CMPs) from WT and p53-KD CHRF cells [206]. As shown below, CMPs can also induce Mk differentiation of HSPCs, although less strongly so compared to MkMPs. We chose to use CMPs in this part of the work for simplicity and cost effectiveness as we can quickly and inexpensively generate CMPs in contrast to MkMPs. As expected, co-culture with WT CMPs induced Mk differentiation of CD34⁺ HSPCs; however, CMPs from p53-KD CHRF cells displayed attenuated function (Figure 5.6). The number of CD41⁺ Mks induced by co-culture with CMPs from p53-KD CHRF cells decreased significantly (Figure 5.6). All ploidy classes had significantly decreased numbers of Mks, demonstrating that expansion of Mks in all ploidy classes was negatively impacted (Figure 5.6). This confirms that TIPA plays a role not only in the number of MkMPs produced (Figure 5.5) but also the “quality” of these MkMPs in their ability to program HSPCs toward megakaryocytic differentiation in the absence of thrombopoietin (Tpo).

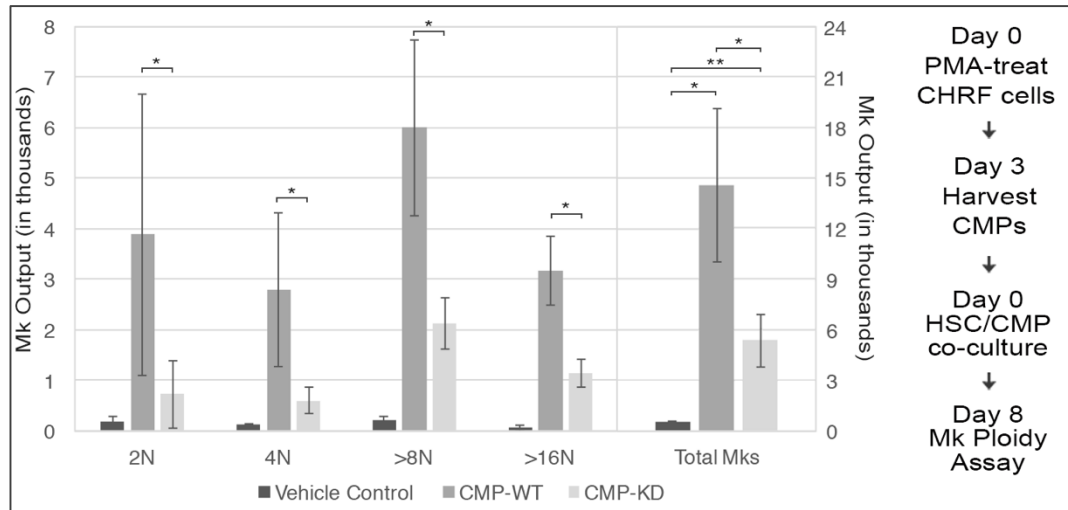


Figure 5.6 CHRF-derived MPs (CMPs) from p53-KD CHRF cells induce megakaryocytic differentiation of HSCs to a lesser extent than CMPs from wild-type CHRF cells. Number of Mks in each ploidy class and overall (as labeled) following and 8-day co-culture of CD34+ HSCs with vehicle control (black) or CMPs from wild-type (dark gray) or p53-KD (light gray) CHRF cells; Unpaired t-test, * $p > 0.05$, ** $p > 0.01$, $n = 4$ (biological replicates).

5.4 Discussion

For this study, we hypothesized that p53 is involved in the physiologically significant shear-stress response of Mks during Mk maturation and thrombopoiesis for three reasons: p53 is a well-characterized modulator of apoptosis [229], is important for Mk maturation [206-208, 226], and plays a role in the shear stress response of ECs [210]. There are several studies demonstrating that cytoplasmic p53 binds and activates Bax, leading to its translocation and insertion into the mitochondrial membrane, thus initiating the intrinsic apoptosis cascade [214, 230].

Here, we have shown that p53 is differentially acetylated in response to shear, but the acetylation pattern is different from that of ECs. In response to shear flow in

ECs, the p53 Lysine residues K320 and K373 were deacetylated, but there was increased acetylation at K382 [210]. In this study, we found (Figure 5.1A) that all three Lysine residues displayed increased acetylation in response to shear in immature day 9 Mk cells. These differences make sense given the profoundly different phenotypic responses to shear of ECs and Mks. In ECs, this specific acetylation pattern is important for inducing a quiescent state in response to laminar flow [210], while in Mks, it is responsible for creating the complex phenotype as described here and our prior work [74, 205]. To some extent, p53 acetylation occurs independent of shear flow between days 9 and 12, as we see increased acetylation in mature Mks at day 12 (Figure 5.1B). Given the low abundance of acetyl-p53 at day 9 compared to day 12 (Figure 5.1B), it is logical that shear flow would stimulate acetylation of p53 only in day 9 Mks (Figure 5.1A). While it is known that hyperacetylation induces cytoplasmic localization of p53 [215] and that preventing acetylation blocks Bax binding [216], it is not currently known whether p53 acetylation serves a specific role, other than increasing proximity, for inducing Bax interaction. Shear flow may modulate this interaction either by increasing p53 acetylation in Mks in earlier days (represented by the data of Day 9) or by translocating more acetyl-p53 K373 to the cytoplasm (where the interaction with Bax takes place) at later days represented by the data of Day 12.

We also examined how transcription-independent p53-induced apoptosis (TIPA) is involved in the Mk shear stress response of immature (day 9) and mature (day 12) Mks. While several studies have implicated intrinsic apoptosis in the

maturation of statically-grown Mks [231-234], there have been limited studies that examine the role it plays in more physiologically-relevant culture systems, such as following shear-flow exposure. Previous work in our lab had shown that enhanced Mk-particle biogenesis, Caspase 3 activation, and PS externalization, which can result from activation of the intrinsic apoptosis cascade [212], are observed in Mks following shear-flow exposure [74]. However, it had not yet been determined how these events were being initiated in response to shear flow. To examine the role of TIPA, we modulated TIPA activity by expressing the p53-S46A mutant that cannot bind Bax. We found that TIPA was involved in the number of PPT and MkMPs and the “quality” of PLPs and MkMPs. Interestingly, as shown in Figure 5.5B, expression of p53-S46A decreased the number of MkMPs below that of wild-type (this trend was also seen with Caspase 9 activation; Figure 5.4C). Although the Mks still expressed wild-type p53 from their genomes, it is possible that the p53-S46A had a dominant negative function against the wild-type p53. Mayo, *et al.* discovered that a Serine-to-Alanine mutation at S46 (the same mutation performed to prevent Bax binding) targeted nuclear p53 to the promoter of *MDM2* (the gene that encodes the p53 inhibitor) instead of promoters for apoptotic genes [227]. This would increase the number of WT p53 molecules in inhibitory complexes with MDM2 and possibly explain how expression of the mutant p53 would decrease Caspase 9 activation and MkMP biogenesis below that of WT Mks.

Our data have shown that shear-induced Caspase 9 activation and Mk-particle generation are TIPA-dependent, while PS externalization is likely TIPA-independent.

It is possible that shear-induced PS externalization occurs independent of any apoptotic mechanism. Several studies have demonstrated that PS externalization can occur without the engagement of apoptotic cascades [235, 236]. Our previous study showed that the JNK and p38 signaling pathways were important for transducing shear-flow stimuli in Mks [205] and inhibition of JNK causes delayed PS externalization [237]. Therefore, it is possible that shear-induced PS externalization is directly modulated by the JNK pathway.

The information provided by this study could be useful for optimizing *in vitro* culture of primary stem-cell derived Mks for the purpose of generating high yields of high-quality PLPs and MkMPs. This information may also explain physiological and pathophysiological phenotypes that relate to the role of p53 and shear flow in normal or aberrant thrombopoiesis and MkMP biogenesis, and inspire strategies for physiological or pharmacological interventions. A physiological phenotype, such as the role of physical activity in enhanced thrombopoiesis, is discussed in [74]. Several pathophysiological phenotypes, including phenotypes related to the large number of p53 mutations in a variety of cancer phenotypes, have been discussed by us previously [206, 226].

Acknowledgements

I would like to acknowledge and thank Dr. Stephanie Luff for her expertise and contribution of the original idea of this project.

Chapter 6

CONCLUSIONS AND FUTURE DIRECTIONS

6.1 Conclusions

This study aimed to investigate the natural targeting of hematopoietic stem/progenitor cells (HSPCs) by the megakaryocyte-derived MPs (MkMPs), and the MkMP ability to deliver important cargo such, as RNA, to HSPCs to induce megakaryocytic differentiation. Moreover, based on the HSPC-target specificity, we further aimed to examine engineering the MkMPs to develop a nucleic-acid delivery system to HSPCs.

The Papoutsakis lab had demonstrated the ability of MkMPs in inducing Mk differentiation of HSPCs [74]. However, how MkMPs target and are taken up by HSPCs was not known. In Chapter 2, we reported detailed studies on the uptake of MkMPs by HSPCs through both endocytosis (Figure 2.3) and membrane fusion (Figure 2.4 & 2.5). Using CFSE-stained MkMPs, we identified individual intact MPs in target cells thus demonstrating MkMP uptake through endocytosis (Figure 2.3). To identify MkMP uptake via membrane fusion, we used both confocal and electron microscopies. Using confocal fluorescent microscopy, we have shown the generation of gradients of CFSE dye carried by MkMPs into HSPCs, thus suggesting the delivery through membrane fusion (Figure 2.4A). With scanning electron microscopy (SEM), we demonstrated the fusion of MkMPs to HSPCs in four stages (Figure 2.4C), with

microvilli on the HSPC surface noted near the “landing” site of MkMPs on the HSPCs. With transmission electron microscopy (TEM), fusion events of MkMPs into HSPCs were detailed based on different TEM textures of MkMPs compared to those of the target cells (Figure 2.5), further supporting the likely role of HSPC microvilli for MkMP recognition. Next, we interrogate the process by which MkMPs recognize HSPCs. We identified important ligand-receptor interactions mediated by several surface antigens on MkMPs and HSPCs (CD54, CD11b, CD18 and CD43), and that the preferential targeting site on the HSPCs is the uropod (“back tail”)(Figure 2.8). Using specific inhibitors, we have also demonstrated that macropinocytosis, lipid raft-mediated endocytosis, and dynamin-mediated endocytosis are involved in the MkMP uptake by HSPCs (Figure 2.6). Our findings documented, for the first time, that receptor-mediated recognition, membrane fusion, and cell endocytosis in the same EV-to-target-cell interaction.

In Chapter 3, we developed the technology for and demonstrated the loading of plasmid DNA (pDNA; 3.5 or 6.3 kb) by electroporation into MkMPs. With optimized the electroporation process, and demonstrated that up to 4200 copies of pDNA can be loaded per MkMP, which is significantly higher payload compared to what is possible for exosome loading with plasmid DNA (less than 10 copies per exosome) [51]. We further confirmed the loaded plasmid DNA (pDNA) into MkMPs, for the first time, using Structured-Illumination (SIM) super-resolution microscopy (Figure 3.1). Efficient loading of a pDNA expressing green fluorescent protein (GFP) into MkMPs enabled effective pDNA delivery to HSPCs and to the HSPC nuclei, with up to 81%

of nuclei containing pDNA, thus resulting in functional GFP expression (Figure 3.3 & 3.4).

We further optimized and examined functional delivery of the small interfering RNA (siRNA) and microRNA (miRNA) to HSPCs by MkMPs. Delivery of siRNA targeting *c-myb* enabled MYB silencing resulted in enhanced Mk differentiation beyond that of unloaded MkMPs: the % of CD41+ and CD34-CD41+ cells increased by 29 % (Figure 3.5) and 25 %, respectively, on day 8 of co-culture versus control (unloaded MkMPs), indicating the functional delivery of siR-MYB via MkMPs. Similarly, loading and delivery of a miR-486-5p mimic to HSPCs via MkMPs enhanced Mk differentiation of CD34+ cells with higher CD41 expression (Figure 3.6).

Overall, this is the first report showing functional MP-mediated pDNA delivery to any cell type. Moreover, functional siRNA delivery via these MkMPs demonstrated the potential of this delivery system for targeting the stem-cell compartment. MkMPs constitute a potentially useful therapeutic delivery system for gene- and cell-therapy, with applications in regenerative and transfusion medicine. Our data also support the use of the larger MPs for delivering larger cargo payloads and larger size-cargo to target cells.

In Chapter 4, we explored the role of miRNAs from MkMPs in triggering Mk differentiation of HSPCs. Based on RNA sequencing analysis, we chose to examine the seven most abundant miRNAs in MkMPs (Figure 4.3). We examined the impact of the individual miRNAs and their combinations by directly transfecting miRNA

mimics to CD34+ HSPCs. We identified that miR-486-5p and miR-92a-3p are able to induce and promote Mk differentiation of CD34+ HSPCs in the absence of Tpo, while miR-22-3p plays a role in HSPCs expansion (Figure 4.4). We also demonstrated the importance of miRNA combinations, with miRNA combinations C2 and C7 significantly inducing and enhancing Mk differentiation of CD34+ HSPCs (Figure 4.5). We further investigated the signaling pathway(s) that may be mediating the observed MkMP-induced Mk differentiation, and identified the JNK, p38, or PI3K/mTOR signaling pathways as being involved in this programming phenotype, with the JNK pathway further regulating the maintenance of HSPC potency (Figure 4.6). Finally, we confirmed the important role of miR-486-5p, by loading the miR-486-5p inhibitor into MkMPs for delivery to CD34+ HSPCs to show that this inhibitor abolished the ability of MkMPs to trigger Mk differentiation of CD34+ HSPCs (Figure 4.7).

In Chapter 5, we investigated the role of p53 and transcription-independent p53-induced apoptosis (TIPA) in shear-stimulated Mk maturation and MkMPs/platelet generation. We demonstrated that shear flow stimulates p53 acetylation and Caspase 9 activation, and also that TIPA is involved in shear-induced Caspase 9 activation and the biogenesis of MkMPs. We also discovered that while shear-induced PS externalization is p53-dependent, it is not likely TIPA-dependent. These findings provide context to previous observations from our lab demonstrating that shear flow induces Caspase 3 activation and MkMP biogenesis.

6.2 Future Directions

Understanding the mechanisms of EV-to-target recognition and its specificity will be crucial for developing more effective technologies for cell therapies or for using parts of the EVs or their parent cells to construct semi-synthetic delivery systems. Are there any reasons as to why some EVs have exquisite target specificity while other do not? Can we determine if a cell's EVs will have some specific targets and which targets? Can we use modular engineering of one EV type to specifically target different cell types? This would enable to use of a single biomanufacturing process with post-manufacturing EV engineering to develop the final product.

Similarly, a better understanding at the molecular level the mechanistic aspects of EV uptake by the target cells will enable better technologies to enhance the uptake process and deliver EV cargo to the desirable target-cell location. For example, if the nucleus is the target location, one would expect that endocytotic EV uptake might be undesirable due to the likely EV-cargo degradation through endosomal processing. Instead, understanding the mechanism of EV fusion to the plasma membrane (Figure 1.1) might enable means to enhance this fusion process and suppress endocytotic uptake. A related issue is that of the dichotomy of target recognition versus EV uptake by the target. We have shown that PMPs, which have similar ontogeny as the MkMPs, can recognize and bind to HSPCs, but they are not apparently taken up by HSPCs [23]. The mechanism that underlies this observation is unknown, but the phenomenon most likely is not unique, and can be exploited in several possible ways, including the

development of competitive inhibition of undesirable EV uptake by a specific cell type.

Another related, but distinct and totally unexplored, issue is the mechanism that determines EV stability in circulation and biodistribution post infusion into the patient. The process by which transplanted cells home to the desirable organ (or not) has been investigated in some transplantation cases, but remains generally, not well understood. How much of that limited knowledge applies to EVs is unknown.

Another important area is the development of synthetic-biology tools and/or vesicle technologies to enable to combine components from different EVs or cell sources and/synthetic membranes to create and load cargo to new synthetic vehicles of desirable cargo capacity. This would allow one to combine a broader spectrum of targeting mechanisms and cargo loading. Could one embed specific antibodies to the EV membrane for even more specific or enhanced target recognition? Could one load EVs with “toxin” proteins to target cancer and other aberrant cells? Could one use EVs for targeted immunotherapy?

As stated in Chapter 1 (specifically 1.7), while some early efforts in biomanufacturing of exosomes have been reported, biomanufacturing of the larger MPs remains an unexplored field. Both exosome and MP biomanufacturing would benefit from methods to quickly and accurately determine the loading efficiency of any cargo molecule (DNA, RNA, protein, or drugs). Similarly, biomanufacturing of both exosomes and MPs would benefit from the development of scalable, high-resolution purification methods, as well as “finishing”, formulation, and storage

technologies for the final product. The stability of the EV product, whether in its final formulation state or earlier, is also critical, as this would permit a wider spectrum of clinical applications, such as the case of the MkMPs, which can be stored frozen and could be possibly used as a substitute for platelet transfusions to overcome the inability to store and transport platelets [23].

REFERENCES

1. Tan, X., et al., *Mesenchymal stem cell-derived microparticles: a promising therapeutic strategy*. Int J Mol Sci, 2014. **15**(8): p. 14348-63.
2. Raposo, G. and W. Stoorvogel, *Extracellular vesicles: exosomes, microvesicles, and friends*. J Cell Biol, 2013. **200**(4): p. 373-83.
3. Curtis, A.M., et al., *Endothelial microparticles: sophisticated vesicles modulating vascular function*. Vasc Med, 2013. **18**(4): p. 204-14.
4. Gyorgy, B., et al., *Membrane vesicles, current state-of-the-art: emerging role of extracellular vesicles*. Cell Mol Life Sci, 2011. **68**(16): p. 2667-88.
5. Schwechheimer, C. and M.J. Kuehn, *Outer-membrane vesicles from Gram-negative bacteria: biogenesis and functions*. Nat Rev Microbiol, 2015. **13**(10): p. 605-19.
6. El-Andaloussi, S., et al., *Extracellular vesicles: biology and emerging therapeutic opportunities*. Nat Rev Drug Discov, 2013. **12**(5): p. 347-57.
7. van Dongen, H.M., et al., *Extracellular vesicles exploit viral entry routes for cargo delivery*. Microbiology and Molecular Biology Reviews, 2016. **80**(2): p. 369-386.
8. Fais, S., et al., *Evidence-based clinical use of nanoscale extracellular vesicles in nanomedicine*. Acs Nano, 2016. **10**(4): p. 3886-3899.
9. McKelvey, K.J., et al., *Exosomes: mechanisms of uptake*. J Circ Biomark, 2015. **4**: p. 7.
10. Mulcahy, L.A., R.C. Pink, and D.R. Carter, *Routes and mechanisms of extracellular vesicle uptake*. J Extracell Vesicles, 2014. **3**(1): p. 24641.
11. Ghosh, A., et al., *Platelet CD36 mediates interactions with endothelial cell-derived microparticles and contributes to thrombosis in mice*. J Clin Invest, 2008. **118**(5): p. 1934-43.
12. Janowska-Wieczorek, A., et al., *Platelet-derived microparticles bind to hematopoietic stem/progenitor cells and enhance their engraftment*. Blood, 2001. **98**(10): p. 3143-9.
13. Baj-Krzyworzeka, M., et al., *Platelet-derived microparticles stimulate proliferation, survival, adhesion, and chemotaxis of hematopoietic cells*. Exp Hematol, 2002. **30**(5): p. 450-9.
14. Turturici, G., et al., *Extracellular membrane vesicles as a mechanism of cell-to-cell communication: advantages and disadvantages*. Am J Physiol Cell Physiol, 2014. **306**(7): p. C621-33.

15. Faille, D., et al., *Endocytosis and intracellular processing of platelet microparticles by brain endothelial cells*. J Cell Mol Med, 2012. **16**(8): p. 1731-8.
16. Obregon, C., et al., *Exovesicles from human activated dendritic cells fuse with resting dendritic cells, allowing them to present alloantigens*. Am J Pathol, 2006. **169**(6): p. 2127-36.
17. Horibe, S., et al., *Mechanism of recipient cell-dependent differences in exosome uptake*. BMC Cancer, 2018. **18**(1): p. 47.
18. Costa Verdera, H., et al., *Cellular uptake of extracellular vesicles is mediated by clathrin-independent endocytosis and macropinocytosis*. J Control Release, 2017. **266**: p. 100-108.
19. Feng, D., et al., *Cellular internalization of exosomes occurs through phagocytosis*. Traffic, 2010. **11**(5): p. 675-87.
20. Tian, T., et al., *Exosome uptake through clathrin-mediated endocytosis and macropinocytosis and mediating miR-21 delivery*. J Biol Chem, 2014. **289**(32): p. 22258-67.
21. Svensson, K.J., et al., *Exosome uptake depends on ERK1/2-heat shock protein 27 signaling and lipid Raft-mediated endocytosis negatively regulated by caveolin-1*. J Biol Chem, 2013. **288**(24): p. 17713-24.
22. del Conde, I., et al., *Tissue-factor-bearing microvesicles arise from lipid rafts and fuse with activated platelets to initiate coagulation*. Blood, 2005. **106**(5): p. 1604-1611.
23. Jiang, J., C.Y. Kao, and E.T. Papoutsakis, *How do megakaryocytic microparticles target and deliver cargo to alter the fate of hematopoietic stem cells?* J Control Release, 2017. **247**: p. 1-18.
24. Prada, I. and J. Meldolesi, *Binding and fusion of extracellular vesicles to the plasma membrane of their cell targets*. Int J Mol Sci, 2016. **17**(8): p. 1296.
25. Huang, Y., et al., *Exosomes function in tumor immune microenvironment*. Adv Exp Med Biol, 2018. **1056**: p. 109-122.
26. Kahlert, C. and R. Kalluri, *Exosomes in tumor microenvironment influence cancer progression and metastasis*. J Mol Med (Berl), 2013. **91**(4): p. 431-7.
27. Fu, Q., et al., *Primary tumor-derived exosomes facilitate metastasis by regulating adhesion of circulating tumor cells via SMAD3 in liver cancer*. Oncogene, 2018: p. 1.
28. Lee, Y.S., et al., *Exosome-mediated ultra-effective direct conversion of human fibroblasts into neural progenitor-like cells*. ACS Nano, 2018. **12**(3): p. 2531-2538.
29. Derigibus, M.C., et al., *Endothelial progenitor cell derived microvesicles activate an angiogenic program in endothelial cells by a horizontal transfer of mRNA*. Blood, 2007. **110**(7): p. 2440-8.
30. McNeer, N.A., et al., *Systemic delivery of triplex-forming PNA and donor DNA by nanoparticles mediates site-specific genome editing of human hematopoietic cells in vivo*. Gene Ther, 2013. **20**(6): p. 658-69.

31. Bruno, S., et al., *Mesenchymal stem cell-derived microvesicles protect against acute tubular injury*. J Am Soc Nephrol, 2009. **20**(5): p. 1053-67.
32. Di Trapani, M., et al., *Differential and transferable modulatory effects of mesenchymal stromal cell-derived extracellular vesicles on T, B and NK cell functions*. Sci Rep, 2016. **6**: p. 24120.
33. Bruno, S., et al., *Microvesicles derived from mesenchymal stem cells enhance survival in a lethal model of acute kidney injury*. PLoS One, 2012. **7**(3): p. e33115.
34. Dong, L., et al., *Human umbilical cord mesenchymal stem cell-derived extracellular vesicles promote lung adenocarcinoma growth by transferring miR-410*. Cell Death Dis, 2018. **9**(2): p. 218.
35. Wu, X., et al., *Exosomes derived from endothelial progenitor cells ameliorate acute lung injury by transferring miR-126*. Exp Cell Res, 2018. **370**(1): p. 13-23.
36. Zhou, Y., et al., *Exosomes from endothelial progenitor cells improve the outcome of a murine model of sepsis*. Mol Ther, 2018. **26**(5): p. 1375-1384.
37. Cantaluppi, V., et al., *Microvesicles derived from endothelial progenitor cells protect the kidney from ischemia-reperfusion injury by microRNA-dependent reprogramming of resident renal cells*. Kidney Int, 2012. **82**(4): p. 412-27.
38. Kuravi, S.J., et al., *Ability of platelet-derived extracellular vesicles to promote neutrophil-endothelial cell interactions*. Inflammation, 2018: p. 1-16.
39. Straat, M., et al., *Monocyte-mediated activation of endothelial cells occurs only after binding to extracellular vesicles from red blood cell products, a process mediated by beta-integrin*. Transfusion, 2016. **56**(12): p. 3012-3020.
40. Keshtkar, S., N. Azarpira, and M.H. Ghahremani, *Mesenchymal stem cell-derived extracellular vesicles: novel frontiers in regenerative medicine*. Stem Cell Res Ther, 2018. **9**(1): p. 63.
41. Flaumenhaft, R., et al., *Megakaryocyte-derived microparticles: direct visualization and distinction from platelet-derived microparticles*. Blood, 2009. **113**(5): p. 1112-21.
42. Tao, S.C., S.C. Guo, and C.Q. Zhang, *Platelet-derived extracellular vesicles: an emerging therapeutic approach*. Int J Biol Sci, 2017. **13**(7): p. 828-834.
43. Ohno, S., et al., *Systemically injected exosomes targeted to EGFR deliver antitumor microRNA to breast cancer cells*. Mol Ther, 2013. **21**(1): p. 185-91.
44. Akao, Y., et al., *Microvesicle-mediated RNA molecule delivery system using monocytes/macrophages*. Mol Ther, 2011. **19**(2): p. 395-9.
45. Zhang, Y., et al., *Microvesicle-mediated delivery of transforming growth factor beta1 siRNA for the suppression of tumor growth in mice*. Biomaterials, 2014. **35**(14): p. 4390-400.
46. Mizrak, A., et al., *Genetically engineered microvesicles carrying suicide mRNA/protein inhibit schwannoma tumor growth*. Mol Ther, 2013. **21**(1): p. 101-8.

47. Fuhrmann, G., et al., *Active loading into extracellular vesicles significantly improves the cellular uptake and photodynamic effect of porphyrins*. J Control Release, 2015. **205**: p. 35-44.
48. Tang, K., et al., *Delivery of chemotherapeutic drugs in tumour cell-derived microparticles*. Nat Commun, 2012. **3**: p. 1282.
49. Wahlgren, J., et al., *Plasma exosomes can deliver exogenous short interfering RNA to monocytes and lymphocytes*. Nucleic Acids Res, 2012. **40**(17): p. e130.
50. Cooper, J.M., et al., *Systemic exosomal siRNA delivery reduced alpha-synuclein aggregates in brains of transgenic mice*. Mov Disord, 2014. **29**(12): p. 1476-85.
51. Lamichhane, T.N., R.S. Raiker, and S.M. Jay, *Exogenous DNA loading into extracellular vesicles via electroporation is size-dependent and enables limited gene delivery*. Mol Pharm, 2015. **12**(10): p. 3650-7.
52. Momen-Heravi, F., et al., *Exosome-mediated delivery of functionally active miRNA-155 inhibitor to macrophages*. Nanomedicine, 2014. **10**(7): p. 1517-27.
53. Alvarez-Erviti, L., et al., *Delivery of siRNA to the mouse brain by systemic injection of targeted exosomes*. Nat Biotechnol, 2011. **29**(4): p. 341-5.
54. Kao, C.Y. and E.T. Papoutsakis, *Engineering human megakaryocytic microparticles for targeted delivery of nucleic acids to hematopoietic stem and progenitor cells*. Sci Adv, 2018. **4**: p. eaau6762
55. Kanada, M., et al., *Differential fates of biomolecules delivered to target cells via extracellular vesicles*. Proc Natl Acad Sci U S A, 2015. **112**(12): p. E1433-42.
56. Tian, Y., et al., *A doxorubicin delivery platform using engineered natural membrane vesicle exosomes for targeted tumor therapy*. Biomaterials, 2014. **35**(7): p. 2383-90.
57. Kooijmans, S.A.A., et al., *PEGylated and targeted extracellular vesicles display enhanced cell specificity and circulation time*. J Control Release, 2016. **224**: p. 77-85.
58. Sato, Y.T., et al., *Engineering hybrid exosomes by membrane fusion with liposomes*. Sci Rep, 2016. **6**: p. 21933.
59. Piffoux, M., et al., *Modification of extracellular vesicles by fusion with liposomes for the design of personalized biogenic drug delivery systems*. ACS Nano, 2018. **12**(7): p. 6830-6842.
60. Lin, Y., et al., *Exosome-liposome hybrid nanoparticles deliver CRISPR/Cas9 system in MSCs*. Adv Sci, 2018. **5**(4): p. 1700611.
61. Hu, C.M., et al., *Erythrocyte membrane-camouflaged polymeric nanoparticles as a biomimetic delivery platform*. Proc Natl Acad Sci U S A, 2011. **108**(27): p. 10980-5.
62. Yang, R., et al., *Cancer cell membrane-coated adjuvant nanoparticles with mannose modification for effective anticancer vaccination*. ACS Nano, 2018. **12**(6): p. 5121-5129.

63. Takasugi, M., *Emerging roles of extracellular vesicles in cellular senescence and aging*. Aging cell, 2018. **17**(2): p. e12734.
64. Morhayim, J., et al., *Osteoblasts secrete miRNA-containing extracellular vesicles that enhance expansion of human umbilical cord blood cells*. Sci Rep, 2016. **6**: p. 32034.
65. Fujita, Y., Y. Yoshioka, and T. Ochiya, *Extracellular vesicle transfer of cancer pathogenic components*. Cancer Sci, 2016. **107**(4): p. 385-90.
66. Hessvik, N.P. and A. Llorente, *Current knowledge on exosome biogenesis and release*. Cell Mol Life Sci, 2018. **75**(2): p. 193-208.
67. Andriolo, G., et al., *Exosomes from human cardiac progenitor cells for therapeutic applications: development of a GMP-grade manufacturing method*. Front Physiol, 2018. **9**: p. 1169.
68. Mendt, M., et al., *Generation and testing of clinical-grade exosomes for pancreatic cancer*. JCI Insight, 2018. **3**(8): p. e99263.
69. Thom, S.R., V.M. Bhopale, and M. Yang, *Neutrophils generate microparticles during exposure to inert gases due to cytoskeletal oxidative stress*. J Biol Chem, 2014. **289**(27): p. 18831-45.
70. Yano, Y., et al., *The role of protein phosphorylation and cytoskeletal reorganization in microparticle formation from the platelet plasma membrane*. Biochem J, 1994. **299**(1): p. 303-8.
71. Sapet, C., et al., *Thrombin-induced endothelial microparticle generation: identification of a novel pathway involving ROCK-II activation by caspase-2*. Blood, 2006. **108**(6): p. 1868-76.
72. Sebbagh, M., et al., *Caspase-3-mediated cleavage of ROCK I induces MLC phosphorylation and apoptotic membrane blebbing*. Nat Cell Biol, 2001. **3**(4): p. 346-52.
73. Morel, O., et al., *Cellular mechanisms underlying the formation of circulating microparticles*. Arterioscler Thromb Vasc Biol, 2011. **31**(1): p. 15-26.
74. Jiang, J., D.S. Woulfe, and E.T. Papoutsakis, *Shear enhances thrombopoiesis and formation of microparticles that induce megakaryocytic differentiation of stem cells*. Blood, 2014. **124**(13): p. 2094-103.
75. Pasquet, J.M., J. Dachary-Prigent, and A.T. Nurden, *Calcium influx is a determining factor of calpain activation and microparticle formation in platelets*. Eur J Biochem, 1996. **239**(3): p. 647-54.
76. Xiao, H., et al., *Thrombin-induced platelet microparticles improved the aggregability of cryopreserved platelets*. Cryobiology, 2002. **44**(2): p. 179-88.
77. Alberio, L., et al., *Surface expression and functional characterization of alpha-granule factor V in human platelets: effects of ionophore A23187, thrombin, collagen, and convulxin*. Blood, 2000. **95**(5): p. 1694-702.
78. Salzer, U., et al., *Ca(++)-dependent vesicle release from erythrocytes involves stomatin-specific lipid rafts, synexin (annexin VII), and sorcin*. Blood, 2002. **99**(7): p. 2569-77.

79. Johnson, B.L., 3rd, et al., *Mechanisms underlying mouse TNF-alpha stimulated neutrophil derived microparticle generation*. Biochem Biophys Res Commun, 2013. **437**(4): p. 591-6.
80. Alexy, T., et al., *TNF-alpha alters the release and transfer of microparticle-encapsulated miRNAs from endothelial cells*. Physiol Genomics, 2014. **46**(22): p. 833-40.
81. Khaspekova, S.G., et al., *Activity of tissue factor in microparticles produced in vitro by endothelial cells, monocytes, granulocytes, and platelets*. Biochemistry (Mosc), 2016. **81**(2): p. 114-21.
82. Pachler, K., et al., *A Good Manufacturing Practice-grade standard protocol for exclusively human mesenchymal stromal cell-derived extracellular vesicles*. Cytotherapy, 2017. **19**(4): p. 458-472.
83. Colao, I.L., et al., *Manufacturing exosomes: a promising therapeutic platform*. Trends Mol Med, 2018. **24**(3): p. 242-256.
84. Lopatina, T., et al., *Platelet-derived growth factor regulates the secretion of extracellular vesicles by adipose mesenchymal stem cells and enhances their angiogenic potential*. Cell Commun Signal, 2014. **12**: p. 26.
85. Collins, P.C., W.M. Miller, and E.T. Papoutsakis, *Stirred culture of peripheral and cord blood hematopoietic cells offers advantages over traditional static systems for clinically relevant applications*. Biotechnol Bioeng, 1998. **59**(5): p. 534-43.
86. Kunas, K.T. and E.T. Papoutsakis, *Damage mechanisms of suspended animal cells in agitated bioreactors with and without bubble entrainment*. Biotechnology and Bioengineering, 2009. **102**(4): p. 980-987.
87. Cherry, R. and E. Papoutsakis, *Hydrodynamic effects on cells in agitated tissue culture reactors*. Bioprocess Engineering, 1986. **1**(1): p. 29-41.
88. McDowell, C.L. and E.T. Papoutsakis, *Increased agitation intensity increases CD13 receptor surface content and mRNA levels, and alters the metabolism of HL60 cells cultured in stirred tank bioreactors*. Biotechnology and Bioengineering, 1998. **60**(2): p. 239-250.
89. Cocucci, E., G. Racchetti, and J. Meldolesi, *Shedding microvesicles: artefacts no more*. Trends Cell Biol, 2009. **19**(2): p. 43-51.
90. Barteneva, N.S., et al., *Circulating microparticles: square the circle*. BMC Cell Biol, 2013. **14**: p. 23.
91. Ratajczak, M.Z., et al., *Pivotal role of paracrine effects in stem cell therapies in regenerative medicine: can we translate stem cell-secreted paracrine factors and microvesicles into better therapeutic strategies?* Leukemia, 2012. **26**(6): p. 1166-73.
92. Aatonen, M., M. Gronholm, and P.R. Siljander, *Platelet-derived microvesicles: multitasking participants in intercellular communication*. Semin Thromb Hemost, 2012. **38**(1): p. 102-13.
93. Chamouard, P., et al., *Circulating Cell-Derived Microparticles in Crohn's Disease*. Digestive Diseases and Sciences, 2005. **50**(3): p. 574-580.

94. Baj-Krzyworzeka, M., et al., *Platelet-derived microparticles stimulate proliferation, survival, adhesion, and chemotaxis of hematopoietic cells*. Experimental Hematology, 2002. **30**(5): p. 450-459.
95. Pluskota, E., et al., *Expression, activation, and function of integrin alpha(M)beta(2) (Mac-1) on neutrophil-derived microparticles*. Blood, 2008. **112**(6): p. 2327-2335.
96. Martinez, M.C., et al., *Transfer of differentiation signal by membrane microvesicles harboring hedgehog morphogens*. Blood, 2006. **108**(9): p. 3012-20.
97. Martinez-Lorenzo, M.J., et al., *Activated human T cells release bioactive Fas ligand and APO2 ligand in microvesicles*. J Immunol, 1999. **163**(3): p. 1274-81.
98. Ansa-Addo, E.A., et al., *Human Plasma Membrane-Derived Vesicles Halt Proliferation and Induce Differentiation of THP-1 Acute Monocytic Leukemia Cells*. Journal of Immunology, 2010. **185**(9): p. 5236-5246.
99. Turturici, G., et al., *Extracellular membrane vesicles as a mechanism of cell-to-cell communication: advantages and disadvantages*. Vol. 306. 2014. C621-C633.
100. Mause, S.F. and C. Weber, *Microparticles: protagonists of a novel communication network for intercellular information exchange*. Circ Res, 2010. **107**(9): p. 1047-57.
101. Yuan, A., et al., *Transfer of microRNAs by embryonic stem cell microvesicles*. PLoS One, 2009. **4**(3): p. e4722.
102. Mause, S.F., et al., *Platelet microparticles enhance the vasoregenerative potential of angiogenic early outgrowth cells after vascular injury*. Circulation, 2010. **122**(5): p. 495-506.
103. Panuganti, S., et al., *Three-stage ex vivo expansion of high-ploidy megakaryocytic cells: toward large-scale platelet production*. Tissue Eng Part A, 2013. **19**(7-8): p. 998-1014.
104. Lobb, R.J., et al., *Optimized exosome isolation protocol for cell culture supernatant and human plasma*. J Extracell Vesicles, 2015. **4**: p. 27031.
105. Vlassov, A.V., et al., *Exosomes: current knowledge of their composition, biological functions, and diagnostic and therapeutic potentials*. Biochim Biophys Acta, 2012. **1820**(7): p. 940-8.
106. Hevehan, D.L., E.T. Papoutsakis, and W.M. Miller, *Physiologically significant effects of pH and oxygen tension on granulopoiesis*. Experimental Hematology, 2000. **28**(3): p. 267-275.
107. Lindsey, S. and E.T. Papoutsakis, *The aryl hydrocarbon receptor (AHR) transcription factor regulates megakaryocytic polyploidization*. Br J Haematol, 2011. **152**(4): p. 469-84.
108. Minciacchi, V.R., M.R. Freeman, and D. Di Vizio, *Extracellular vesicles in cancer: exosomes, microvesicles and the emerging role of large oncosomes*. Semin Cell Dev Biol, 2015. **40**: p. 41-51.

109. Dalli, J., et al., *Heterogeneity in neutrophil microparticles reveals distinct proteome and functional properties*. Mol Cell Proteomics, 2013. **12**(8): p. 2205-19.
110. Boilard, E., A.C. Duchez, and A. Brisson, *The diversity of platelet microparticles*. Curr Opin Hematol, 2015. **22**(5): p. 437-44.
111. Bjornson, C.R.R., et al., *Turning brain into blood: A hematopoietic fate adopted by adult neural stem cells in vivo*. Science, 1999. **283**(5401): p. 534-537.
112. Sanchez-Ramos, J., et al., *Adult bone marrow stromal cells differentiate into neural cells in vitro*. Experimental Neurology, 2000. **164**(2): p. 247-256.
113. Zhang, S., et al., *Both cell fusion and transdifferentiation account for the transformation of human peripheral blood CD34-Positive cells into cardiomyocytes in vivo*. Circulation, 2004. **110**(17): p. 138-138.
114. Frid, M.G., V.A. Kale, and K.R. Stenmark, *Mature vascular endothelium can give rise to smooth muscle cells via endothelial-mesenchymal transdifferentiation - In vitro analysis*. Circulation Research, 2002. **90**(11): p. 1189-1196.
115. Badorff, C.M., et al., *Transdifferentiation of blood-derived human adult endothelial progenitor cells into functionally active cardiomyocytes*. Circulation, 2002. **106**(19): p. 138-139.
116. Aliotta, J.M., et al., *Microvesicle entry into marrow cells mediates tissue-specific changes in mRNA by direct delivery of mRNA and induction of transcription*. Experimental hematology, 2010. **38**(3): p. 233-245.
117. Fonseca, A.V., et al., *Polarization and Migration of Hematopoietic Stem and Progenitor Cells Rely on the RhoA/ROCK I Pathway and an Active Reorganization of the Microtubule Network*. Journal of Biological Chemistry, 2010. **285**(41): p. 31661-31671.
118. Salaun, C., D.J. James, and L.H. Chamberlain, *Lipid rafts and the regulation of exocytosis*. Traffic, 2004. **5**(4): p. 255-64.
119. Gorlin, J.B., et al., *Human endothelial actin-binding protein (ABP-280, nonmuscle filamin): a molecular leaf spring*. J Cell Biol, 1990. **111**(3): p. 1089-105.
120. Umeda, T., et al., *Limited proteolysis of filamin is catalyzed by caspase-3 in U937 and Jurkat cells*. J Biochem, 2001. **130**(4): p. 535-42.
121. Giebel, B., et al., *Segregation of lipid raft markers including CD133 in polarized human hematopoietic stem and progenitor cells*. Blood, 2004. **104**(8): p. 2332-8.
122. Vodyanik, M.A., J.A. Thomson, and Slukvin, II, *Leukosialin (CD43) defines hematopoietic progenitors in human embryonic stem cell differentiation cultures*. Blood, 2006. **108**(6): p. 2095-105.
123. Ostberg, J.R., R.K. Barth, and J.G. Frelinger, *The Roman god Janus: a paradigm for the function of CD43*. Immunol Today, 1998. **19**(12): p. 546-50.

124. Murray, P., G. Frampton, and P.N. Nelson, *Cell adhesion molecules. Sticky moments in the clinic*. BMJ, 1999. **319**(7206): p. 332-4.
125. Hagiwara, T., et al., *Expression of adhesion molecules on cytoplasmic processes of human megakaryocytes*. Exp Hematol, 1996. **24**(6): p. 690-5.
126. Remold-O'Donnell, E., et al., *Expression on blood cells of sialophorin, the surface glycoprotein that is defective in Wiskott-Aldrich syndrome*. Blood, 1987. **70**(1): p. 104-109.
127. Nagata, Y., et al., *Thrombopoietin induces megakaryocyte differentiation in hematopoietic progenitor FDC-P2 cells*. J Biol Chem, 1995. **270**(34): p. 19673-5.
128. Gunji, Y., et al., *Expression and function of adhesion molecules on human hematopoietic stem cells: CD34+ LFA-1- cells are more primitive than CD34+ LFA-1+ cells*. Blood, 1992. **80**(2): p. 429-36.
129. Cho, J.Y., et al., *Regulation of CD43-induced U937 homotypic aggregation*. Exp Cell Res, 2003. **290**(1): p. 155-67.
130. Bazil, V., et al., *A monoclonal antibody recognizing CD43 (leukosialin) initiates apoptosis of human hematopoietic progenitor cells but not stem cells*. Blood, 1996. **87**(4): p. 1272-81.
131. Serrador, J.M., et al., *CD43 interacts with moesin and ezrin and regulates its redistribution to the uropods of T lymphocytes at the cell-cell contacts*. Blood, 1998. **91**(12): p. 4632-44.
132. Anzai, N., et al., *Modulation of integrin function in hematopoietic progenitor cells by CD43 engagement: possible involvement of protein tyrosine kinase and phospholipase C-gamma*. Blood, 1999. **93**(10): p. 3317-26.
133. Seveau, S., et al., *Leukosialin (CD43, sialophorin) redistribution in uropods of polarized neutrophils is induced by CD43 cross-linking by antibodies, by colchicine or by chemotactic peptides*. J Cell Sci, 1997. **110** (Pt 13): p. 1465-75.
134. Ratajczak, J., et al., *Embryonic stem cell-derived microvesicles reprogram hematopoietic progenitors: evidence for horizontal transfer of mRNA and protein delivery*. Leukemia, 2006. **20**(5): p. 847-56.
135. Skog, J., et al., *Glioblastoma microvesicles transport RNA and proteins that promote tumour growth and provide diagnostic biomarkers*. Nat Cell Biol, 2008. **10**(12): p. 1470-6.
136. Chao, T.Y. and R.T. Raines, *Mechanism of Ribonuclease A Endocytosis: Analogies to Cell-Penetrating Peptides*. Biochemistry, 2011. **50**(39): p. 8374-8382.
137. Eller, C.H., J.E. Lomax, and R.T. Raines, *Bovine Brain Ribonuclease Is the Functional Homolog of Human Ribonuclease 1*. Journal of Biological Chemistry, 2014. **289**(38): p. 25996-26006.
138. Ismail, N., et al., *Macrophage microvesicles induce macrophage differentiation and miR-223 transfer*. Blood, 2013. **121**(6): p. 984-95.

139. Njock, M.S., et al., *Endothelial cells suppress monocyte activation through secretion of extracellular vesicles containing antiinflammatory microRNAs*. *Blood*, 2015. **125**(20): p. 3202-3212.
140. Smallwood, D.T., et al., *Extracellular vesicles released by CD40/IL-4-stimulated CLL cells confer altered functional properties to CD4(+) T cells*. *Blood*, 2016. **128**(4): p. 542-552.
141. Losche, W., et al., *Platelet-derived microvesicles transfer tissue factor to monocytes but not to neutrophils*. *Platelets*, 2004. **15**(2): p. 109-15.
142. Mause, S.F., et al., *Platelet microparticles: a transcellular delivery system for RANTES promoting monocyte recruitment on endothelium*. *Arterioscler Thromb Vasc Biol*, 2005. **25**(7): p. 1512-8.
143. Mettlen, M., et al., *Dissecting dynamin's role in clathrin-mediated endocytosis*. *Biochem Soc Trans*, 2009. **37**(Pt 5): p. 1022-6.
144. Preta, G., et al., *Protective role of the dynamin inhibitor Dynasore against the cholesterol-dependent cytolysin of *Trueperella pyogenes**. *FASEB J*, 2015. **29**(4): p. 1516-28.
145. Park, R.J., et al., *Dynamin triple knockout cells reveal off target effects of commonly used dynamin inhibitors*. *J Cell Sci*, 2013. **126**(Pt 22): p. 5305-12.
146. Colombo, M., G. Raposo, and C. Thery, *Biogenesis, secretion, and intercellular interactions of exosomes and other extracellular vesicles*. *Annu Rev Cell Dev Biol*, 2014. **30**: p. 255-89.
147. Jeyaram, A. and S.M. Jay, *Preservation and Storage Stability of Extracellular Vesicles for Therapeutic Applications*. *AAPS J*, 2017. **20**(1): p. 1.
148. Zhu, X., et al., *Comprehensive toxicity and immunogenicity studies reveal minimal effects in mice following sustained dosing of extracellular vesicles derived from HEK293T cells*. *J Extracell Vesicles*, 2017. **6**(1): p. 1324730.
149. Zhuang, X., et al., *Treatment of brain inflammatory diseases by delivering exosome encapsulated anti-inflammatory drugs from the nasal region to the brain*. *Mol Ther*, 2011. **19**(10): p. 1769-79.
150. Thomas, C.E., A. Ehrhardt, and M.A. Kay, *Progress and problems with the use of viral vectors for gene therapy*. *Nat Rev Genet*, 2003. **4**(5): p. 346-58.
151. Yu, K.R., H. Natanson, and C.E. Dunbar, *Gene Editing of Human Hematopoietic Stem and Progenitor Cells: Promise and Potential Hurdles*. *Hum Gene Ther*, 2016. **27**(10): p. 729-740.
152. Schomber, T., et al., *Gene silencing by lentivirus-mediated delivery of siRNA in human CD34+ cells*. *Blood*, 2004. **103**(12): p. 4511-3.
153. Diener, Y., et al., *RNA-based, transient modulation of gene expression in human haematopoietic stem and progenitor cells*. *Sci Rep*, 2015. **5**: p. 17184.
154. Wiehe, J.M., et al., *mRNA-mediated gene delivery into human progenitor cells promotes highly efficient protein expression*. *J Cell Mol Med*, 2007. **11**(3): p. 521-30.

155. Wu, M.H., et al., *Efficient expression of foreign genes in human CD34(+) hematopoietic precursor cells using electroporation*. *Gene Ther*, 2001. **8**(5): p. 384-90.
156. McNeer, N.A., et al., *Nanoparticles deliver triplex-forming PNAs for site-specific genomic recombination in CD34+ human hematopoietic progenitors*. *Mol Ther*, 2011. **19**(1): p. 172-80.
157. Escobar, C., *Human megakaryocytic microparticles target murine hematopoietic stem cells to stimulate in vivo platelet biogenesis*. 2018, University of Delaware.
158. Fuhrken, P.G., et al., *Comparative, genome-scale transcriptional analysis of CHRF-288-11 and primary human megakaryocytic cell cultures provides novel insights into lineage-specific differentiation*. *Exp Hematol*, 2007. **35**(3): p. 476-489.
159. Naughton, B.J., D.D. Han, and H.H. Gu, *Fluorescence-based evaluation of shRNA efficacy*. *Anal Biochem*, 2011. **417**(1): p. 162-4.
160. Nabbi, A. and K. Riabowol, *Rapid Isolation of Nuclei from Cells In Vitro*. *Cold Spring Harb Protoc*, 2015. **2015**(8): p. 769-72.
161. Schermelleh, L., R. Heintzmann, and H. Leonhardt, *A guide to super-resolution fluorescence microscopy*. *J Cell Biol*, 2010. **190**(2): p. 165-75.
162. Taanman, J.W., *The mitochondrial genome: structure, transcription, translation and replication*. *Biochim Biophys Acta*, 1999. **1410**(2): p. 103-23.
163. Latulippe, D.R. and A.L. Zydney, *Radius of gyration of plasmid DNA isoforms from static light scattering*. *Biotechnol Bioeng*, 2010. **107**(1): p. 134-42.
164. Lehmusvaara, S., et al., *Utility of cell-permeable peptides for enhancement of virus-mediated gene transfer to human tumor cells*. *Biotechniques*, 2006. **40**(5): p. 573-4, 576.
165. Aluigi, M., et al., *Nucleofection is an efficient nonviral transfection technique for human bone marrow-derived mesenchymal stem cells*. *Stem Cells*, 2006. **24**(2): p. 454-461.
166. Dean, D.A., D.D. Strong, and W.E. Zimmer, *Nuclear entry of nonviral vectors*. *Gene Therapy*, 2005. **12**(11): p. 881-890.
167. de Queiroz, F.M., et al., *Nucleofection induces non-specific changes in the metabolic activity of transfected cells*. *Molecular Biology Reports*, 2012. **39**(3): p. 2187-2194.
168. Benjaminsen, R.V., et al., *The possible "proton sponge" effect of polyethylenimine (PEI) does not include change in lysosomal pH*. *Mol Ther*, 2013. **21**(1): p. 149-57.
169. El-Sayed, A., S. Futaki, and H. Harashima, *Delivery of macromolecules using arginine-rich cell-penetrating peptides: ways to overcome endosomal entrapment*. *AAPS J*, 2009. **11**(1): p. 13-22.
170. Bai, H., et al., *Cytoplasmic transport and nuclear import of plasmid DNA*. *Biosci Rep*, 2017. **37**(6).

171. Vacik, J., et al., *Cell-specific nuclear import of plasmid DNA*. Gene Ther, 1999. **6**(6): p. 1006-14.
172. Bianchi, E., et al., *c-myb supports erythropoiesis through the transactivation of KLF1 and LMO2 expression*. Blood, 2010. **116**(22): p. e99-110.
173. Bianchi, E., et al., *MYB controls erythroid versus megakaryocyte lineage fate decision through the miR-486-3p-mediated downregulation of MAF*. Cell Death Differ, 2015. **22**(12): p. 1906-21.
174. Wang, L.S., et al., *MicroRNA-486 regulates normal erythropoiesis and enhances growth and modulates drug response in CML progenitors*. Blood, 2015. **125**(8): p. 1302-13.
175. Laffont, B., et al., *Activated platelets can deliver mRNA regulatory Ago2*microRNA complexes to endothelial cells via microparticles*. Blood, 2013. **122**(2): p. 253-61.
176. Cai, Y., et al., *A brief review on the mechanisms of miRNA regulation*. Genomics Proteomics Bioinformatics, 2009. **7**(4): p. 147-54.
177. Das, S. and M.K. Halushka, *Extracellular vesicle microRNA transfer in cardiovascular disease*. Cardiovasc Pathol, 2015. **24**(4): p. 199-206.
178. Chen, J., C. Hu, and P. Pan, *Extracellular Vesicle MicroRNA Transfer in Lung Diseases*. Front Physiol, 2017. **8**: p. 1028.
179. Vinas, J.L., et al., *Transfer of microRNA-486-5p from human endothelial colony forming cell-derived exosomes reduces ischemic kidney injury*. Kidney Int, 2016. **90**(6): p. 1238-1250.
180. Lu, C., B.C. Meyers, and P.J. Green, *Construction of small RNA cDNA libraries for deep sequencing*. Methods, 2007. **43**(2): p. 110-7.
181. Kozomara, A. and S. Griffiths-Jones, *miRBase: annotating high confidence microRNAs using deep sequencing data*. Nucleic Acids Res, 2014. **42**(Database issue): p. D68-73.
182. Robinson, M.D., D.J. McCarthy, and G.K. Smyth, *edgeR: a Bioconductor package for differential expression analysis of digital gene expression data*. Bioinformatics, 2010. **26**(1): p. 139-40.
183. Kamat, V., et al., *MicroRNA screen of human embryonic stem cell differentiation reveals miR-105 as an enhancer of megakaryopoiesis from adult CD34+ cells*. Stem Cells, 2014. **32**(5): p. 1337-46.
184. Liao, F.L., et al., *Hematopoietic stem cell-derived exosomes promote hematopoietic differentiation of mouse embryonic stem cells in vitro via inhibiting the miR126/Notch1 pathway*. Acta Pharmacol Sin, 2018. **39**(4): p. 552-560.
185. Kim, N., et al., *Combination of small RNAs for skeletal muscle regeneration*. FASEB J, 2016. **30**(3): p. 1198-206.
186. Cursons, J., et al., *Combinatorial Targeting by MicroRNAs Co-ordinates Post-transcriptional Control of EMT*. Cell Syst, 2018. **7**(1): p. 77-91 e7.
187. Kaushansky, K., *Molecular mechanisms of thrombopoietin signaling*. J Thromb Haemost, 2009. **7 Suppl 1**: p. 235-8.

188. de Graaf, C.A. and D. Metcalf, *Thrombopoietin and hematopoietic stem cells*. Cell Cycle, 2011. **10**(10): p. 1582-9.
189. Drachman, J.G., K.M. Millett, and K. Kaushansky, *Thrombopoietin signal transduction requires functional JAK2, not TYK2*. J Biol Chem, 1999. **274**(19): p. 13480-4.
190. Geddis, A.E., N.E. Fox, and K. Kaushansky, *Phosphatidylinositol 3-kinase is necessary but not sufficient for thrombopoietin-induced proliferation in engineered Mpl-bearing cell lines as well as in primary megakaryocytic progenitors*. J Biol Chem, 2001. **276**(37): p. 34473-9.
191. Rojnuckarin, P., J.G. Drachman, and K. Kaushansky, *Thrombopoietin-induced activation of the mitogen-activated protein kinase (MAPK) pathway in normal megakaryocytes: role in endomitosis*. Blood, 1999. **94**(4): p. 1273-82.
192. Kirito, K., N. Fox, and K. Kaushansky, *Thrombopoietin stimulates Hoxb4 expression: an explanation for the favorable effects of TPO on hematopoietic stem cells*. Blood, 2003. **102**(9): p. 3172-8.
193. Miyazaki, R., H. Ogata, and Y. Kobayashi, *Requirement of thrombopoietin-induced activation of ERK for megakaryocyte differentiation and of p38 for erythroid differentiation*. Ann Hematol, 2001. **80**(5): p. 284-91.
194. Severin, S., C. Ghevaert, and A. Mazharian, *The mitogen-activated protein kinase signaling pathways: role in megakaryocyte differentiation*. J Thromb Haemost, 2010. **8**(1): p. 17-26.
195. Baker, J.E., et al., *Thrombopoietin receptor agonists protect human cardiac myocytes from injury by activation of cell survival pathways*. J Pharmacol Exp Ther, 2015. **352**(3): p. 429-37.
196. Guerriero, R., et al., *Inhibition of TPO-induced MEK or mTOR activity induces opposite effects on the ploidy of human differentiating megakaryocytes*. J Cell Sci, 2006. **119**(Pt 4): p. 744-52.
197. Hattori, K., B. Heissig, and S. Rafii, *The regulation of hematopoietic stem cell and progenitor mobilization by chemokine SDF-1*. Leuk Lymphoma, 2003. **44**(4): p. 575-82.
198. Schulze, H. and R.A. Shivdasani, *Mechanisms of thrombopoiesis*. J Thromb Haemost, 2005. **3**(8): p. 1717-24.
199. Italiano, J.E., Jr. and R.A. Shivdasani, *Megakaryocytes and beyond: the birth of platelets*. J Thromb Haemost, 2003. **1**(6): p. 1174-82.
200. Kaushansky, K., *Historical review: megakaryopoiesis and thrombopoiesis*. Blood, 2008. **111**(3): p. 981-6.
201. Whitaker, B.I., R.a. Henry, and S. Hinkins, *Report of the US Department of Health and Human Services. The 2011 national blood collection and utilization survey report*. 2013.
202. Lambert, M.P., et al., *Challenges and promises for the development of donor-independent platelet transfusions*. Blood, 2013. **121**(17): p. 3319-24.
203. Junt, T., et al., *Dynamic visualization of thrombopoiesis within bone marrow*. Science, 2007. **317**(5845): p. 1767-70.

204. Dunois-Larde, C., et al., *Exposure of human megakaryocytes to high shear rates accelerates platelet production*. Blood, 2009. **114**(9): p. 1875-83.
205. Luff, S.A. and E.T. Papoutsakis, *Megakaryocytic Maturation in Response to Shear Flow Is Mediated by the Activator Protein 1 (AP-1) Transcription Factor via Mitogen-activated Protein Kinase (MAPK) Mechanotransduction*. J Biol Chem, 2016. **291**(15): p. 7831-43.
206. Fuhrken, P.G., et al., *Tumor suppressor protein p53 regulates megakaryocytic polyploidization and apoptosis*. J Biol Chem, 2008. **283**(23): p. 15589-600.
207. Apostolidis, P.A., et al., *Tumor Suppressor Protein p53 Affects Megakaryocytic Maturation: In Vivo and Ex Vivo Post-Translational Modification Studies*. Blood, 2008. **112**(11): p. 850-850.
208. Apostolidis, P.A., et al., *Proposed megakaryocytic regulon of p53: the genes engaged to control cell cycle and apoptosis during megakaryocytic differentiation*. Physiol Genomics, 2012. **44**(12): p. 638-50.
209. Knights, C.D., et al., *Distinct p53 acetylation cassettes differentially influence gene-expression patterns and cell fate*. J Cell Biol, 2006. **173**(4): p. 533-44.
210. Zeng, L., et al., *The role of p53 deacetylation in p21Waf1 regulation by laminar flow*. J Biol Chem, 2003. **278**(27): p. 24594-9.
211. Kroemer, G., et al., *Classification of cell death: recommendations of the Nomenclature Committee on Cell Death 2009*. Cell Death Differ, 2009. **16**(1): p. 3-11.
212. Elmore, S., *Apoptosis: a review of programmed cell death*. Toxicol Pathol, 2007. **35**(4): p. 495-516.
213. Fridman, J.S. and S.W. Lowe, *Control of apoptosis by p53*. Oncogene, 2003. **22**(56): p. 9030-40.
214. Chipuk, J.E., et al., *Direct activation of Bax by p53 mediates mitochondrial membrane permeabilization and apoptosis*. Science, 2004. **303**(5660): p. 1010-4.
215. Kawaguchi, Y., et al., *Charge modification at multiple C-terminal lysine residues regulates p53 oligomerization and its nucleus-cytoplasm trafficking*. J Biol Chem, 2006. **281**(3): p. 1394-400.
216. Yamaguchi, H., et al., *p53 acetylation is crucial for its transcription-independent proapoptotic functions*. J Biol Chem, 2009. **284**(17): p. 11171-83.
217. Sykes, S.M., et al., *Acetylation of the DNA binding domain regulates transcription-independent apoptosis by p53*. J Biol Chem, 2009. **284**(30): p. 20197-205.
218. Bode, A.M. and Z. Dong, *Post-translational modification of p53 in tumorigenesis*. Nat Rev Cancer, 2004. **4**(10): p. 793-805.
219. Kодиha, M., R. Umar, and U. Stochaj, *Optimized immunofluorescence staining protocol to detect the nucleoporin Nup98 in different subcellular compartments*. 2009.
220. Brooks, C.L. and W. Gu, *The impact of acetylation and deacetylation on the p53 pathway*. Protein Cell, 2011. **2**(6): p. 456-62.

221. Luff, S.A., C.Y. Kao, and E.T. Papoutsakis, *Role of p53 and transcription-independent p53-induced apoptosis in shear-stimulated megakaryocytic maturation, particle generation, and platelet biogenesis*. PLoS One, 2018. **13**(9): p. e0203991.
222. Pietsch, E.C., et al., *Oligomerization of BAK by p53 utilizes conserved residues of the p53 DNA binding domain*. J Biol Chem, 2008. **283**(30): p. 21294-304.
223. Leu, J.I., et al., *Mitochondrial p53 activates Bak and causes disruption of a Bak-Mcl1 complex*. Nat Cell Biol, 2004. **6**(5): p. 443-50.
224. Baker, S.J., et al., *Suppression of human colorectal carcinoma cell growth by wild-type p53*. Science, 1990. **249**(4971): p. 912-5.
225. Follis, A.V., et al., *Pin1-Induced Proline Isomerization in Cytosolic p53 Mediates BAX Activation and Apoptosis*. Mol Cell, 2015. **59**(4): p. 677-84.
226. Apostolidis, P.A., et al., *Role of tumor suppressor p53 in megakaryopoiesis and platelet function*. Exp Hematol, 2012. **40**(2): p. 131-42 e4.
227. Mayo, L.D., et al., *Phosphorylation of human p53 at serine 46 determines promoter selection and whether apoptosis is attenuated or amplified*. J Biol Chem, 2005. **280**(28): p. 25953-9.
228. Ohtsuka, T., et al., *ASC is a Bax adaptor and regulates the p53-Bax mitochondrial apoptosis pathway*. Nat Cell Biol, 2004. **6**(2): p. 121-8.
229. Vousden, K.H. and C. Prives, *Blinded by the Light: The Growing Complexity of p53*. Cell, 2009. **137**(3): p. 413-31.
230. Caelles, C., A. Heimberg, and M. Karin, *p53-Dependent Apoptosis in the Absence of Transcriptional Activation of p53-Target Genes*. Nature, 1994. **370**: p. 220-223.
231. Avanzi, M.P., et al., *Actin inhibition increases megakaryocyte proplatelet formation through an apoptosis-dependent mechanism*. PLoS One, 2015. **10**(4): p. e0125057.
232. Cantor, A.B., *Death-defying apoptotic caspases in thrombopoiesis*. Blood, 2012. **119**(18): p. 4098-9.
233. De Botton, S., et al., *Platelet formation is the consequence of caspase activation within megakaryocytes*. Blood, 2002. **100**(4): p. 1310-7.
234. Josefsson, E.C., et al., *Megakaryocytes possess a functional intrinsic apoptosis pathway that must be restrained to survive and produce platelets*. J Exp Med, 2011. **208**(10): p. 2017-31.
235. Balasubramanian, K., B. Mirnikjoo, and A.J. Schroit, *Regulated externalization of phosphatidylserine at the cell surface: implications for apoptosis*. J Biol Chem, 2007. **282**(25): p. 18357-64.
236. Smrz, D., L. Draberova, and P. Draber, *Non-apoptotic phosphatidylserine externalization induced by engagement of glycosylphosphatidylinositol-anchored proteins*. J Biol Chem, 2007. **282**(14): p. 10487-97.
237. Krilleke, D., et al., *Inhibition of JNK signaling diminishes early but not late cellular stress-induced apoptosis*. Int J Cancer, 2003. **107**(4): p. 520-7.

Appendix A

SUPPLEMENTARY MATERIAL FOR CHAPTER 2

HOW DO MEGAKARYOCYTIC MICROPARTICLES TARGET AND DELIVER CARGO TO ALTER THE FATE OF HEMATOPOIETIC STEM CELLS?

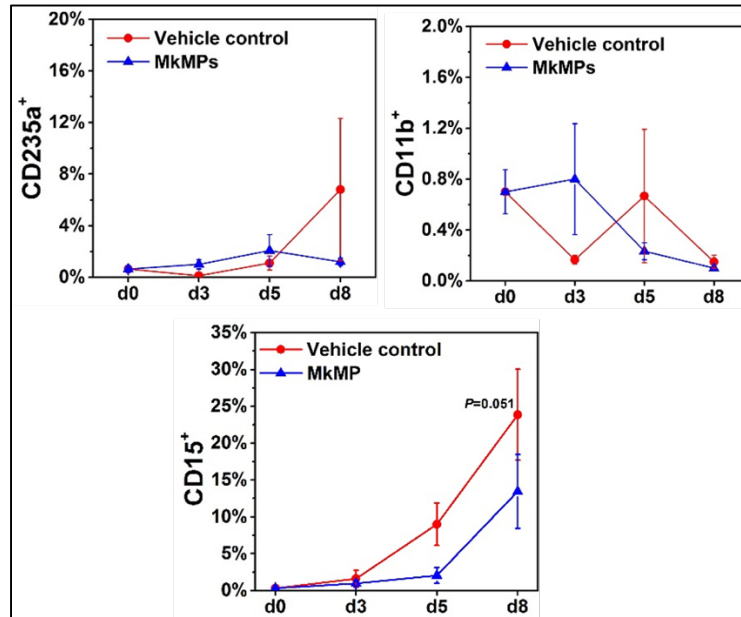


Figure A.1 CD235a, CD11b and CD15 expressions of cells in MkMP co-cultures and vehicle control cultures.

60K primitive Lineage⁻ cells were enriched from CD34⁺ cells and co-cultured with MkMPs at concentration of 10 MkMPs/cell for 8 days. At d0, d3, d5 and d8, some cells were harvested for antibody staining and flow cytometry analysis. Co-culture of HSPCs with MkMPs significantly decreased the percentage of CD15⁺ monocytes compared to vehicle control cultures. Error bars represent standard error of mean (n=3).

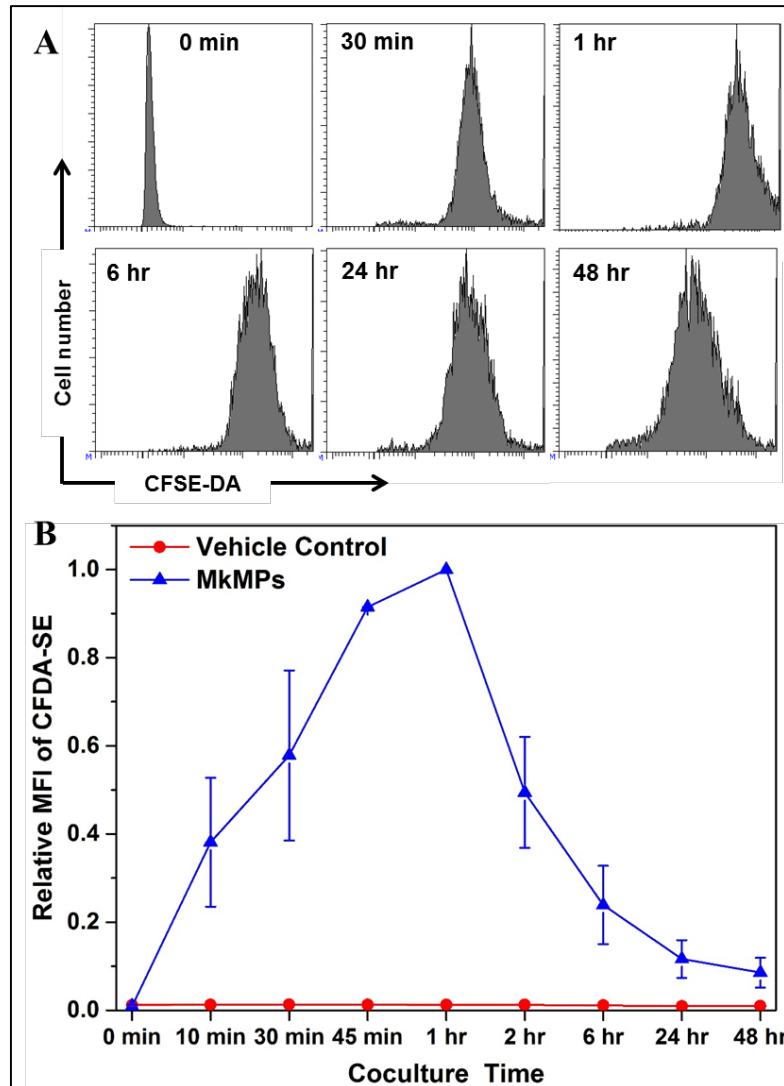


Figure A.2 Kinetics of MkMP binding to cells. MkMPs were stained with dye CFDA-SE and then co-cultured with d3 HPCs. At the time as indicated, some cells were harvested for analysis of mean fluorescence intensity (MFI) of CFDA-SE by flow cytometry. **(A)** Flow cytometry histogram of cell CFDA-SE intensity from a single experiment at several representative time points. **(B)** CFDA-SE MFI of cells at different time points were normalized to MFI at 1 hour. Error bar represents standard error of mean (n=3).

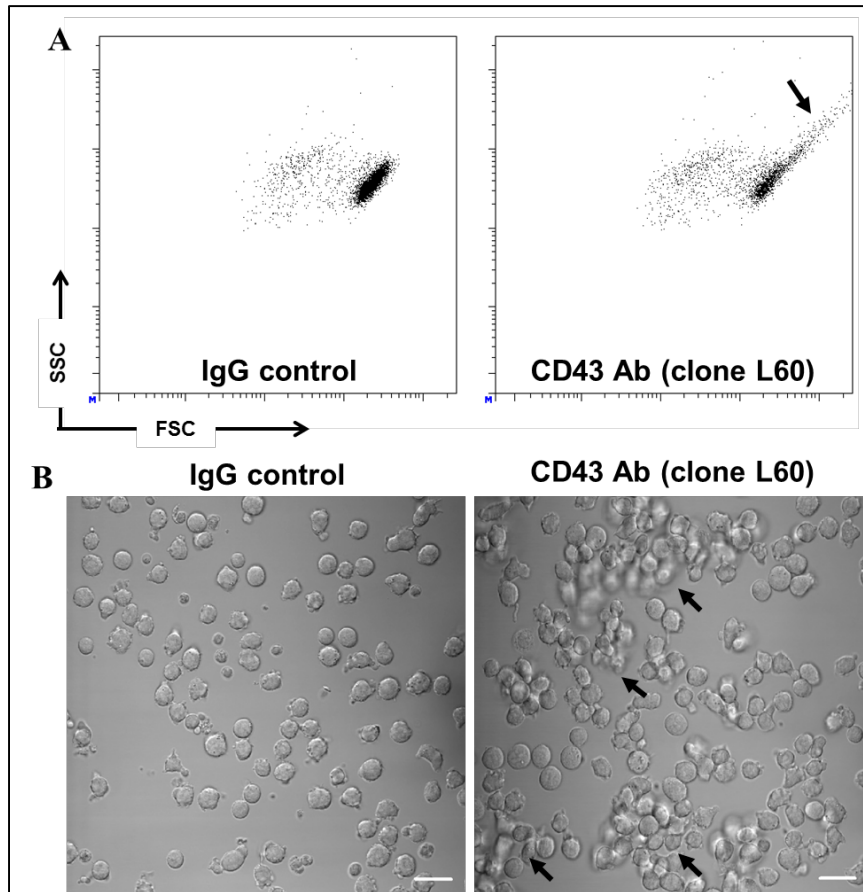


Figure A.3 CD43 antibody induces cell aggregation of d3 HPCs. Day 3 HSPCs were treated with IgG or CD43 antibody (clone L60) for 1 hour and 15 minutes before analysis by flow cytometry (A) or confocal microscopy (B). Cell aggregations are indicated by arrows. Scale bar in (B) is 20 μm .

Appendix B

SUPPLEMENTARY MATERIAL FOR CHAPTER 3

ENGINEERING HUMAN MEGAKARYOCYTIC MICROPARTICLES FOR TARGETED DELIVERY OF NUCLEIC ACIDS TO HEMATOPOIETIC STEM & PROGENITOR CELLS

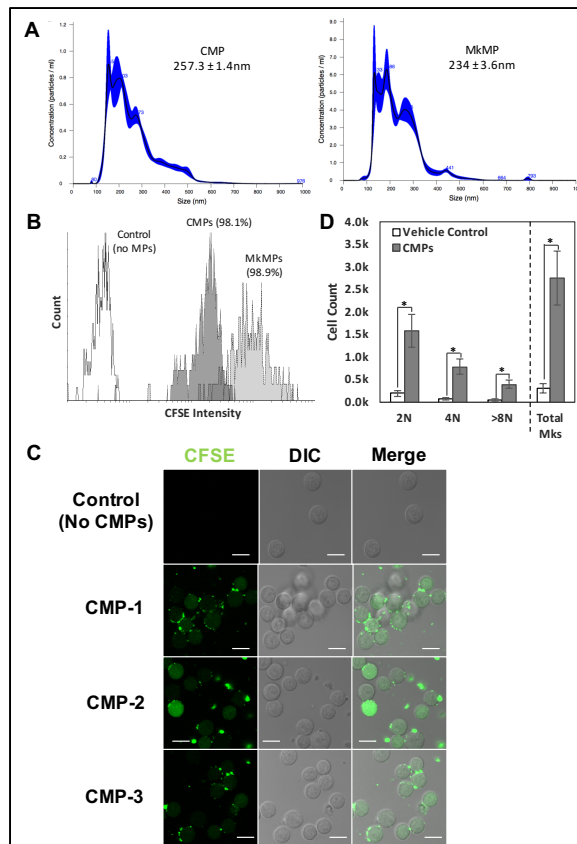


Figure B.1 Physical and functional characterization of CMP. (A) Size distribution measurement of CMPs and MkMPs by NTA. (B, C) CD34⁺ HSPCs were co-culture with CFSE-stained CMPs, MkMPs or vehicle control. After 30 minutes of co-culture, cells were harvested for (B) flow cytometry analysis on CFSE intensity, and (C) the uptake of CMPs with CFSE delivery to HSPCs were examined by confocal microscopy. (D) CMPs were co-cultured with CD34⁺ HSPCs and programed Mk differentiation. Cells were harvested at day 8 of co-culture and cell count of each ploidy class (2N, 4N, >8N), or total cell count were measured by flow cytometry. Scale bar in (C) represent 10 μ M.

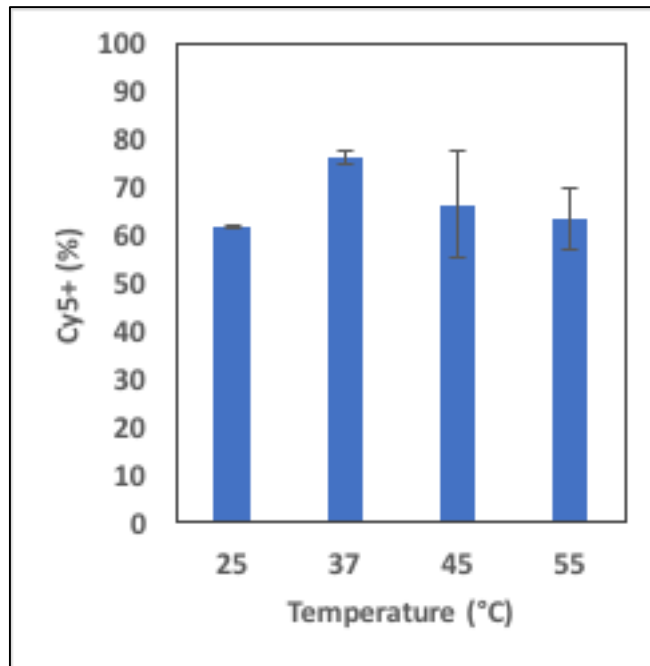


Figure B.2 The effect of electroporation temperature on pDNA loading efficiency. pGFPns was first stained with Cy5 fluorescent dye, then loaded into CMPs via electroporation at 100V, 100 μ F, in 2-mm cuvette at various temperature (25, 37, 45, or 55 °C). Cy5+ percentage of CMPs from each electroporation was quantified by flow cytometry analysis. Error bar represents SEM of three biological replicates.

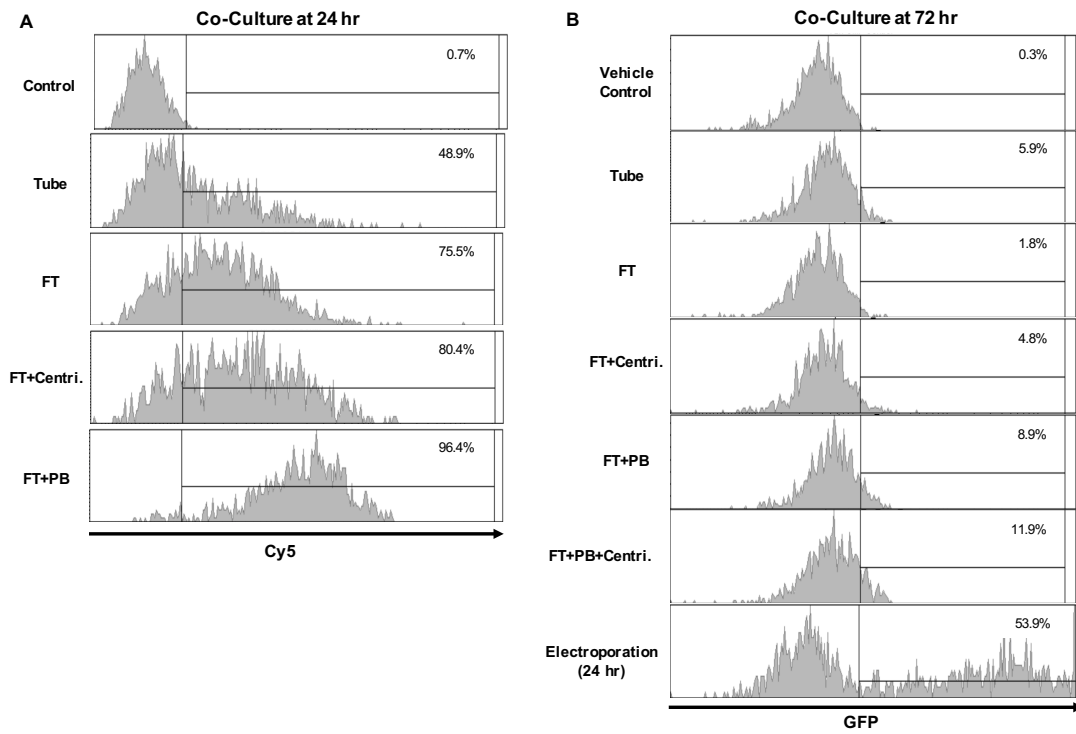


Figure B.3 Flow cytometry histograms. HSPCs were co-cultured with (A) Cy5-pGFPns-loaded CMPs, (B) pmaxGFP-loaded CMPs, and were harvested for flow cytometry analysis at (A) 24 hours for Cy5 signal, or (B) 72 hour for GFP expression. (A) Representative figures of Cy5 percentage associated with Figure 2D. (B) Representative figures of GFP expression associated with Figure 2F.

Table B.1 Primers for amplification in PCR and q-RT-PCR

| Gene | Forward Primer | Reverse Primer |
|--------------|------------------------|------------------------|
| <i>GAPDH</i> | CCCTTCATTGACCTCAACTACA | ATGACAAGCTTCCCGTTCTC |
| <i>GFP</i> | TCAAGATCCGCCACAACATC | GTGCTCAGGTAGTGGTTGTC |
| <i>CMV</i> | GGGTCATTAGTTCATAGCCATA | GCCAAGTAGGAAAGTCCCATAA |
| <i>c-myb</i> | CTGCCTGGACGAACTGATAAT | TTGAAGACTCCTGCAGATAACC |

Table B.2 Estimation of DNA copies in loaded-EVs from literature

| EV Type | DNA Type | DNA Size | Loaded DNA copy per EV | Ref. |
|---------------------------|-----------------|-----------------|-------------------------------|------------------------|
| Exosome (85nm) | Linear | 250 bp | 462 | [51] |
| MP (167nm) | Linear | 250 bp | 1347 | |
| Exosome (85nm) | Plasmid | 6 kb | 1-2 | |
| MP (167nm) | Plasmid | 6 kb | 8 | |
| MP (257nm) | Plasmid | 6.29 kb | 3455 | Our Result |
| MP (234 nm) | Plasmid | 3.49 kb | 4264 | Our Best Result |
| MP (257 or 234 nm) | Plasmid | 9.8 kb | 1700-2100 | Estimation* |

*Estimation of pDNA copy number in loaded-EVs from Latulippe *et al* [163] and our result.

Appendix C

SUPPLEMENTARY MATERIAL FOR CHAPTER 4

ROLE OF MICRORNAS FROM MEGAKARYOCYtic MICROPARTICLES (MKMPS) IN MKMP-INDUCED MEGAKARYOCYtic DIFFERENTIATION OF HEMATOPOIETIC STEM/PROGENITOR CELLS

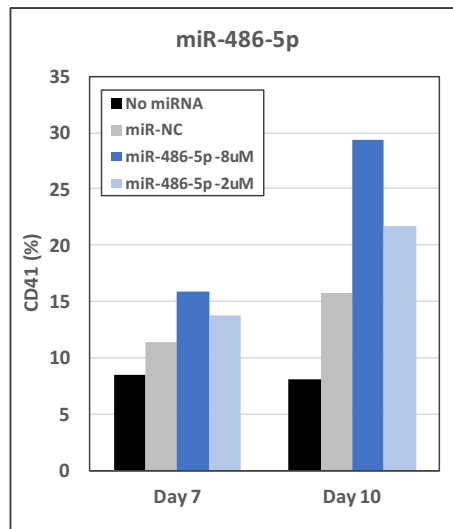


Figure C1 Dose effect of miRNA transfection to HSPCs. 2 μ M or 8 μ M of miR-486-5p mimics, or miR-NC (non-targeting miRNA), or “No miRNA” control were transfected into HSPCs by nucleofection under program U-08. Cells were harvested for flow cytometric analysis on CD41 expression at day 7 and day 10.

Appendix D

SUPPLEMENTARY MATERIAL FOR CHAPTER 5

ROLE OF P53 AND TRANSCRIPTION-INDEPENDENT P53-INDUCED APOPTOSIS IN SHEAR-STIMULATED MEGAKARYOCYTIC MATURATION, PARTICLE GENERATION, AND PLATELET BIOGENESIS

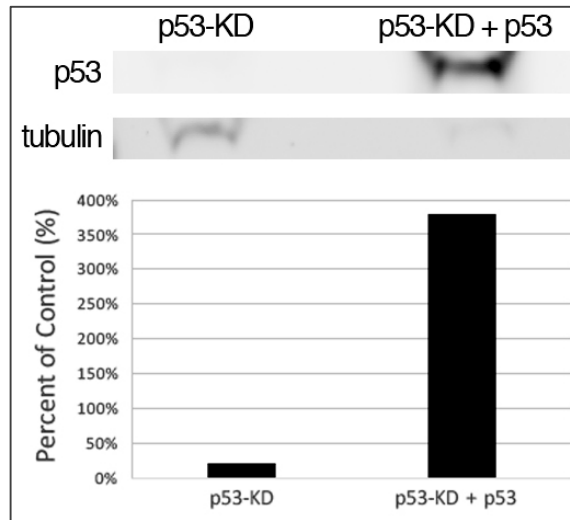


Figure D1 Western blotting analysis of p53 expression in CHRF cells with p53 knock-down (p53-KD) or p53-KD followed by rescuing with wild-type p53. p53 levels are presented as percentage of control (WT cells).

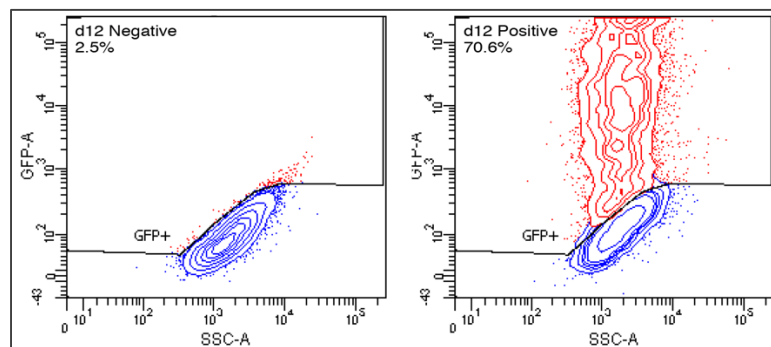


Figure D2 Transfection efficiency from pmaxGFP-transfected or negative control d12 Mks. GFP expression was analyzed by flow cytometry.

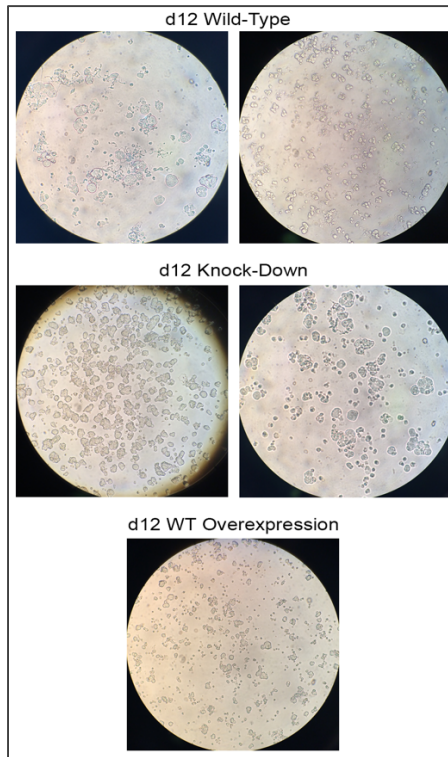


Figure D3 Representative images of wild-type, p53 knock-down, or p53 overexpression d12 Mks.

Appendix E

PUBLICATION PERMISSIONS



RightsLink®

- [Home](#)
- [Create Account](#)
- [Help](#)



Title: How do megakaryocytic microparticles target and deliver cargo to alter the fate of hematopoietic stem cells?

Author: Jinlin Jiang, Chen-Yuan Kao, Eleftherios T. Papoutsakis

Publication: Journal of Controlled Release

Publisher: Elsevier

Date: 10 February 2017

© 2016 Elsevier B.V. All rights reserved.

LOGIN

If you're a [copyright.com](#) user, you can login to RightsLink using your copyright.com credentials. Already a [RightsLink user](#) or want to [learn more?](#)

Please note that, as the author of this Elsevier article, you retain the right to include it in a thesis or dissertation, provided it is not published commercially. Permission is not required, but please ensure that you reference the journal as the original source. For more information on this and on your other retained rights, please visit: <https://www.elsevier.com/about/our-business/policies/copyright#Author-rights>

- [BACK](#)
- [CLOSE WINDOW](#)

Copyright © 2018 [Copyright Clearance Center, Inc.](#) All Rights Reserved. [Privacy statement](#). [Terms and Conditions](#). Comments? We would like to hear from you. E-mail us at customercare@copyright.com



RightsLink®

Home

Create Account

Help



Title: Extracellular vesicles: exosomes, microparticles, their parts, and their targets to enable their biomanufacturing and clinical applications

Author: Chen-Yuan Kao, Eleftherios T Papoutsakis

Publication: Current Opinion in Biotechnology

Publisher: Elsevier

Date: December 2019

© 2019 Elsevier Ltd. All rights reserved.

LOGIN
If you're a **copyright.com** user, you can login to RightsLink using your copyright.com credentials. Already a **RightsLink user** or want to [learn more?](#)

Please note that, as the author of this Elsevier article, you retain the right to include it in a thesis or dissertation, provided it is not published commercially. Permission is not required, but please ensure that you reference the journal as the original source. For more information on this and on your other retained rights, please visit: <https://www.elsevier.com/about/our-business/policies/copyright#Author-rights>

BACK

CLOSE WINDOW

Copyright © 2019 [Copyright Clearance Center, Inc.](#) All Rights Reserved. [Privacy statement.](#) [Terms and Conditions.](#) Comments? We would like to hear from you. E-mail us at customer@copyright.com

Appendix F

IRB APPROVAL LETTER FOR BLOOD COLLECTION



RESEARCH OFFICE

210 Hullihen Hall
University of Delaware
Newark, Delaware 19716-1551
Ph: 302/831-2136
Fax: 302/831-2828

DATE: June 18, 2018

TO: Eleftherios Papoutsakis, PhD
FROM: University of Delaware IRB

STUDY TITLE: [622751-5] Generation of Platelet-derived Microparticles

SUBMISSION TYPE: Continuing Review/Progress Report

ACTION: APPROVED

APPROVAL DATE: June 18, 2018

EXPIRATION DATE: June 23, 2019

REVIEW TYPE: Expedited Review

REVIEW CATEGORY: Expedited review category # (2)

Thank you for your submission of Continuing Review/Progress Report materials for this research study. The University of Delaware IRB has APPROVED your submission. This approval is based on an appropriate risk/benefit ratio and a study design wherein the risks have been minimized. All research must be conducted in accordance with this approved submission.

This submission has received Expedited Review based on the applicable federal regulation.

Please remember that informed consent is a process beginning with a description of the study and insurance of participant understanding followed by a signed consent form. Informed consent must continue throughout the study via a dialogue between the researcher and research participant. Federal regulations require each participant receive a copy of the signed consent document.

Please note that any revision to previously approved materials must be approved by this office prior to initiation. Please use the appropriate revision forms for this procedure.

All SERIOUS and UNEXPECTED adverse events must be reported to this office. Please use the appropriate adverse event forms for this procedure. All sponsor reporting requirements should also be followed.

Please report all NON-COMPLIANCE issues or COMPLAINTS regarding this study to this office.

Please note that all research records must be retained for a minimum of three years.

Based on the risks, this project requires Continuing Review by this office on an annual basis. Please use the appropriate renewal forms for this procedure.

Appendix G

IRB EXEMPT LETTER OF USING HUMAN CD34+ CELLS



RESEARCH OFFICE

210 Halliher Hall
University of Delaware
Newark, Delaware 19716-1551
Ph: 302/831-2136
Fax: 302/831-2828

DATE: April 30, 2018

TO: Eleftherios Papoutsakis, PhD
FROM: University of Delaware IRB

STUDY TITLE: [753050-2] Utilizing Primary Human Cells in the Papoutsakis Lab

SUBMISSION TYPE: Continuing Review/Progress Report

ACTION: DETERMINATION OF EXEMPT STATUS
DECISION DATE: April 30, 2018

REVIEW CATEGORY: Exemption category # (4)

Thank you for your submission of Continuing Review/Progress Report materials for this research study. The University of Delaware IRB has determined this project is EXEMPT FROM IRB REVIEW according to federal regulations.

We will put a copy of this correspondence on file in our office. Please remember to notify us if you make any substantial changes to the project.

If you have any questions, please contact Nicole Farnese-McFarlane at (302) 831-1119 or nicolefm@udel.edu. Please include your study title and reference number in all correspondence with this office.